# Chemical Activity-based Risk Assessment of Perfluorooctane Sulfonate (PFOS)

**by**

**Shu Han (Sophia) Hsu**

B.Sc. (Hons., Biology), McGill University, 2019

Thesis Submitted in Partial Fulfillment of the
Requirements for the Degree of
Master of Resource Management

in the
School of Resource and Environmental Management
Faculty of Environment


SIMON FRASER UNIVERSITY
Summer 2023

## Declaration of Committee

| | |
|---|---|
| **Name:** | **Shu Han (Sophia) Hsu** |
| **Degree:** | **Master of Resource Management** |
| **Title:** | **Chemical Activity-based Risk Assessment of Perfluorooctane Sulfonate (PFOS)** |
| **Committee:** | **Chair:** **Brett van Poorten**<br>Assistant Professor, Resource and Environmental Management |
| | **Frank Gobas**<br>Supervisor<br>Professor, Resource and Environmental Management |
| | **Barry Kelly**<br>Committee Member<br>Adjunct Professor, Resource and Environmental Management |
| | **Juan José Alava**<br>Examiner<br>Adjunct Professor, Resource and Environmental Management |

# Abstract

Traditional methods for assessing the environmental risks associated with perfluorooctane sulfonate (PFOS) have faced challenges due to its ionic, poorly lipid-soluble, non-volatile, and surface-active nature. To support current environmental management practices for PFOS, this thesis applies the concept of chemical activity to facilitate the comparison of its exposure and toxicity concentrations. Through this approach, a wide range of concentration data from various media, units, and sources are integrated, enabling a more comprehensive evaluation of its environmental distribution and potential risks. To support the measurement of apparent chemical activity, a technique of solid-phase microextraction (SPME) through thin-films of ethylene vinyl acetate (EVA) is developed. This technique can also be used to determine samples' concentration, sorptive capacity, and partition coefficient of PFOS. Results show that the sorptive capacity of PFOS in aqueous solutions is influenced by factors such as ionic strength and potentially temperature, while the partition coefficients between EVA and solution ($K_{EVA\text{-}Soln}$) and serum albumin and solution ($K_{BSA\text{-}Soln}$) are dependent on the concentrations of PFOS and serum albumin. These observations are likely attributed to the surfactant nature of PFOS, which complicates its behaviour in solution and interaction with receptor media such as EVA and serum albumin. Given the complex physicochemical properties of PFOS that may be influenced by varying conditions, direct measurements through EVA SPME offer a practical tool for supporting a chemical activity-based environmental risk assessment of PFOS.



**Keywords**: perfluorooctane sulfonate; PFAS; chemical activity; environmental; risk assessment

# Acknowledgements

I am sincerely grateful to many people for their invaluable contributions to the completion of this thesis.

Dr. Frank Gobas—thank you for your continued support, encouragement, and dedication throughout my graduate studies. Your passion for science, immense insight, and openness to learning have been an inspiration to me. I feel incredibly fortunate to have had this opportunity to work and learn from you.

Dr. Barry Kelly—thank you for your invaluable feedback and guidance. Your expertise in PFAS and assistance in technical work have been instrumental in this research.

Dr. Yung-Shan Lee—thank you for sharing your time and expertise to help me navigate the world of lab work and experiment setup. I am very grateful for your technical advice, guidance, and unwavering emotional support.

Furthermore, I would like to thank everyone in the Fugacity Club for your advice, support, and positivity. Learning with and from all of you has been a pleasure. Special thanks to Mark and Alex for your help and troubleshooting with the LC MS/MS, and to Beatrice and Samantha for your support with my experiments.

Finally, I am deeply grateful to my mom, dad, brother, and all my family and friends for their support, patience, and love. Thank you for believing in me throughout this journey.

# Table of Contents

# List of Tables

# List of Figures

# List of Acronyms

| | |
|---|---|
| AFFF | Aqueous Film Forming Foam |
| BAFB | Barksdale Air Force Base |
| BSA | Bovine Serum Albumin |
| $C_{EVA}$ | PFOS Concentration in EVA |
| $C_W$ | PFOS Concentration in Water |
| DoD | US Department of Defense |
| EVA | Ethylene Vinyl Acetate |
| *F* | Fugacity Ratio |
| $K_{BSA-PBS}$ | Partition Coefficient of PFOS between BSA and PBS |
| $K_{EVA-Soln}$ | Partition Coefficient of PFOS between EVA and solution |
| $K_{OW}$ | Octanol-water Partition Coefficient |
| LC MS/MS | Liquid Chromatography with Tandem Mass Spectrometry |
| MeOH | Methanol |
| MS | Mass Spectrometry |
| OECD | The Organization for Economic Co-operation and Development |
| PBS | Phosphate Buffered Saline |
| PDMS | Polydimethylsiloxane |
| PFAS | Per- and Polyfluoroalkyl Substances |
| PFHxS | Perfluorohexanesulfonic Acid |
| PFNA | Perfluorononanoic Acid |
| PFOA | Perfluorooctanoic Acid |
| PFOS | Perfluorooctane Sulfonate |
| PFOS-K | Potassium Perfluorooctanesulfonate |
| $pK_a$ | Acid Dissociation Constant |
| SD | Standard Deviation |
| SE | Standard Error |
| SPME | Solid-Phase-Micro-Extraction |
| US EPA | US Environmental Protection Agency |
| WAFB | Wurtsmith Air Force Base |

# Glossary

| | |
|---|---|
| Aliphatic | Denotes organic compounds that have an open structure as opposed to aromatic rings (i.e. carbon chains) |
| Aqueous film-forming foam (AFFF) | A highly efficient foam used for suppressing flammable liquid fires. When mixed with water, the resulting solution is able to rapidly spread across the surface of the fuel, effectively preventing re-ignition and extinguishing the flame |
| Bioaccumulation | The accumulation of a chemical in biota as a result of a combination of absorption, distribution, metabolism, and excretion processes, where the concentration of the chemical in biota exceeds those in the environment |
| BSA-water partition coefficient ($K_{BSA-W}$) | The ratio of PFOS concentrations in BSA and water at equilibrium |
| Chemical activity (*a*) | The dimensionless ratio of the fugacity of a substance in a medium relative to the fugacity of the substance at a defined standard state; can also be estimated by the ratio of the chemical's concentration (C, mg/L) and solubility (S, mg/L) for a dilute phase. |
| EVA-water partition coefficient ($K_{EVA-W}$) | The ratio of PFOS concentrations in EVA and water at equilibrium |
| Fugacity | The escaping tendency of a chemical between phases, measured by the partial pressure (Pa) that the chemical exerts |
| Hydrophobicity | The tendency of a substance to repel or be insoluble in water due to its non-polar nature |
| Lipophobicity | The tendency of a substance to be insoluble in lipids |
| Non-polar substances | Substances that are neutral due to equal charge distribution. Examples include hydrocarbons, lipids, and oils |
| Octanol-water partition coefficient ($K_{OW}$) | The ratio of concentrations of a chemical in octanol and water at equilibrium |
| Organic | Denotes compounds that contain carbon and hydrogen. Examples include carbohydrates, lipids, proteins, etc. |
| Perfluoroalkyl substances | Substances whose carbon-chains are fully fluorinated, common functional groups include carboxylates and sulfonates |
| Polar substances | Substances with an unequal charge distribution, where negative and positive charges are distinctly parted. Examples include water and glucose |

| | |
|---|---|
| Polarity | Refers to the distribution of electrical charge in a molecule |
| Polyfluoroalkyl substances | Aliphatic substances whose carbon-chains are not fully fluorinated. The non-fluorinated bond in polyfluoroalkyl substances renders a “weak” point in the carbon tail, hence making the molecule susceptible to degradation |
| Sorptive capacity (S) | Describes the capacity of a medium to sorb or associate with a chemical |

# Chapter 1. Introduction

## 1.1. Per- and Polyfluoroalkyl Substances

Per- and polyfluoroalkyl substances, or PFAS, are a growing class of manufactured chemicals with strong water-, stain-, and heat resistance (Key et al. 1997). Due to these unique properties, they are commonly used in industrial and consumer products to create non-stick and stain-proof products. They are also important components of firefighting foams. Consequently, because of their extensive application, PFAS have become ubiquitous in the environment (Moody and Field 2000, Anderson et al. 2016).

PFAS comprise a diversity of structures, leading to a wide range of physical and chemical properties. They can be divided into polymers and non-polymers; neutral molecules, anions, cations, and zwitterions; solids, liquids, and gases; soluble and insoluble substances; and volatile and involatile substances (Cousins et al. 2020). The common structure of PFAS features a fluorinated alkyl backbone connected to a hydrogen or an acidic functional group. The strong carbon-fluorine bonds in the backbone contributes to the high chemical and thermal stability of PFAS, making PFAS robust to environmental degradations (Buck et al. 2011, Wang et al. 2015, 2017). Additionally, the alkyl backbone is hydrophobic and lipophobic, therefore, combined with the polar and hydrophilic properties of the functional group, PFAS is stain-repellent. While these traits are desirable in various industries, they also contribute to PFAS persistence, bioaccumulation, long-range transport, and toxicity in biota (Giesy and Kannan 2001, Stock et al. 2007, Quist et al. 2015, ATSDR 2021). Their persistence and high water solubility have led to the widespread presence of PFAS in groundwater, rivers, drinking water, and regions far beyond their origin of source (Giesy and Kannan 2001, Kelly et al. 2009, Buck et al. 2011). It is no surprise that PFAS is detected in humans as well as freshwater, marine, and terrestrial species (Kelly et al. 2009, Worley et al. 2017, Lee et al. 2023, Hedgespeth et al. 2023, Kesic et al. 2023).

Recent studies have associated PFAS exposure with serious health issues such as cancer, kidney disease, liver problems, high cholesterol, immunotoxicity, and autoimmune disorders, raising significant ecological and human health concerns (Fair et al. 2013, Convertino et al. 2018, Budtz-Jørgensen and Grandjean 2018, Bassler et al.

2019, Li et al. 2022). As evidence of the environmental and health impacts of PFAS emerged, manufacturers like 3M Company voluntarily began phasing out the production of perfluorooctane sulfonate (PFOS), perfluorooctanoic acid (PFOA), and related precursors in the 2000s (3M Company 2000).

In Canada, PFOS was declared a toxic substance in 2004, through which PFOS and its salts were listed in Schedule 1 of the Canadian Environmental Protection Act 1999 (CEPA) (Canada Gazette 2006). This marked the first environmental legislation for any PFAS in Canada, aimed to protect the environment and human health. However, no compliance or enforcement requirements were made in association with the Act. In 2006, the Ecological Screening Assessment concluded that PFOS and its salts and precursors were entering into the environment in a quantity that may lead to immediate or long-term harmful effect on wildlife and that PFOS has the potential to bioaccumulate and biomagnify in mammals and piscivorous birds (Environment Canada 2006). In 2009, PFOS was added to the Virtual Elimination List (CEPA 2009). Subsequently, a tighter restriction was introduced in 2016 through the Prohibition of Certain Toxic Substances Regulations 2012 to prohibit the manufacture, use, sale, and import of PFOS and PFOA, as well as their salts and precursors. However, these regulations exempted the use of PFOA and PFOS in aviation hydraulic fluids, photolithography, photographic films, papers, and printing plates. More recently, drinking water guidelines were developed by Health Canada for PFOS and PFOA at 0.6 µg/L and 0.2 µg/L, respectively (CEPA 2018a, 2018b). Similarly, British Columbia has set a drinking water guideline at 0.6 µg/L for PFOS (BC Ministry of Environment and Climate Change Strategy 2020), while Ontario had developed an interim drinking water advice for a combined level of 11 select PFAS at 0.07 µg/L (Ontario Minister of the Environment 2021). In support of risk assessment, management and monitoring of PFOS, federal environmental quality guidelines have also been developed for freshwater (at 6.8 µg/L) and wildlife (fish tissue at 9.4 mg/kg wet weight, mammalian diet at 4.6 µg/kg diet wet weight, avian diet at 8.2 µg/kg diet wet weight, and bird egg tissue at 1.9 µg/g wet weight) (CEPA 2018).

Internationally, PFOS was added to Annex B of the Stockholm Convention List of globally restricted Persistent Organic Pollutants in 2009, with PFOA added in 2015. As a result, the Conference Parties were required to restrict their production and use (KEMI 2017). In 2022, the US Environmental Protection Agency (EPA) revised its lifetime health advisory as well as the drinking water guideline for PFOS and PFOA to 0.02 ppt

(US EPA 2022a), down from 70 ppt (US EPA 2016). Despite these preemptive measures, many PFAS persist and remain widespread, meanwhile, short-chained and structurally similar alternative PFAS are still being produced and used (Buck et al. 2011). Given this rapidly changing landscape of PFAS, there is still a large knowledge gap, making it crucial to improve strategies for managing PFAS to minimize their environmental and human health impacts (East et al. 2021).

## 1.2. PFAS at US Military Sites

Since the 1970s, the US Department of Defense (DoD) has been using aqueous film forming foams (AFFF) containing mixtures of PFAS as fire retardants. These fluorinated foams effectively extinguish a fire by rapidly spreading across the surface of a hydrocarbon fuel spill, preventing vapour re-ignitions. As a result, the use of AFFF with PFAS is required by US DoD, where they are used for fire training, equipment maintenance, and emergency response purposes (US DoD 2017). Consequently, the groundwater, surface water, sediment, and biota on many US DoD sites are contaminated with PFAS.

PFAS are often found as complex mixtures in the environment and biota (East et al. 2021). The types of PFAS present are influenced by the manufacturing process of the foams (Anderson et al. 2016). In general, PFAS synthesized for AFFF can be manufactured via either electrochemical fluorination or telomerization. The former results in fully fluorinated acids like PFOS and other perfluoroalkyl sulfonamides. These sulfonamides and their derivatives can break down into PFOS and other smaller chains of perfluoroalkyl moieties. In contrast, telomerization produces a diversity of PFAS, where often the carbon tails are not fully fluorinated. These fluorotelomers can then degrade into PFOA and perfluoroalkyl carboxylic acids (Buck et al. 2011). As such, multiple PFAS are often found on DoD sites (East et al. 2021).

A previous analysis on US Air Force installations with historical AFFF release found that the overall mixtures of PFAS was predominantly of PFOS and perfluorohexanesulfonic acid (PFHxS) (Anderson et al. 2016). A key concern was that those existing levels of PFOS exceeded the toxicity benchmarks for aquatic and terrestrial organisms (Salice et al. 2018, Larson et al. 2018). Several field studies have also attributed PFOS for the apparent effects in wildlife when exposed to mixtures of

PFAS (Custer et al. 2014, Groffen et al. 2019). Because of these reasons, PFOS will be selected as a focus compound in representation for other PFAS. More details are described in Section 1.6 Research Objectives.

## 1.3. Physicochemical Properties of PFOS

PFOS is synthesized as a non-polymer solid, some of its forms include potassium salt (CAS No. 2795-39-3), ammonium salt (CAS No.29081-56-9), diethanolamine salt (CAS No. 70225-14-8), lithium salt (CAS No. 29457-72-5), and sodium salt (CAS No. 4021-47-0) (CEPA 2018c). PFOS is also produced as a by-product in the manufacture of other perfluorinated precursors such as perfluoroalkyl sulfonamides and telomers (Giesy and Kannan 2001).

Unlike neutral persistent organic pollutants, PFOS is hydrophilic and poorly soluble in neutral lipids. It is bioaccumulative in protein-rich (Giesy and Kannan 2001, Aas et al. 2014, Robuck et al. 2021) and phospholipid-rich (Armitage et al. 2013, Droge 2019, Ebert et al. 2020) tissues. Additionally, PFOS is a surfactant, exhibiting tendencies to accumulate on interfaces and self-assemble into micelles at higher concentrations (Krafft and Riess 2015, Rewerts et al. 2021). Despite being non-volatile, its high structural stability and water solubility facilitates its long range transport within water bodies (Health Canada 2018). In the environment, PFOS is often found dissociated as an ion ($C_8F_{17}SO_3^-$) due to its strong acid nature. However, under very low pH conditions, it may be present as an acid (CAS No. 1763-23-1) (Vierke et al. 2013).

In biota, PFOS is frequently detected as the predominant form of PFAS due to its widespread environmental distribution (Giesy and Kannan 2001, Kelly et al. 2009, Anderson et al. 2016, Salice et al. 2018, Larson et al. 2018). Additionally, the biotransformation of precursor compounds, such as N-ethyl perfluorooctanesulfonamide (N-EtPFOSA), into PFOS, also contributes to the load of PFOS in biota (Tomy et al. 2004). As such, PFOS is frequently found in the blood, kidney, liver, and cell membranes. In particular, it has been found that PFOS exhibits strong associations with serum albumin (Jones et al. 2003, Bischel et al. 2010), α globulins (Han et al. 2004), and fatty acid-binding proteins (Luebker et al. 2002).

The physicochemical properties of PFOS are crucial to understanding its environmental fate and assessing processes such as transfer between environmental media (i.e., partition coefficient), bioaccumulation, and biotransformation. However, many of these data remain inconsistent or missing altogether, due to the unique characteristics of PFOS that have made experimental measurements as well as predictions through computer programs difficult. Notably, PFOS does not exist as ions in a pure phase for direct measurements. Computational models are consequently the primary means of estimating these properties, however, without experimental data to calibrate and validate these models, predictions of PFOS properties can vary widely and associated with considerable errors, often spanning several orders of magnitude (Arp et al. 2006, Lampic and Parnis 2020, Endo et al. 2023). This variability is exemplified by the solubility data of PFOS-K in water presented in Table A1, as well as other physical and chemical properties, where predicted values vary by up to 4 logarithmic units compared to those experimentally measured. In contrast, direct measurements using PFOS salts exhibit more consistency. Nonetheless, these have their own limitations, as the interfacial active nature of PFOS causes it to aggregate at interfaces or form micelles, resulting in major concentration differences, up to eightfold, between the bulk solution and surface (Schaefer et al. 2019, Costanza et al. 2020).

Table A1 to Table A6 present a comprehensive overview of the physical and chemical properties of PFOS, including water solubility, melting temperature, vapor pressure, Henry's constant, critical micelle concentrations, and acid dissociation constant ($pK_a$). Despite the wide range of variations in reported data, it is evident that PFOS is water-soluble, sparingly volatile, and a strong acid.

## 1.4. Risk Assessment Context for PFOS

Environmental risk assessments of substances typically involve comparing the exposure concentration with the concentration associated with the most sensitive potential adverse biological effect. Numerous studies since the early 2000s have linked PFOS exposures with toxicological endpoints, providing valuable insights into the environmental and health implications of PFOS. However, the assessment of PFOS's environmental risk poses a notable challenge regarding the evaluation involving varying media, units, and methodological conditions. Often, field conditions and those employed in toxicological studies such as temperature, media composition, exposure duration, and

subject species, do not align, thus comparing these data of different metrics can be likened to “comparing apples to oranges”. Consequently, only a few toxicity references that have comparable metrics are included in analyses, leaving out other valuable data for risk assessments. In this context, guidelines are applied with uncertainty factors to account for data extrapolation, leading to varying guidelines across organizations. For instance, as shown in Table 1, the drinking water guideline for PFOS varies by up to a factor of 30,000. Evidently, there is a need to develop an approach that effectively make use of available data and make sense of the relationships between exposure and effects for the environmental management of PFOS.

**Table 1. Drinking water guidelines for PFOS**

| Agency | Guideline (ng/L) | Year |
|---|---|---|
| Health Canada | 600 | (2018) |
| UK Health Protection Agency | 300 | (2007) |
| Australia Department of Health | 70 | (2017) |
| US EPA | 70* | (2016) |
| World Health Organization | 18 | (2017, 2022) |
| US EPA | 0.02† | (2022a) |
| US EPA | 4‡ | (2023a) |

* health advisory; non-regulatory and non-legally enforceable

† interim health advisory; non-regulatory and non-legally enforceable

‡ proposed maximum contaminant level (enforceable regulatory drinking water standard)

To overcome these challenges and facilitate the environmental risk assessment of PFOS, this study aims to apply the concept of chemical activity. This approach is rooted in thermodynamic principles that have been successfully applied to understand and predict the environmental fate of legacy pollutants and ionizable substances (Franco and Trapp 2010, Mackay et al. 2010, Gobas et al. 2017, 2018). The chemical activity concept provides a metric that allows for the expression of concentration data from different media, units, and studies in a common quantity, enabling accurate comparisons. Moreover, this approach has to potential to incorporate vast amounts of data, providing a more comprehensive understanding of the risks associated with PFOS.

## 1.5. Research Objectives

The overall aim of this thesis is to investigate the application of a chemical activity-based approach for environment risk assessments of PFOS. Specifically, this

study develops and tests the use of solid-phase microextraction (SPME) using EVA thin-films to measure the apparent chemical activities of PFOS and applies this method to evaluate the environmental risks of PFOS at AFFF-affected sites of the US Air Force Bases. To do this, this study:

1) Measures the solubility of PFOS in water and phosphate buffered saline at pH 7.4.

2) Develops and calibrates EVA thin-film solid-phase microextraction for measuring the chemical activity of PFOS in media types.

3) Measures the sorptive capacity of PFOS in bovine serum albumin through rapid EVA thin-film solid-phase microextraction.

4) Applies the chemical activity approach at AFFF-impacted sites to evaluate the environmental risks of PFOS contamination.

# Chapter 2. Theory

## 2.1. Chemical Activity

Chemical activity, like fugacity, is a thermodynamic concept used to describe the distribution of chemicals in the environment. These concepts were introduced by Gilbert N. Lewis in the early 1900s to understand the "escaping tendency" of chemicals from mixtures and solutions. Fugacity is a measure based on pressures, allowing the ideal gas law to be applied to non-gaseous substances such as liquids and solids. As such, the distribution of substances between phases can be better understood through pressures or gaseous concentrations. On the other hand, chemical activity applies the concept of ideal solutions to describe the behaviour of chemicals, taking into account their deviations from ideality. It can be defined using pressures or mole fractions of the substance, such as the case of their concentrations in aqueous solutions. This makes chemical activity a suitable descriptor for both neutral and charged species, extending its applicability to substances such as ions, metals, or polymers (Lewis 1907, Mackay 2001). Considering that PFOS is ionizable and not expected to exhibit significant volatility, the chemical activity approach will be applied in this thesis.

The chemical activity concept has been proposed as a tool for assessing chemical risks and developing guidelines (Mackay et al. 2010, Mackay and Arnot 2011, Gobas et al. 2015, 2017, 2018). This approach has been applied to neutral hydrophobic substances as well as ionizable compounds. For instance, chemical activity was used to evaluate the toxic potentials of polycyclic aromatic hydrocarbons (PAHs) in marine sediments (Witt et al. 2009) and assess the fate of pentachlorobenzene across different regions (Mackay et al. 2010). The chemical activity approach also facilitated the evaluation of the environmental risks of decamethylcyclopentasiloxane (D5) and di-ethylhexyl phthalate (DEHP), that was otherwise difficult to address through traditional concentration-based approaches (Gobas et al. 2015, 2017). Furthermore, chemical activity-based models have shown improved predictions of exposure scenarios for organic ionizable substances such as 2,4-dichlorophenoxyacetic acid (2,4-D), aniline and trimethoprim compared to conventional fugacity models (Franco and Trapp 2010).

Chemical activity (a, unitless) for a substance can be expressed as the ratio of its fugacity in a medium (f, Pa) to its reference fugacity ($f^R$, Pa) defined at standard state

using its pure chemical form (Equation 1). The reference phase can be selected based on practicality. In the case of ions, an ideal unimolar solution of 1 mol/$m^3$ for solutes has been used (Franco and Trapp 2010). However, the pure liquid phase is often chosen as the reference phase due to its ease of manipulation and direct measurability.

$$a = \frac{f}{f^R} \tag{1}$$

In that case, chemical activities vary from 0 to 1 for substances in the liquid phase. For substances that are in a solid state at the system's temperature or in a sub-cooled liquid form, the fugacity ratio (F, unitless, Equation 2) is applied to convert the vapour pressure of the solid into the vapour pressure of the subcooled liquid. As a result, chemical activities for solids range from 0 to F (unitless). The fugacity ratio can be estimated using the following formula, where $T_M$ is the melting point of the chemical in Kelvin, and T is the system's temperature, also in Kelvin (Mackay 2001).

$$F = e^{\left\{-6.79 \cdot \left[\left(\frac{T_M}{T}\right)-1\right]\right\}} \tag{2}$$

Chemical activity has also been defined as $x \cdot \gamma$ , where $x$ is the mole fraction (mol solute/mol solvent) and $\gamma$ (unitless) is the activity coefficient. The activity coefficient accounts for deviations from the ideal solution behaviour, making chemical activity a more accurate representation of the substance's effective concentration in a medium compared to its simple molar concentration.

$$a = \frac{f}{f^R} = x \cdot \gamma \tag{3}$$

When selecting the pure liquid phase as the reference state, the activity coefficient can be determined when the substance is saturated, i.e., the fugacity (f) of the substance is equal to the reference fugacity ($f^R$), resulting in the chemical activity at the thermodynamic maximum at either a value of 1 for liquids or F for solids. The activity coefficient ($\gamma_L$, unitless) of the substance in liquids can then be determined experimentally as the reciprocal of the sorptive capacity of the liquid for the substance (X, mol/mol).

$$\gamma_L = \frac{1}{X} \tag{4}$$

For solids at the system's temperature, the activity coefficient ($\gamma_s$, unitless) can be determined as the reciprocal of the sorptive capacity of the solid for the substance (X, mol/mol), adjusted with the fugacity ratio (F, unitless).

$$\gamma_S = \frac{F}{X} \tag{5}$$

Assuming that γ (unitless) is constant within the concentration range from 0 to X, which is reasoned for hydrophobic organic substances at dilute conditions, the activity coefficient in Equation (3) can be substituted with either Equations (4) or (5). In other words, the chemical activity for liquids ($a_L$, unitless) can be approximated by dividing the concentration of the chemical by its solubility (S, mol/m$^3$) in the medium in which it is dissolved.

$$a_L = (\frac{1}{X}) \cdot x = \frac{C}{S} \tag{6}$$

The chemical activity for solids ($a_S$, unitless) follows the same approximation, with the addition of the fugacity ratio.

$$a_S = \left(\frac{F}{X}\right) \cdot x = \frac{F}{S} \cdot C \tag{7}$$

As chemical activity reflects the effective concentration of a substance in a medium, the chemical activity concept can be used to predict the partitioning behaviour of the substance between environmental media, such as water and air. At equilibrium, the chemical activity (a, unitless) of a substance in one medium is equal to another:

$$a_1 = a_2 = x_1 \cdot \gamma_1 = x_2 \cdot \gamma_2 \tag{8}$$

Assuming that the substance is dilute in the media, the molar fraction (x, mol/mol) can be substituted with $C \cdot v$, where C is the concentration (mol/m$^3$) of the substance in the medium and v is the volume (m$^3$) of the medium. Equation (8) can be rearranged as follows:

$$\frac{x_1}{x_2} = \frac{\gamma_2}{\gamma_1} = \frac{C_1 \cdot v_1}{C_2 \cdot v_2} \tag{9}$$

The partition coefficient ($K_{12}$, unitless) of the substance between the two media can then be calculated from the concentrations of the substance in the media. The partition coefficient ($K_{12}$, unitless) can then be used to assess the substance's environmental fate and transport.

$$K_{12} = \frac{C_1}{C_2} = \frac{\gamma_2 \cdot v_2}{\gamma_1 \cdot v_1} \tag{10}$$

Similarly, chemical activity can support the understanding of biomagnification by calculating the biomagnification factor (BMF) using the chemical activities of the substance in the predator and prey:

$$BMF = \frac{a_{Predator}}{a_{Prey}} \tag{11}$$

The concept of chemical activity has traditionally been applied to neutral substances, as their pure liquids or solids make it possible for the determination of their standard fugacities. While there is no pure ionic PFOS available for direct measurement and determination of its standard fugacity, the chemical activity concept can still be useful for PFOS. Notably, the predicted ionic solubility displayed in Figure A1 indicates that PFOS exhibits measurable solubilities through PFOS salts in water. The consistency in the aqueous solubilities between different PFOS salts further suggests that the counter-ions (e.g. $K^+$, $Li^+$, $Na^+$, etc.) do not significantly contribute to the aqueous solubility, and that it is mainly the PFOS moiety that is responsible for its solvation limit. Therefore, by using its concentration and solubility in the medium, the apparent chemical activity of ionic PFOS can be approximated through Equation (7). It should be noted that the apparent chemical activities calculated in this thesis may differ from absolute chemical activities. However, the apparent values obtained are sufficiently accurate for the purpose of comparing concentration data within the context of environmental risk assessments.

Using chemical activity as a tool to evaluate concentration data can enhance current environmental risk assessments of PFOS. Not only does the concept enable direct comparisons between exposure and toxicity data, it also significantly reduces variability compared to using concentrations alone (Mackay et al. 2009, Gobas et al.

2017). In addition, this approach can determine whether PFOS was correctly dosed in exposure studies (Mackay 2001).

## 2.2. Measurement and Estimation of Chemical Activities

Table A1 summarizes both measured and predicted aqueous solubilities of PFOS in the forms of acid, ion, and salts. Among them, the average experimentally measured solubilities of PFOS-K in pure water was found to be 635 ± 169 mg/L (n = 5), based on data from multiple sources including 3M Company (2000), Ellefson (2001), OECD (2002), Inoue et al. (2012), and US EPA (2023b). As shown in Figure A1, these solubilities closely match the predicted solubility for ionic PFOS by OPERA. It can also be observed that the aqueous solubilities predicted by the same models are consistent among different salts. These observations indicate that the counter-ions do not significantly contribute to the aqueous solubility and suggest that the aqueous solubility of PFOS can be measured through the dissolution of PFOS salts.

The aqueous solubility of PFOS has also been measured in seawater and ion-buffered solutions. The solubility of PFOS-K was measured to be 12.4 mg/L in natural seawater (3.5% salinity) and 20mg/L in a 3.5% sodium chloride solution at 23 °C (OECD 2002). 3M Company has also measured the solubilities of PFOS-K in freshwater and filtered sea water to be 370 mg/L and 25 mg/L, however, it should be noted that these measurements did not follow the OECD Principles of Good Laboratory Practice (3M Company 2000).

Likewise, the sorptive capacity of biological samples such as serum, tissues, and organisms for PFOS can be determined. In a biological medium, the solubility of PFOS can be thought of as the maximum amount of PFOS that the medium can hold. Already, studies have detected PFOS frequently in biological phases such as polar lipids, serum albumin, structural proteins, and to a minor extent—neutral lipids (Droge 2019, Ebert et al. 2020, Allendorf et al. 2021). Following this, if the sorptive capacity for PFOS in these biological phases can be determined, the sorptive capacity in tissues or organisms may also be approximated based on the composition of their biological compartments. Accordingly, the sorptive capacity of biota or biological samples for PFOS ($S_{Biota}$, mg/L) can be estimated through summing the sorptive capacities of each constituent ($S_i$, mg/L)

for PFOS, adjusted by their mass fraction ($\phi$, unitless) within the biota. (W= buffered water, PL= polar lipids, AB= serum albumin, SP= structural protein, NL= neutral lipids)

$$S_{Biota} = (S_w \cdot \phi_w) + (S_{PL} \cdot \phi_{PL}) + (S_{AB} \cdot \phi_{AB}) + (S_{SP} \cdot \phi_{SP}) + (S_{NL} \cdot \phi_{NL}) \quad (12)$$

The chemical activity of PFOS ($a_{Biota}$, unitless) in biota can then be calculated by dividing the concentration of PFOS ($C_{Biota}$, mg/L) in the biota by its sorptive capacity for PFOS ($S_{Biota}$, mg/L), and finally multiplied by the fugacity ratio, as follows.

$$a_{Biota} = \frac{C_{Biota}}{S_{Biota}} \cdot F \quad (13)$$

## 2.3. Solid-phase Microextraction via EVA thin-film

Solid-phase microextraction (SPME) is a commonly used passive equilibrium-sampling method for quantifying chemical concentrations in environmental matrices. Compared to complex environmental media, the sorbent in SPME allows for simpler and more reproducible analyses. Moreover, the sorbent can be made negligible compared to the volume of the environmental matrix, ensuring that the sampling process is non-depletive. During SPME, chemicals equilibrate between the matrix and sorbent, allowing the concentration, fugacity, and chemical activity of the matrix to be determined through the sorbent. Partition coefficients between the sorbent and matrix can also be determined. Together, these properties can be used to predict the fate of chemicals in the environment and their bioavailability for uptake by organisms (Wilcockson and Gobas 2001, Mayer et al. 2003, Golding et al. 2008, Meloche et al. 2009).

The partition coefficient between the sorbent and matrix is determined by the concentrations of the chemical in the respective phases ($C_{Sorbent}$ and $C_{Matrix}$) at equilibrium. The partition coefficient also defines the relative solubilities of the chemical in the sorbent ($S_{Sorbent}$) and matrix ($S_{Matrix}$), as demonstrated in the following equation. The units of C and S can be selected for practicality, as long as they are consistent with each other.

$$K_{Sorbent-Matrix} = \frac{C_{Sorbent}}{C_{Matrix}} = \frac{S_{Sorbent}}{S_{Matrix}} \quad (14)$$

In this study, SPME will be conducted through thin-films of ethylene vinyl acetate (EVA). EVA thin-films will be used to 1) measure the freely dissolved PFOS in prepared matrices, 2) determine partition coefficients between EVA and matrices, and 3) to serve as a reference standard phase in the measurement of apparent chemical activities for PFOS. This partitioning matrices in this thesis will include pure water, phosphate buffered saline at pH 7.4 to mimic cellular conditions, and bovine serum albumin (BSA), which is commonly used as a surrogate protein for serum albumin in studies.

Serum albumin is one of many biological media that associates strongly with PFOS (Jones et al. 2003, Bischel et al. 2010, 2011), and is the most abundant protein in blood plasma, with concentrations ranging from 35 to 50 g/L. Serum albumin is found throughout the body, including the skin, muscle, liver, gut, and subcutaneous compartment (Peters 1996). Additionally, it also has the ability to bind a diversity of ligands, functioning as a transporter of fatty acids, bilirubin, heme, thyroid hormones, and drugs (He and Carter 1992, Peters 1996, Bhattacharya et al. 2000). Therefore, BSA is an appropriate model biological phase for PFOS in this study.

Compared to commercial SPME fibers, EVA offers a significantly higher surface-area-to-volume ratio up to approximately 2000 times. This enables rapid equilibration between the EVA thin-film and chemicals from the partitioning medium. EVA also exhibits high sorption for PFOS, whereas commercial SPME fibers made of polyacrylic or polydimethylsiloxane (PDMS) tend to show weaker sorption, resulting in lower and inconsistent sorption and desorption (Liu and Sun 2021, Figure B1).

Another advantage of using EVA in the form of a thin-film coating in this study is its ability to prevent potential glass-sorption of PFOS, which is not possible with dialysis equilibrium. Notably, when using dialysis, PFAS solutions are in direct contact with the test apparatus, which necessitate additional steps to account for those that are glass-sorbed (Allendorf et al. 2019, 2021; Ebert et al. 2020).

## 2.4. Chemical Activity-Based Approach

In light of the current challenges in the environmental risk assessment of PFOS, the concept of chemical activity holds great potential for improving the assessment process. Given the unique properties of PFOS that render traditional approaches difficult

to apply, the objective of this thesis is to develop and test a chemical activity-based risk assessment of PFOS. The EVA thin-film is used as a reference standard state to for the determination of the apparent chemical activity of PFOS through SPME. The approach provides a means to interpret PFOS concentration data from monitoring and toxicity studies. By presenting concentration data in chemical activities, they can be used in hazard quotients or in cumulative distributions, where all available data that would otherwise be excluded due to differences in units, quantities, and methodology can be considered together.

Accordingly, a comprehensive assessment of PFOS can be facilitated, encompassing factors such as surface water contamination, environmental guidelines, wildlife concentration, and the wealth of information from high throughput *in-vitro* toxicity assays.

# Chapter 3. Methods

## 3.1. General Methodology

To meet the objectives of this thesis in developing a chemical activity-based approach towards the environmental risk assessment on PFOS, the methodology was divided into several sections. The first step involved measuring the aqueous solubility of PFOS to calculate its apparent chemical activities in water. Next, the methodology of EVA thin-film SPME was established to determine the partition coefficient for EVA-solution ($K_{EVA-W}$ and $K_{EVA-PBS}$, unitless) and the sorptive capacity of EVA for PFOS ($S_{EVA}$, mg/L). EVA thin-film SPME was then used as a proxy for measuring PFOS chemical activities. The partition coefficient of BSA-water ($K_{BSA-W}$, unitless) was also determined through EVA partitioning, which in turn was used to determine the sorptive capacity of BSA for PFOS ($S_{BSA}$, mg/L). Finally, the chemical activity-based approach was applied to evaluate field data, toxicity references, and water guidelines for PFOS.

Section 2.2 outlines the reagents involved and the general steps taken to minimize PFOS-glass sorption and background contamination. Section 2.3 explains how the solubilities of PFOS in water and buffered saline were measured. Section 2.4 describes the preparation and application of the EVA-thin film, including partition experiments of PFOS from water to EVA. The sorptive capacity of EVA for PFOS was determined, which allows for the direct measurement of chemical activities of PFOS through EVA equilibration. This technique was relied on for the measurement of the sorptive capacity of bovine serum albumin for PFOS, where results from equilibration of PFOS in BSA to EVA were analyzed through chemical activity calculations as well as regression analyses. Section 2.5 demonstrates the application of chemical activity on the environmental risk assessment on PFOS at AFFF-affected study sites. This section covers background information on the study sites and details of field and toxicity data on PFOS. Methods for calculations of sorptive capacities of biological media and chemical activities of PFOS are also presented. Finally, PFOS data of various media, toxicity references, and guidelines were integrated and compared in terms of apparent chemical activities. Section 2.6 briefly describes the statistical methodologies, and Section 2.7 lists the details for analysis through Liquid Chromatography-Tandem Mass Spectrometry (LC MS/MS).

## 3.2. Chemicals

The neat chemical of PFOS (CAS 2795-39-3) used in this study was the Heptadecafluorooctanesulfonic acid potassium (PFOS-K) salt of ≥ 98.0 % purity from Sigma-Alrich (Product # 77282) with a molecular weight of 538.22 g/mol (Figure A2). Concentration differences between the anion and acid forms were assumed to be inconsequential, since the weight difference between the anion form (499.12 g/mol) and the acid form is minimal.

PFOS stock solutions were prepared directly in deionized water from the NANOpure ultrapure water system without pre-solvation in methanol. To mimic cellular conditions, a phosphate buffered saline (PBS) matrix with a pH of 7.4 was prepared at 30 mM. PBS was prepared by dissolving potassium phosphate dibasic ($K_2HPO_4$, VWR Analytical, BDH9266) and potassium dihydrogen phosphate ($KH_2PO_4$, Caledon Laboratories Ltd, 6660-1) in deionized water (Table A7). The pH of the solution was then adjusted with potassium hydroxide (KOH, Caledon Laboratories Ltd, 6160-1) while being closely monitored using a pH meter. With a 30 mM concentration of $K_2HPO_4$ and $KH_2PO_4$, the ionic strength of the solution was calculated to be 71.74 mM (Table A8).

Analytical standards from Wellington Laboratories were used for PFOS quantification by Liquid Chromatography with tandem Mass Spectrometry (LC MS/MS). The technical grade (TPFOS0220) of potassium perfluorooctanesulfonate, containing 68.3% of the linear isomer, was used to detect native PFOS. Sodium perfluoro-[$^{13}C_8$]octanesulfonate (M8PFOS0121) was used as the internal standard at a constant concentration in all samples being quantified by the LC MS/MS.

Mobile phases for the LC were prepared every two weeks using HPLC-grade water (Honeywell), HPLC-grade ammonium acetate (Sigma-Aldrich), and LC/MS-grade methanol (Honeywell). The LC mobile phase A was 20 mM ammonium acetate in water, whereas mobile phase B was methanol.

To avoid potential glass-sorption of PFOS, solutions containing PFOS were prepared and stored in polypropylene or high-density polyethylene vials, tubes, or bottles, whenever possible. Polypropylene autosampler vials and screw caps, sourced from Agilent Technologies (Part no. 5191-8150 and 5191-8151), were used for LC

MS/MS analysis. An exception was made for the methanol-based analytical standards, which were stored in glass vials in the freezer to minimize volatilization.

BSA was used as a biological medium with a high sorptive capacity for PFOS. Fatty-acid free, lyophilized powders of BSA from Sigma-Alrich (No. A3803) were prepared daily in 30 mM PBS at pH 7.4. The molecular weight of BSA is 66,430 g/mol.

Lastly, to avoid background contamination of PFOS, equipment or materials of polytetrafluoroethylene (PTFE) and aluminum foil were avoided. Instead, parafilm was used as an alternative for sealing purposes. Laboratory supplies, such as graduated cylinders, beakers, glass syringes, lab spatula, and glass pipettes were triply rinsed with LC/MS-grade methanol before use.

## 3.3. Measurement of Solubility of PFOS in Water and Phosphate Buffered Saline at pH 7.4

Solutions of PFOS in water were made in triplicate solutions at above the reported solubilities of PFOS in pure and salt water at approximately 0.02 g of PFOS-K salt per 25 mL of MS-grade water and approximately 0.002 g of PFOS-K salt per 25 mL of 30 mM PBS at pH 7.4. The solutions were capped and placed on a horizontal mixer roller at 60 rpm at room temperature (approximately 22.5 °C) for continuous mixing. A 21-day time course analysis was then conducted to monitor the time it took for PFOS to reach solubility in water and buffered saline at room temperature. The collected solubility data ($C_{Soln}$, mg/L) were plotted against time (t, day) and fitted to the model:

$$C_{Soln} = S_{Soln}\left(1 - e^{-kt}\right) \quad (15)$$

where $S_{Soln}$ (mg/L) is the aqueous solubility of PFOS in either water or buffered saline, and k ($day^{-1}$) is the rate constant.

The effect of temperature on the aqueous solubility of PFOS was also investigated. After determining the saturation time for PFOS in solution at room temperature, the aqueous solubility experiments were repeated at 12 °C and 37 °, as described earlier. The measurements were taken on days 3 and 7. The experimental temperatures at 12 °C and 37 °C were maintained by placing the solutions in a Grant OLS200 water bath. The orbital shaker was used for continuous mixing.

The effect of temperature on the solubility of PFOS in deionized water and PBS was investigated through scatterplots. As well, the Van't Hoff plot through the following the equation was examined.

$$\ln S_{Soln} = -\frac{\Delta H}{R} \cdot \frac{1}{T} + c \qquad (16)$$

Where $S_{Soln}$ (unitless) is the aqueous solubility, ΔH (J/mol) is the change in enthalpy of the solution, R ($J \cdot K^{-1} \cdot mol^{-1}$) is the ideal gas constant, T is temperature (K), and c is the intercept. A positive slope ($-\frac{\Delta H}{R}$) would indicate for an endothermic reaction, whereas a negative slope would indicate for an exothermic reaction.

Sampling of PFOS solutions in water and PBS began with centrifugation to separate the undissolved PFOS-K salt from the solution. Then, the top layer of the solution was sampled and diluted as needed through deionized water, PBS, and methanol until the expected concentrations fell within the calibration range of the LC MS/MS. After adjusting the sample matrix to 90% methanol, the diluted samples were injected onto LC MS/MS Quantified PFOS concentrations in matrices of 90% methanol obtained by the LC MS/MS were back calculated to determine the aqueous solubility of PFOS.

In addition, this study explored the relationship between pH and the concentration of PFOS in water and PBS. Stock solutions of PFOS-K were centrifuged to remove excess, undissolved salts. The solutions were then diluted to between 1 % and 70 % of the PFOS solubility in deionized water and in PBS at room temperature. These samples were divided into three 15 mL Nalgene vials for independent pH readings.

The pH electrode (Thermo Fisher, Orion™ 9156BNWP) with a refillable Ag/AgCl electrode solution (Thermo Fisher, No. 900011) was calibrated using pH standard solutions at pH 7 and 4 to at least a slope ($\frac{\Delta U}{\Delta pH}$) of 95 %—a good indication of the pH sensor at detecting electrode potential differences between the two standard pH's. Between pH readings, the pH electrode was rinsed with deionized water and gently blotted with a Kimwipe. To prevent PFOS contamination in dilute samples, the pH electrode was additionally immersed in deionized water for further removal of PFOS.

pH data were compiled and compared to concentrations of PFOS in water and PBS. Results are displayed in Appendix A.

## 3.4. EVA Thin-Film

### 3.4.1. Thin Film Preparation

In this study, two sizes of EVA thin-films were made to extract different concentrations of PFOS from incubation solutions (Table 2). To prepare for coating, EVA pellets (Elvax 40W, Dupont Chemical Co., Wilmington, DE, USA) were dissolved in dichloromethane. The resulting EVA solution was then added to a silane-treated vial using a Hamilton glass syringe. The vial was promptly capped and rolled horizontally to ensure even coating of the interior surface. The cap was then removed for the solution to evaporate, resulting in an EVA film thickness of 0.1 µm.

**Table 2. Details of the EVA thin-film preparation, including the incubation solution volume, type of vial, EVA thin-film volume, EVA solution concentration used for making the films, and EVA coating volume.**

| Partitioning PFOS concentration (mg/L) | ≤ 1 | > 1 |
|---|---|---|
| **Vial type** | Supelco, No. 27217 | Agilent, No. 5183-2072 |
| **Cap type** | Supelco, No. 27141* | Agilent, No. 5191-8151 |
| **EVA solution concentration (g/L)** | 1.38 | 3.21 |
| **EVA coating volume (µL)** | 100 | 25 |
| **EVA thin-film volume (mL)** | $1.43 \times 10^{-4}$ | $8.33 \times 10^{-5}$ |
| **Incubation volume (mL)** | 4.8 | 2 |

* A sheet of parafilm is used to seal incubation solution underneath the cap to prevent contact between the incubation solution and the PTFE material in the cap.

Solid-phase microextraction through use of commercial fibers of polyacrylate (Supelco, No. 57304) and polydimethylsiloxane (PDMS) (Supelco, No. 57308) was also attempted as alternatives to EVA thin-films. Prior to equilibrium partitioning, the SPME fiber and a magnetic stir bar were placed in methanol to desorb and eliminate background contaminants. After desorption, the SPME fiber was inserted into the incubation solution through a silicon-septum cap. The incubation solution was gently stirred on a magnetic stir plate. After equilibration, the SPME fiber was blotted with a Kimwipe and transferred to 90% methanol for PFOS extraction. The extraction was held for 15 minutes without stirring, following which the extract was quantified by LC MS/MS.

The fiber was analyzed at various time points throughout 120 minutes of equilibrium partitioning. Overall, both polyacrylate and PDMS commercial fibers showed inconsistent and low sorption of PFOS (Figure B1), hence the EVA thin-film was used for solid-phase microextraction in this study.

### 3.4.2. EVA-Thin Film Solid-Phase Microextraction

Incubation solutions with PFOS were added to EVA-coated vials and gently rotated on the roller at 60 rpm at room temperature. For vials with Supelco caps (No. 27141), a sheet of parafilm was applied before capping to prevent contact between the incubation solution and the PTFE material in the cap. Incubation was then stopped at various time intervals over the course of 120 minutes for EVA extraction to determine the time required for equilibration.

To extract PFOS from the EVA thin-film, the incubation solution was first removed using a Pasteur pipette. Any remaining droplets on the EVA thin-film were blotted away using tightly rolled-up Kimwipes. Subsequently, 90% methanol was added to the vial to extract PFOS from EVA. The vial was then rotated on the roller at 60 rpm for 10 minutes. Afterwards, the methanol extract was quantified by LC MS/MS. EVA extraction efficiency tests were conducted to ensure that PFOS was efficiently extracted into methanol from EVA (Figure B2).

To analyze the uptake of PFOS by EVA over time, the PFOS concentration in EVA ($C_{EVA}$, mg/L) was fitted to Equation (17), where $C_{Soln}$ (mg/L) is the PFOS concentration in the incubation solution, $k_2$ ($min^{-1}$) is the elimination rate constant of PFOS from EVA to the solution, and t is time (min). $k_1$* ($min^{-1}$) represents the product of $k_1 \cdot \frac{V_{Soln}}{V_{EVA}}$, where $k_1$ ($min^{-1}$) is the EVA uptake rate constant, $V_{Soln}$ (mL) is the volume of the solution, and $V_{EVA}$ (mL) is the volume of the EVA thin-film.

$$C_{EVA} = C_{Soln} \cdot \left(\frac{k_1^*}{k_2}\right) \cdot (1 - e^{-k_2 t}) \quad (17)$$

The time to reach 95% ($t_{95}$, min) of the theoretical maximum concentration of PFOS in EVA ($C_{EVA}$, mg/L) was determined as:

$$t_{0.95} = \frac{-\ln 0.05}{k_2} \quad (18)$$

### 3.4.3. Determination of Partition Coefficient for EVA-Water ($K_{EVA-W}$) and EVA-PBS ($K_{EVA-PBS}$)

To study the partitioning relationship of PFOS between EVA and water, as well as between EVA and the PBS solution, a series of experiments involving equilibrium partitioning between EVA thin-film and incubation solutions with various concentrations of PFOS were conducted.

At equilibrium, $C_{EVA}$ (mg/L) was obtained following the steps outlined in Section 3.4.2. $C_{EVA}$ (mg/L) was then used to adjust $C_W$ and $C_{PBS}$ (mg/L) to account for any loss of PFOS to EVA. Subsequently, the partition coefficients of PFOS between EVA-water ($K_{EVA-W}$, unitless) and EVA-PBS ($K_{EVA-PBS}$, unitless) were calculated by dividing $C_{EVA}$ (mg/L) by the mass-adjusted $C_W$ or $C_{PBS}$ (mg/L).

$$K_{EVA-W} = \frac{C_{EVA}}{C_W} \quad (19)$$

$$K_{EVA-PBS} = \frac{C_{EVA}}{C_{PBS}} \quad (20)$$

### 3.4.4. Determination of the Sorptive Capacity of EVA for PFOS

The sorptive capacity of EVA for PFOS ($S_{EVA}$, mg/L) is the maximum concentration of PFOS that can be dissolved in EVA. To determine $S_{EVA}$ (mg/L), a linear regression analysis was first performed to establish the relationship between $C_{EVA}$ (mg/L) and mass-adjusted $C_{Soln}$ (mg/L). Subsequently, $S_{EVA}$ (mg/L) was modeled based on the aqueous solubilities in water ($S_W$, mg/L) and PBS ($S_{PBS}$, mg/L).

### 3.4.5. Measurement of Apparent Chemical Activity of PFOS

EVA thin-film SPME has been applied to measure the fugacities of chlorobenzenes and polychlorinated biphenyls in biological tissues and contaminated sediment (Wilcockson and Gobas 2001, Otton 2004, Golding et al. 2008, Meloche et al. 2009). The same approach is applied to determine the apparent chemical activity of

PFOS in environmental matrices. Briefly, a medium of PFOS is let to equilibrate with EVA. Once the equilibrium is established, the chemical activities (a, unitless) of PFOS in EVA and the medium become equal:

$$a_{EVA} = a_{Medium} \tag{21}$$

Using Equation (21), the apparent chemical activity of PFOS in the medium at equilibrium can be determined by dividing the PFOS concentration in EVA ($C_{EVA}$, mg/L) by the sorptive capacity of EVA for PFOS ($S_{EVA}$, mg/L) and adjusted with the fugacity ratio (F, unitless).

$$a_{Medium} = a_{EVA} = \frac{C_{EVA}}{S_{EVA}} \cdot F \tag{22}$$

Based on the method described, the apparent chemical activities of PFOS in water and PBS were measured using EVA thin-film SPME. The same approach was applied to determine the apparent chemical activities of PFOS in solutions of BSA.

### 3.4.6. Measurement of the Sorptive Capacity of Bovine Serum Albumin for PFOS

#### *EVA Thin-Film Solid-Phase Microextraction*

EVA SPME was used to measure the apparent chemical activities of PFOS in solutions of BSA. To prepare the BSA solutions, BSA powders were dissolved in PBS at pH 7.4 and left overnight in the refrigerator. The solubilized BSA in PBS was then brought to room temperature and spiked with a stock PFOS solution. The resulting solution, containing PFOS and BSA, was then equilibrated with EVA thin-film at room temperature using the procedure outlined in Section 2.4.2.

The incubation solution encompassed a range of PFOS to BSA molar ratios (mol/mol) spanning from $10^{-5}$ to 100, covering $C_{Soln}$ ranging from $10^{-3}$ mg/L to 10 mg/L, and BSA concentrations ranging from 0.01 g/L to 50 g/L. A specific PFOS:BSA molar ratio of 0.02 mol/mol was tested to replicate the conditions used in dialysis equilibration by Allendorf et al. (2019).

The time to reach 95% ($t_{95}$, min) of the theoretical maximal PFOS concentration in EVA ($C_{EVA}$, mg/L) was determined using Equations (17) and (18).

### *Determination of the Sorptive Capacity of BSA for PFOS ($S_{BSA}$, mg/L)*

The apparent chemical activity of PFOS in the incubation solution of PFOS and BSA ($a_{Soln}$, unitless) was first measured by EVA SPME, as described in Equation (22). Subsequently, the sorptive capacity of the incubation solution for PFOS ($S_{Soln}$, mg/L) was calculated using Equation (7), where the mass-adjusted $C_{Soln}$ or $C_{PBS}$ (mg/L) was divided by the apparent chemical activity of PFOS in BSA solution ($a_{Soln}$, unitless):

$$S_{Soln} = \frac{C_{Soln}}{a_{Soln}} \tag{23}$$

The sorptive capacity of the incubation solution for PFOS ($S_{Soln}$, mg/L) can then be broken down into the individual sorptive capacities of PBS and BSA for PFOS ($S_{PBS}$ and $S_{BSA}$, mg/L), adjusted by their mass fractions ($\phi_{PBS}$ *and* $\phi_{BSA}$, L/L), similar to Equation (12):

$$S_{Soln} = (S_{PBS} \cdot \phi_{PBS}) + (S_{BSA} \cdot \phi_{BSA}) \tag{24}$$

Following Equation (24), the sorptive capacity of BSA for PFOS ($S_{BSA}$, mg/L) can be calculated as:

$$S_{BSA} = \frac{S_{Soln} - (S_{PBS} \cdot \phi_{PBS})}{\phi_{BSA}} \tag{25}$$

### *Determination of the Partition Coefficient for BSA-Solution ($K_{BSA\text{-}PBS}$)*

Using the sorptive capacity of BSA for PFOS ($S_{BSA}$, mg/L), the BSA-solution partition coefficient for PFOS ($K_{BSA\text{-}PBS}$, unitless) can then be calculated as:

$$K_{BSA-PBS} = \frac{S_{BSA}}{S_{PBS}} \tag{26}$$

## 3.5. Illustration of Chemical Activity-based Assessment of PFOS

### 3.5.1. Field Site Description

Field data were collected from two US DoD installations at Barksdale Air Force Base (BAFB) and Wurtsmith Air Force Base (WAFB) between 2010 and 2014. BAFB,

located in northwest Louisiana, covers over 22,000 acres of land and currently serves as an active site for fire training involving AFFF. The base includes bodies of freshwater such as rivers and lakes (Salice et al. 2018). Surface water samples from BAFB revealed the presence of PFOS, ranging from 0.01 to 7.07 ng/mL (n = 50). Additionally, several fish species such as bass, sunfish, gambusia, carps, minnows, and catfish were found to contain PFOS at levels varying from 134 to 9,349 ng/g dry weight (n = 25).

WAFB is a decommissioned site located in northeastern Michigan within the coastal zone of Lake Huron. The base covers 5,223 acres and is surrounded by forests, lakes, and recreational properties such as campgrounds. For over four decades, WAFB conducted fire-fighting procedures as part of military training until its decommissioning in 1993. WAFB also consisted of two landfills, receiving wastes from base activities as well as domestic sources. In 1994, due to the detection of extensive contamination of heavy metals, volatile organic compounds, polycyclic aromatic hydrocarbons, and PFAS, WAFB was listed as a Superfund site (Former WAFB 2013). Notably, PFOS was found in surface water at concentrations ranging from $3.4 \times 10^{-5}$ to 7.4 ng/mL (n = 8). In fish, with freshwater species similar to those found at BAFB, PFOS levels were detected from 1 to 73,200 ng/g (n = 36). Additionally, PFOS was detected in tree swallow eggs at 1,220 ng/g (n = 1) and plasma at 1,840 ng/g (n = 1) (Moody et al. 2003).

### 3.5.2. PFOS Toxicity Data

Available toxicity data for PFOS in fish and birds were compiled (see Supplementary Information). These include a range of biological effects observed *in vivo* at lowest-observed-effect-levels (LOEL), no-observed-effect-levels (NOEL), median effective concentrations (EC50), and *in vitro* at concentrations where 50% of maximum activity was observed (AC50). The AC50 data in particular were obtained from high-throughput bioactivity tests, which involved a diversity of cellular responses and biomolecular activities, sourced from the US EPA Toxicity Forecaster (US EPA 2022b).

In fish, toxic effects were observed at external water concentrations ranging from 230 ng/mL to 113,000 ng/mL for EC50 (n = 12) and 3.1 ng/mL to 16,000 ng/mL (n = 7) for NOEL. The tests were conducted at temperatures between 25 °C to 28 °C, and the observed effects were changes in growth, reproduction, physiology, development, and behaviour. The AC50s (n = 16) were measured at concentrations from 273 ng/mL to

21,170 ng/mL, the observed effects at these concentrations included changes in embryo morphogenesis and teratoma formation. Temperatures for fish AC50s were assumed to be 21 °C, as temperature details were not reported.

In birds, toxic effects were observed at concentrations of 17,000 ng/mL to 140,000 ng/mL for NOELs (n = 35) and 8,700 ng/mL to 200,000 ng/mL for LOELs (n = 8). The effects encompass changes on reproduction, physiology, and mortality. A temperature of 40 °C was assumed for these effects, as they were measured *in vivo*.

### 3.5.3. Apparent Chemical Activity Calculations

The apparent chemical activities (unitless) of PFOS in various environmental media were calculated based on the physical-chemical properties of PFOS and methods provided in Tables 3 and 4. In general, apparent chemical activities of PFOS were estimated using Equation (7). The sorptive capacity of water ($S_w$, mg/L) and buffered solution ($S_{PBS}$, mg/L) for PFOS were based on measured values from this study. The sorptive capacities of fish ($S_{Fish}$, mol/m$^3$), egg ($S_{Egg}$, mol/m$^3$), and plasma ($S_{Plasma}$, mol/m$^3$) for PFOS were estimated by summing the sorptive capacities of transporter proteins ($S_{TP}$, mol/m$^3$), polar lipids ($S_{PL}$, mol/m$^3$), structural proteins ($S_{SP}$, mol/m$^3$), neutral lipids ($S_{NL}$, mol/m$^3$), and buffered water ($S_{PBS}$, mol/m$^3$), adjusted with their respective volume fractions. The sorptive capacities of these biological components were calculated from the partition and distribution coefficients of PFOS between the respective phases to water obtained from the literature (Droge 2019, Ebert et al. 2020, Allendorf et al. 2021) through multiplying $S_{PBS}$ (mol/m$^3$).

**Table 3. Physical-chemical properties and methods for the calculation of the apparent chemical activity and sorptive capacities (S, mol/m$_3$) of various biological media for PFOS**

| Symbol | Description | Value | Units |
|---|---|---|---|
| MW | Molecular weight | 499.1[a] | g/mol |
| $S_W$ | Solubility of PFOS in pure water | 664.3[b] | mg/L |
| $S_{PBS}$ | Solubility of PFOS in phosphate buffered saline at pH 7.4 | 44.1[c] | mg/L |
| $S_{PBS}$ | $S_{PBS}$ (mol/m$^3$) = $S_{PBS}$ (mg/L)÷ MW (g/mol) × $d_{PBS}$ (kg/L)[d] | 0.088 | mol/m$^3$ |
| MP | Melting point | 185[e] | °C |
| $d_{TP}$ | Density of transporter protein | 0.9 | kg/L |
| $d_{PL}$ | Density of polar lipid | 0.9 | kg/L |

| | | | |
|---|---|---|---|
| $d_{SP}$ | Density of structural protein | 0.9 | kg/L |
| $d_{NL}$ | Density of neutral lipid | 0.9 | kg/L |
| $K_{BSA-W}$ | Partition coefficient of BSA-water | $10^{4.67f}$ | unitless |
| $K_{PL-W}$ | Partition coefficient of polar lipid-water | $10^{4.89g}$ | unitless |
| $D_{SP-W}$ | Distribution coefficient of structural protein-water | $10^{2.94h}$ | unitless |
| $D_{NL-W}$ | Distribution coefficient of neutral lipid-water | $10^{-0.56h}$ | unitless |
| $S_{TP}$ | Sorptive capacity of transporter protein<br>$S_{TP} = K_{BSA-W} \times S_{PBS} \times d_{TP}$ | 3719.4 | mol/m$^3$ |
| $S_{PL}$ | Sorptive capacity of polar lipid<br>$S_{PL} = K_{PL-W} \times S_{PBS} \times d_{PL}$ | 6032.2 | mol/m$^3$ |
| $S_{SP}$ | Sorptive capacity of structural protein<br>$S_{SP} = D_{SP-W} \times S_{PBS} \times d_{SP}$ | 69.3 | mol/m$^3$ |
| $S_{NL}$ | Sorptive capacity of neutral lipid<br>$S_{NL} = D_{NL-W} \times S_{PBS} \times d_{NL}$ | 0.022 | mol/m$^3$ |
| $S_{Fish}{}^{i}$ | $S_{Fish} = (S_{TP} \times 0.05) + (S_{PL} \times 0.01) + (S_{SP} \times 0.12) + (S_{NL} \times 0.04) + (S_{PBS} \times 0.78)$ | 254.7 | mol/m$^3$ |
| $S_{Egg}{}^{i}$ | $S_{Egg} = (S_{TP} \times 0.15) + (S_{PL} \times 0.01) + (S_{NL} \times 0.02) + (S_{PBS} \times 0.82)$ | 618.3 | mol/m$^3$ |
| $S_{Plasma}{}^{i}$ | $S_{Plasma} = (S_{TP} \times 0.056) + (S_{PL} \times 0.008) + (S_{NL} \times 0.013) + (S_{PBS} \times 0.923)$ | 256.6 | mol/m$^3$ |

[a] Based on the ionic form
[b] Obtained from this study
[c] Obtained from this study
[d] Density ($d_{PBS}$) = 1 kg/L
[e] Based on the ionic form, obtained from US EPA CompTox
[f] Obtained from Allendorf et al. 2019
[g] Obtained from Droge 2019, Ebert et al. 2020
[h] Obtained from Allendorf et al. 2021
[i] See Equation (12)

**Table 4. Equations for the calculation of the chemical activity of PFOS (a, unitless) in environmental media**

| Medium | Activity (unitless) |
|---|---|
| Surface water, water guideline | $a = \frac{C_W}{S_W} \cdot F$ |
| Fish | $a = \frac{C_{Fish}}{S_{Fish}} \cdot F$ |
| Bird egg | $a = \frac{C_{Egg}}{S_{Egg}} \cdot F$ |
| Bird plasma | $a = \frac{C_{Plasma}}{S_{Plasma}} \cdot F$ |

The fugacity ratio (F) was calculated via Equation (2). Refer to Section 2.5.3 for temperature conditions.

It is important to note that several assumptions were made in the calculation of apparent chemical activities. Firstly, it was assumed that the surface water in the study sites had minimal levels of ions and organic matter, such that the sorptive capacity of surface water for PFOS was approximately that of pure water. The temperatures for surface water and fish were assumed to be 12 °C, while a temperature of 40 °C was assumed for birds. In the case of fish data obtained from AC50 tests, a temperature of 21 °C was assumed due to the absence of specific temperature details in the report. For fish data derived from EC50 and NOEL tests, the temperatures ranging from 25 °C to 28 °C were used, as reported in the studies (See Supplementary Information). In most cases, the calculation of apparent chemical activity was based on the maximum reported concentrations; however, average concentrations were used when they were the only available data. Lastly, in cases where concentrations were below the detection limit, they were assigned as one-half of the reported detection limit.

### 3.5.4. Risk Assessment of PFOS Levels on AFFF-Impacted Sites

Reported levels of PFOS in surface waters, fishes, and birds from BAFB and WAFB were compared in concentrations and apparent chemical activities. To further analyze the findings, the apparent chemical activities of PFOS from BAFB and WAFB were assessed in relation to toxicity concentrations and drinking water guidelines using cumulative probabilities. This approach allowed for the comparison of different media types and the evaluation of the likelihood of these media being associated with specific toxicity effects.

## 3.6. Statistical Analyses

Linear regressions were conducted in Excel, whereas multiple linear regression and non-parametric Kruskal-Wallis tests, followed by multiple comparison analysis, were performed using R Statistical Software (version 1.1.383). Three-dimensional analyses were carried out using the “scatterplot3d” function in R. Logarithmic transformations of the data were performed using the base 10 logarithm.

## 3.7. Liquid Chromatography-Tandem Mass Spectrometry (LC MS/MS)

The calibration standards for LC MS/MS for every sample run were prepared with standard PFOS of technical grade at concentrations of 0, 5, 10, 50, 100, and 200 ng/mL. PFOS samples to be analyzed by LC MS/MS were diluted as needed to bring the expected PFOS concentration into the range of the calibration standards and prepared to a matrix of 90% methanol in water.

Every sample was fortified with isotopically labeled analogue of PFOS (Sodium perfluoro-[$^{13}C_8$]octanesulfonate) as the internal standard at 20 ng/mL and prepared to a total volume of 1 mL. The samples were then analyzed on a Shimadzu liquid chromatographic system (LC-20AD) coupled to a triple quadruple mass spectrometer (Sciex QTRAP 4000 MS/MS System). The interface was a Turbo Ion spray source operating under the electrospray ionization (ESI) mode. PFOS was optimized for MS via standard solutions from Wellington Laboratories (TPFOS0220 and M8PFOS0121) by direct infusion. The column used in the LC was the Phenomenex Gemini LC column at 3 µm C18 110 Å and 50 × 2 mm. The guard column of SecurityGuard Gemini C18 was applied additionally. Details on chromatographic separation and detection of PFOS are provided in Table C1.

To minimize the background signals of PFOS on LC MS/MS, 90 % methanol in water was injected prior to sample analysis. The injections were repeated until the signal was below a peak height of 2000 cps. Then, calibration standards of PFOS in 90% methanol were injected, followed by the samples. Quality controls were conducted every five samples, using a concentration of 10 ng/mL of PFOS in 90% methanol. After the completion of sample injections, a 50-minute long wash method using 100% methanol was run to flush out the LC column. The resulting chromatograms were integrated with the SciexOS Software and exported to Excel for calculations, where the concentration of PFOS in each sample was determined using the response ratio of PFOS and the internal standard. Blank averages in the sample run were used to correct samples for background signals. The average detection limit for PFOS was less than 1.25 ng/mL (n = 31), see Table C2 for further information on study detection limits.

# Chapter 4. Results and Discussion

## 4.1. Solubility of PFOS in Water and Phosphate Buffered Saline at pH 7.4 at Room Temperature

Given that the estimated p$K_a$ values for PFOS (Table A6) are much lower than the pH of both water at a pH of 6 and PBS at a pH of 7.4, the solubilities reported in this study are presumed to be representative of the ionized form of PFOS.

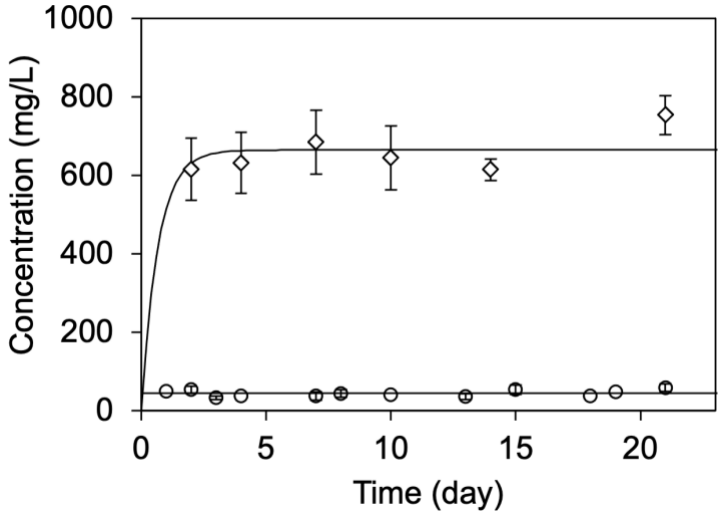


**Figure 1. Concentration (mg/L) of PFOS in MS-grade water (diamonds) and 30mM phosphate buffered saline at pH 7.4 (circles) over time (day) at room temperature of 22.5°C. Errors bars are standard deviations.**

Figure 1 shows the time course of PFOS concentration in MS-grade water at pH 6 (n = 3) and PBS at pH 7.4 (n = 6) at room temperature. Under continuous mixing, saturation of PFOS in water was achieved after approximately 3 days at 664.3 mg/L (SD = 53.7 mg/L). In contrast, saturation of PFOS in PBS was reached on the first day after preparation at 44.1 mg/L (SD = 9.1 mg/L). Throughout the dissolution time course, no foaming was observed in either water or PBS, contrary to the expected behaviour for surfactants. However, the Tyndall effect was observed when the saturated solutions of PFOS were vigorously mixed. Additionally, several PFOS-K salt flakes, measuring less than 3 mm, were observed remaining in both water and PBS even after the solutions have reached saturation. For this reason, the saturated solutions were filtered by centrifugation prior to sampling.

Compared to the nominal concentrations of PFOS in water (mean = 888.6 mg/L, SD = 1.1 mg/L) and PBS (mean = 836.7 mg/L, SD = 115.9 mg/L), the measured saturation levels were lower. This difference between nominal and measured PFOS concentration is also observed by Rewerts and Colleagues (2021), who reported up to 30% difference. Additionally, the authors also noted the lack of foaming during the dissolution of PFOS-K in water.

Compared to the aqueous solubilities reported in the literature for PFOS-K and PFOS-Li salts based on experimental measurements, the measured aqueous solubility of PFOS in this thesis falls within a similar range (Table A1). The similarity in the aqueous solubilities among different PFOS salts suggests that the counter-ions (i.e., $K^+$ or $Li^+$) do not contribute significantly to the saturation of PFOS in solution. Together, the consistent reported values and observations across various PFOS salts and studies indicate that PFOS can achieve a stable equilibrium-based aqueous solubility and that the aqueous solubility of PFOS can be determined in a reproducible manner.

For saturation experiments of PFOS in deionized water (n=3) and PBS (n=3) conducted at 12 °C and 37 °C, a non-parametric Kruskal-Wallis test showed no significant differences between the saturation levels measured at temperatures ranging from 2 °C to 37 °C (Table D1). Based on these results, when averaged across all temperatures, the aqueous solubility was determined to be 502.2 mg/L (SD = 73.7 mg/L) for PFOS in water and 31.9 mg/L (SD = 11.1 mg/L) for PFOS in PBS.

The lack of apparent temperature influence on the solubility of PFOS in water and PBS can be attributed to the limited statistical power to detect potentially small differences in solubility of PFOS in aqueous solutions. The noise in data may be due to the chemical-physical properties of PFOS, which can cause emulsion or micro-crystal suspensions at high concentrations as well as sorption to the solution-container interface, potentially creating a heterogeneous distribution of PFOS in the solution. Thus, increasing the sample size and expanding the temperature range may improve the study's statistical power and help detect any effects related to temperature.

Further analysis using the Van't Hoff equation, as illustrated in Figure 2, was also unable to identify any statistical correlation between temperature (x-axis, K) and the solubility of PFOS (y-axis, natural logarithm of $mol/m^3$) in water ($R^2 = 0.12$, $F(1,16) =$

2.19, p-value = 0.159) and PBS ($R^2$ = 0.059, F(1,13) = 0.81, p-value = 0.384). Nevertheless, the dashed lines in Figure 2 show some evidence of an increase in the aqueous solubility with higher temperatures, the relationship for PFOS in water can be described with standard error as:

$$\ln S_{Soln} = (-392.6 \pm 265.4) \cdot \frac{1}{T} + (1.35 \pm 0.9) \quad (27)$$

and the relationship for PFOS in PBS can be described with standard error as:

$$\ln S_{Soln} = (-790.8 \pm 877.9) \cdot \frac{1}{T} - (0.16 \pm 2.9) \quad (28)$$

The lack of statistical insignificance in the slopes suggests that the temperature dependence was likely too small to be detected given the experimental errors.

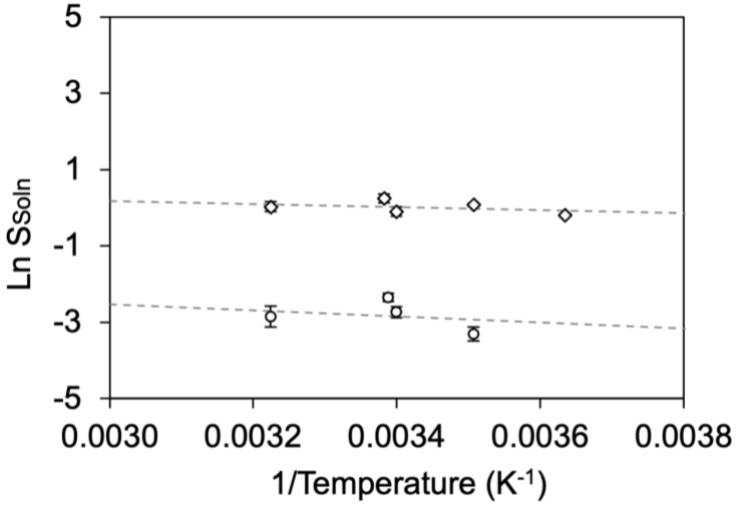


**Figure 2. Van't Hoff plot for PFOS in deionized water (diamonds) and 30mM phosphate buffered saline at pH 7.4 (circles). Dash lines indicate slopes that were found statistically insignificant. Error bars are standard deviations.**

In general, the aqueous solubility of PFOS was found to be much lower in PBS than in pure water. This difference in solubility can be explained by the difference in ionic strength between the two solutions (Mackay 2001). Specifically, the ionic strength of the 30 mM PBS was 71.74 mM, while the ionic strength of water was considered negligible. In PBS, the presence of ions can lead to ion pairing and complex ion formation, thereby interfering with the solvation of PFOS by displacing water molecules from PFOS. Consequently, PFOS becomes less soluble in the presence of buffer ions, leading to a

lower solubility when dissolved in saline or ionized solutions. In contrast, in pure water where ions are highly diluted, PFOS is readily solvated, resulting in a higher solubility in solution.

Additional PFOS saturation experiments were conducted in PBS at pH 7.8 to compare the effect of pH on the solubility of PFOS. The results showed no significant difference in the solubility of PFOS between experiments conducted at pH 7.4 and pH 7.8 (Figure B4), suggesting that the solubility of PFOS in solution may be more influenced by the ionic strength than pH. These findings are consistent with previous studies that have reported lower solubility of PFOS in saline matrices, such as in 3.5 % NaCl solution with an ionic strength of 0.60 M, where the solubility of PFOS was recorded at 20 mg/L, and in seawater with an assumed ionic strength of 0.70 M, where the solubility was found to be even lower at 12.4 mg/L (OECD 2002). Thus, the solubility of PFOS in solution may be appreciably reduced in the presence of ions.

Overall, the aqueous solubility measurements of PFOS obtained in this study are consistent with the range of values reported in the literature (Table A1). The observed variance in aqueous solubilities of PFOS in this study may be attributed to the unique perfluorinated moiety and properties of PFOS. As Table A1 illustrates, the predicted solubilities for PFOS vary widely across different modeling efforts. A study by Lampic and Parnis (2020) also reported a deviation up to 4 logarithmic units at 6.65 log units (mg/L) for the PFOS solubility predicted by COSMOtherm. In contrast, the authors found that the predictions for other perfluorinated compounds such as PFOA, 8:2 Fluorotelomer unsaturated acid (8:2 FTUCA), and long-chained precursors to carboxylic acids showed much lower variance. Given the challenges and uncertainty associated with predicting PFOS solubilities using computational techniques, experimental-based measurements through PFOS salts provide a more reliable foundation for evaluating the properties of PFOS.

Future research could include a larger sample size, a wider range of temperatures, different PFOS salts, and alternative methodologies such as the generator column to help gain a more comprehensive understanding of how factors such as temperature as well as its counter ion may affect the solubility of PFOS in water.

For the purpose of demonstrating the application of chemical activity on PFOS, the solubilities at room temperature, which were measured as 664.3 mg/L in water and 44.1 mg/L in PBS will be used in this thesis.

## 4.2. EVA Thin-Film Non-Depletive Rapid Extraction

### 4.2.1. Equilibrium Partitioning of PFOS into EVA

Equilibrium partitioning of PFOS between the water phase ($C_W$, mg/L) and EVA ($C_{EVA}$, mg/L) was achieved within 10 minutes, as indicated by Equation (14). The air phase was omitted (Appendix B). The concentration of PFOS in the water phase was not found to be depleted by EVA throughout the equilibration process. This is evident from Figure 3 and a linear regression analysis that found no differences in $C_W$ over time (p-value = 0.16). The transfer of PFOS towards EVA occurred rapidly with estimated mass-transfer rate constant $k_1$ (water to EVA) of $7.60 \times 10^{-4}$ $min^{-1}$ and $k_2$ (EVA to water) of $3.54 \times 10^{-1}$ $min^{-1}$. The time required to reach 95% equilibrium concentration ($t_{0.95}$) in the film was determined to be 8.44 minutes. PFOS extraction into 90% MeOH was found to be at least 97.9%, as illustrated in Figure B2.

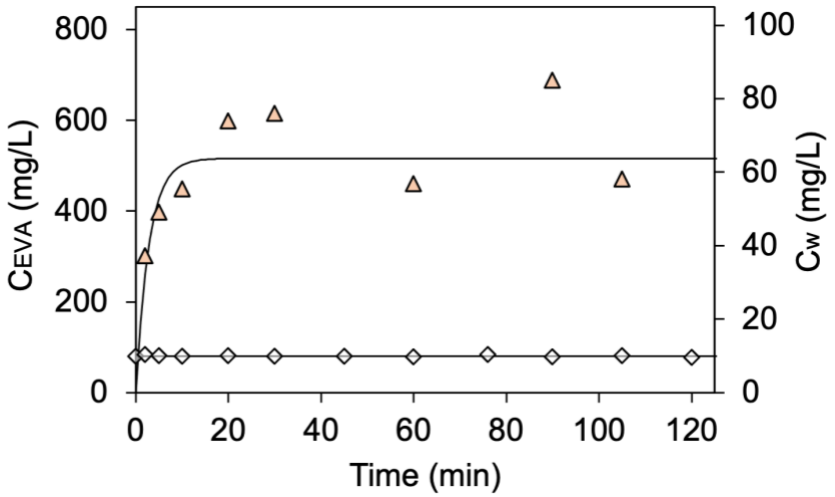


**Figure 3. Equilibration of PFOS from water ($C_W$ at 10 mg/L; diamonds) into EVA thin-film ($C_{EVA}$, mg/L; triangles).**

The relationship between PFOS in EVA ($C_{EVA}$, mg/L) and the incubation solution ($C_W$ and $C_{PBS}$, mg/L) was analyzed using the Freundlich isotherm (Figure 4), which is a suitable model for describing the partitioning behaviour of PFOS. The Freundlich model has been used to describe non-ideal adsorption processes. The model does not impose

fixed assumptions on the number of sorption sites or layer for the sorbent, and it also accomodates interactions between the sorbing molecules (Freundlich 1926). To determine the isotherm, linear regression of $C_{EVA}$ and $C_{Soln}$ was calculated on logarithmic scale. The linear equation between $C_{EVA}$ (mg/L) and $C_W$ (mg/L) was estimated with standard error as ($R^2$ = 0.99, F(1, 38) = 2537, p-value < 0.001):

$$\log C_{EVA} = (0.7258 \pm 0.01) \cdot \log C_W + (1.9158 \pm 0.03) \quad (29)$$

Similarly, the relationship between $C_{EVA}$ (mg/L) and $C_{PBS}$ (mg/L) was ($R^2$ = 0.98, F(1, 34) = 1635, p-value < 0.001):

$$\log C_{EVA} = (0.7836 \pm 0.02) \cdot \log C_{PBS} + (2.7416 \pm 0.03) \quad (30)$$

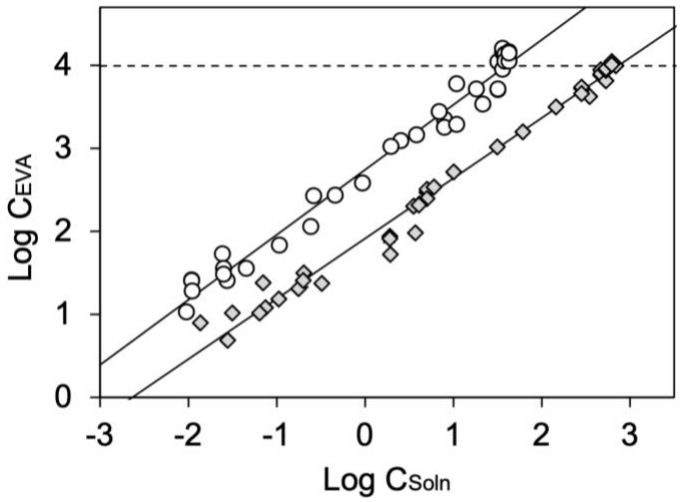


**Figure 4. The concentration of PFOS in EVA ($C_{EVA}$, mg/L) relative to the concentration of PFOS in incubation solution ($C_{Soln}$, mg/L) on logarithmic scale. Circles = PFOS in 30mM phosphte buffered saline at pH 7.4. Diamonds = PFOS in water. Dashed horizontal line indicates the sorptive capacity of EVA for PFOS at $10^{3.997}$.**

The slopes of the Freundlich equations are typically less than 1, reflecting diminishing adsorption as the concentration of the sorbing molecules increases (Freundlich 1926). In this thesis, both slopes in the above equations suggest that the sorption sites of EVA were becoming saturated with increasing PFOS concentrations in the incubation solution. This indicates that as the number of adsorption sites become occupied, EVA adsorption decreases. It is worth noting that if the relationships were strictly linear (i.e., slopes = 1), it would suggest an absorption process, whereas if the

slopes had been larger than 1, it would suggest that PFOS had formed into micelles, turning itself into a sorbing phase.

### 4.2.2. Determination of the Partition Coefficient of PFOS between EVA and Water ($K_{EVA-W}$) and EVA and PBS ($K_{EVA-PBS}$)

Consistent with the findings in Section 4.2.1., where the calculated Freundlich slopes calculated for the partitioning of PFOS between the incubation solution ($C_W$ and $C_{PBS}$, mg/L) and EVA indicate a saturating effect on EVA with increasing $C_{Soln}$, this saturation effect is also reflected in the partition coefficients of PFOS between EVA and water ($K_{EVA-W}$, unitless) and EVA and PBS ($K_{EVA-PBS}$, unitless).

$K_{EVA-W}$ (unitless) and $K_{EVA-PBS}$ (unitless) were found highest at low concentrations of PFOS in the incubation solution, and vice versa. When comparing at the same $C_{Soln}$, $K_{EVA-W}$ (unitless) values were also found approximately 10 times lower than $K_{EVA-PBS}$ (unitless). In Tables F1 and F2, $K_{EVA-W}$ (unitless) decreased from 568 to 14 as the PFOS concentrations in water ranged from 0.014 mg/L to 685 mg/L, whereas $K_{EVA-PBS}$ (unitless) decreased from approximately 1700 to 300 for PFOS concentrations in PBS from 0.010 mg/L to 43 mg/L. These results indicate a reduction in the PFOS-adsorption process on EVA as the concentration of PFOS in the incubation solution increases.

The lowering of $K_{EVA-W}$ (unitless) and $K_{EVA-PBS}$ (unitless) with increasing $C_{Soln}$ can also be attributed to the high surface activity of PFOS. As $C_{Soln}$ increases, PFOS molecules become more likely to aggregate at the air-solution or EVA-solution interfaces, thereby hindering or interfering with the partitioning process of PFOS into EVA. Additionally, PFOS molecules can assemble into micelles or self-interact in the bulk solution, further reducing the partition rate into EVA. These surfactant effects may become more pronounced at higher PFOS concentrations, leading to a greater decrease in $K_{EVA-Soln}$.

Lastly, the difference in $K_{EVA-W}$ and $K_{EVA-PBS}$ could potentially be explained by the solution composition. As previously discussed, PBS contains buffer ions that decrease the aqueous solubility of PFOS. This reduction in solubility may result in an increased partitioning of PFOS from the solution into EVA. Another possible explanation is the occurrence of ion paring between buffer ions and PFOS, which could neutralize PFOS, thereby facilitating its partitioning into EVA compared to the negatively charged PFOS in

pure water. Therefore, the partitioning of PFOS into EVA varies depending on the concentration of PFOS in the solution and the composition of the solution.

### 4.2.3. Determination of the Sorptive Capacity of EVA for PFOS

In Figure 5, it can be observed that despite the 10-fold difference in the maximum solubility of PFOS in water and PBS, their $C_{EVA}$ (mg/L) from equilibrium partitioning were approximately equal. Therefore, the sorptive capacity of EVA for PFOS ($S_{EVA}$, mg/L) was estimated through the linear regression of $C_{EVA}$ (mg/L) and $C_{Soln}$ (mg/L) as described in Section 4.2.1.

Based on $S_W$ (mg/L) at 664.3, the estimated $S_{EVA-W}$ was $10^{3.96}$ mg/L or $10^{4.03}$ mg/L when $S_{PBS}$ (mg/L) at 44.1 was applied. A geometric mean was calculated between $S_{EVA-W}$ and $S_{EVA-PBS}$ to finalize $S_{EVA}$, which was determined to be $10^{3.99}$ mg/L or 9934 mg/L.

It is important to note that $S_{EVA}$ (mg/L) may not be applicable to the entire range of $C_{Soln}$ (mg/L) due to the varying nature of EVA-solution adsorption and partition coefficient ($K_{EVA-W}$ and $K_{EVA-PBS}$) as aforementioned in Section 4.2.2.

### 4.2.4. Measurement of Apparent Chemical Activity of PFOS

Using EVA as a reference phase, the apparent chemical activities of PFOS in the incubation solution were determined by dividing the PFOS concentrations of EVA ($C_{EVA}$, mg/L) by $S_{EVA}$ (mg/L) and adjusted with the fugacity ratio. The results show that the EVA-measured apparent chemical activities of PFOS in PBS were approximately 10 times higher than those in water. As Figure 5 illustrates, the maximum apparent chemical activity of PFOS in solution was achieved at a lower concentration of PFOS in PBS compared to that in water. This suggests that at the same concentration, PFOS exhibits a higher chemical potential in ion-buffered solutions than that in pure water, indicating that PFOS may be more bioavailable in ionized or cellular conditions than when present in pure water. This finding highlights the significance of accounting for solution composition and ionic strength when conducting environmental risk assessments, as they play a crucial role in the chemical fate and potentials risks associated with PFOS.

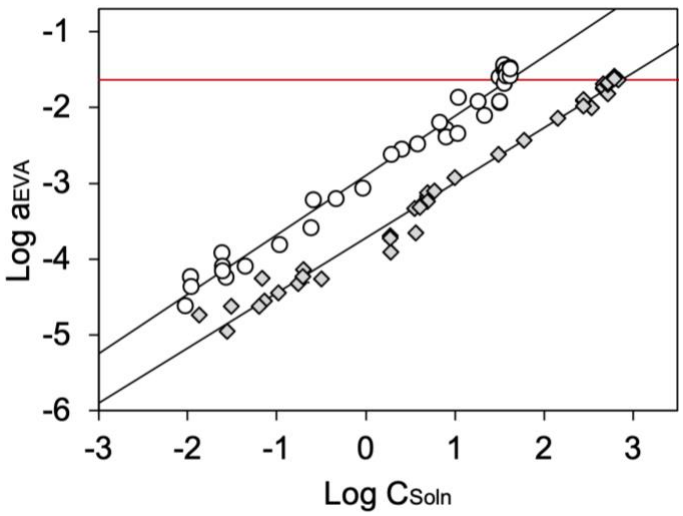


**Figure 5.** **The apparent chemical activity of PFOS in incubation solution ($a_{Soln}$ = $a_{EVA}$ = $C_{EVA} \cdot F \div S_{EVA}$, unitless) relative to the concentration of PFOS in incubation solution ($C_{Soln}$, mg/L) on logarithmic scale. Circles = PFOS in 30mM phosphte buffered saline at pH 7.4. Diamonds = PFOS in water. Red horizontal line indicates the maximum apparent chemical activity (F = 0.023).**

As aforementioned in Sections 4.2.2 and 4.2.3., the varying sorption behaviour of EVA with changing $C_{Soln}$ challenges the use of $S_{EVA}$ for calculating the apparent chemical activity for solutions at low $C_{Soln}$. To address this, a meter to estimate the incubation solution's apparent chemical activity was developed by calibrating the apparent chemical activity using water and PBS solutions with $C_{EVA}$ (Figure 6). The apparent chemical activity of the solutions was calculated by dividing the concentration of PFOS of the incubation solution by its sorptive capacity (i.e., $a_W = C_W \cdot F \div S_W$ ). $C_{EVA}$ was measured from equilibrium partitioning with the solutions. The relationship between the apparent chemical activity of the solutions and $C_{EVA}$ was then analysed through a power regression analysis, where the equation was estimated with standard error as follows ($R^2$ = 0.98, F(1, 74) = 3991, p-value < 0.001):

$$a_{Soln} = 10^{(1.3105 \pm 0.02) \cdot \log C_{EVA} - (6.9058 \pm 0.06)} \quad (31)$$

The apparent chemical activity of PFOS evaluated using the power function (Equation (31)) was subsequently compared to the calculated apparent chemical activity obtained through EVA (i.e., $a_W = a_{EVA} = C_{EVA} \cdot F \div S_{EVA}$). As shown in Figure 7, the activities of PFOS in the incubation solutions calculated using $S_{EVA}$ (mg/L) deviated up to 10-fold from those analyzed using the power function. The discrepancy was particularly

evident at the lower $C_{Soln}$ ranges, reflecting the relative drop in the sorptive capacity of EVA for PFOS with increasing $C_{Soln}$. Considering the $C_{Soln}$-dependent sorptive capacity of EVA, Equation (31) should be relied on for the estimation of apparent chemical activities of PFOS in the incubation media.

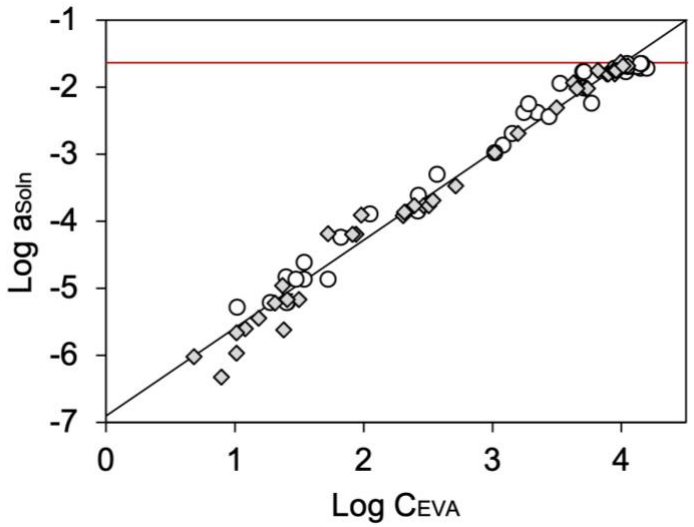


**Figure 6.** **Meter of apparent chemical activity of PFOS in incubation solution ($a_{Soln}$, unitless) based on equilibrated concentration of PFOS in EVA ($C_{EVA}$, mg/L), displayed on logarithmic scale. Circles = PFOS in 30mM phosphte buffered saline at pH 7.4. Diamonds = PFOS in water. Red horizontal line indicates the maximum apparent chemical activity (F = 0.023).**

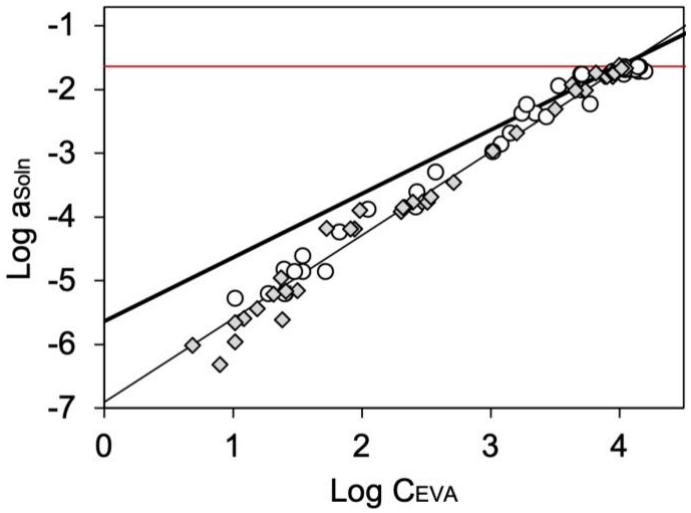


**Figure 7.** **Comparison of apparent chemical activity of PFOS in incubation solution from methods of ($C_{EVA} \cdot F \div S_{EVA}$) (bolded line) and power regression analysis using Equation (31). Circles = PFOS in 30mM phosphate buffered saline at pH 7.4. Diamonds = PFOS in water. Red horizontal line indicates the maximum apparent chemical activity (F = 0.023).**

## 4.3. Sorptive Capacity of Bovine Serum Albumin for PFOS

### 4.3.1. Equilibrium Partitioning

Equilibration between EVA and the solution of PFOS in BSA was reached within 10 minutes (Figure 8). It was also observed that extending the equilibration period to 120 minutes did not significantly affect the concentration of PFOS in EVA ($C_{EVA}$, mg/L).

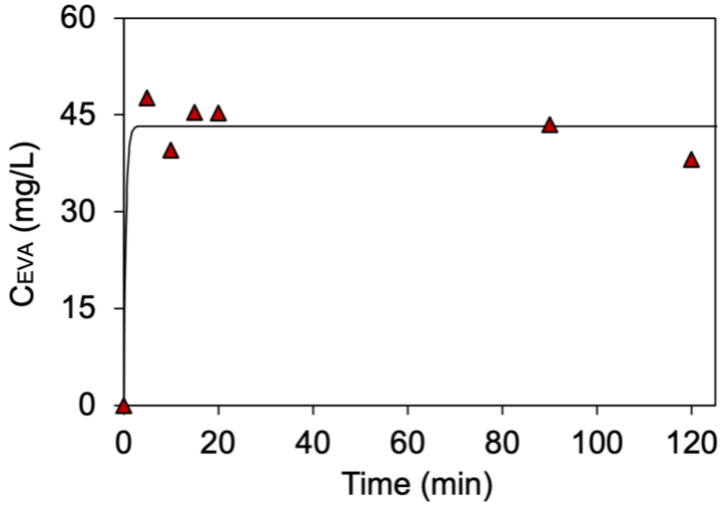


**Figure 8.** **Equilibration of PFOS from BSA solution (BSA at 9.7 g/L and $C_{PBS}$ at 2.64 mg/L) into EVA thin-film ($C_{EVA}$, mg/L).**

Results from equilibrium partitioning showed that $C_{EVA}$ (mg/L) decreased with the concentration of BSA (g/L) in the incubation solution, while $C_{EVA}$ (mg/L) was found to increase with the concentration of PFOS ($C_{PBS}$, mg/L) (Figure 9). The relationship between $C_{EVA}$ and the concentration of BSA and PFOS in the solution can be described as follows on logarithmic scale with standard error ($R^2$ = 0.86, F(2, 77) = 243, p-value < 0.001):

$$\log C_{EVA} = (-0.4672 \pm 0.04) \cdot \log BSA + (0.8983 \pm 0.04) \cdot \log C_{PBS} + (1.9475 \pm 0.04) \quad (32)$$

The inverse relationship observed between $C_{EVA}$ (mg/L) and the concentration of BSA (Figure 9) may be explained by the capacity of BSA to bind PFOS. Notably, when there is a higher concentration of BSA in the solution, more PFOS are bound by BSA, thereby reducing the amount of freely dissolved PFOS available for partitioning into EVA. On the other hand, the increase in $C_{EVA}$ (mg/L) with respect to the concentration of PFOS in incubation solution is consistent with previous results discussed in Section 3.2.3, where higher PFOS concentrations in incubation solutions ($C_W$ and $C_{PBS}$, mg/L) increased $C_{EVA}$ (mg/L).

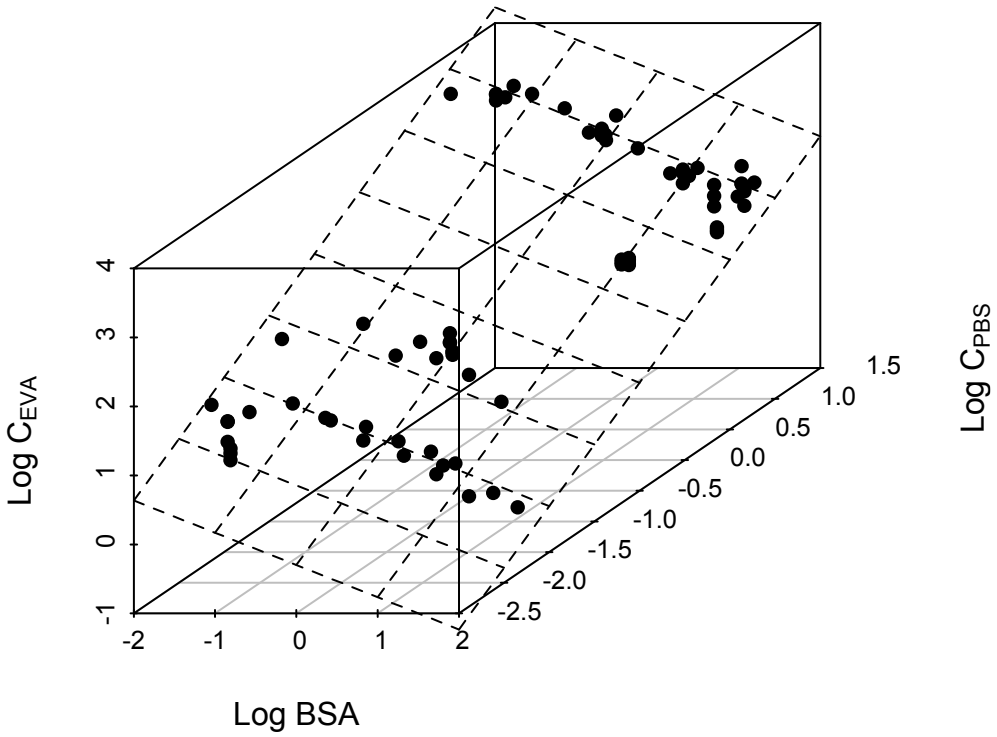


**Figure 9.** **$C_{EVA}$ (mg/L) relative to the concentration of BSA (g/L) and concentration of PFOS (mg/L) in incubation solution on logarithmic scale.**

### 4.3.2. Determination of the Partition Coefficient of PFOS between BSA and Solution ($K_{BSA\text{-}PBS}$)

Based on the two approaches discussed in Section 4.2.4. for estimating the apparent chemical activities of PFOS in the incubation solution ($a_{Soln}$, unitless), the sorptive capacity of the BSA solution for PFOS ($S_{BSA\ Soln}$, mg/L) was first calculated by dividing $C_{PBS}$ (mg/L), having adjusted to account for EVA-losses, by $a_{Soln}$ (unitless). The sorptive capacity of BSA for PFOS ($S_{BSA}$, mg/L) was then calculated using Equation (25), where the partition coefficient of PFOS between BSA and PBS ($K_{BSA\text{-}PBS}$, unitless) was determined through the division of $S_{BSA}$ (mg/L) by $S_{PBS}$ (mg/L).

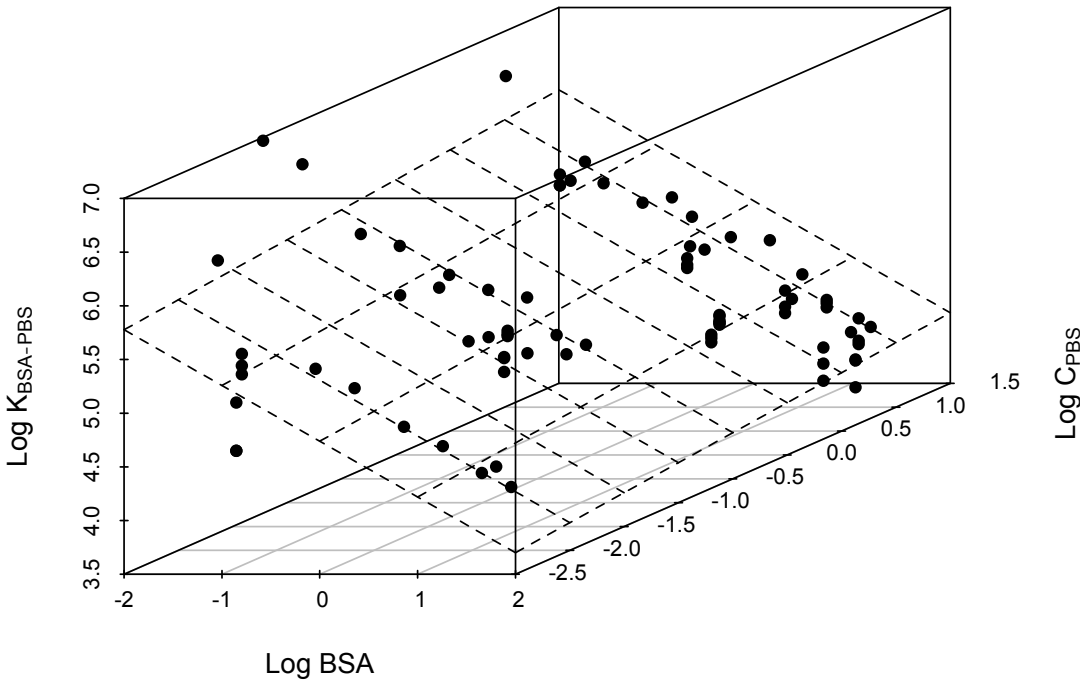


**Figure 10. $K_{BSA\text{-}PBS}$ (unitless) relative to the concentration of BSA (g/L) and concentration of PFOS (mg/L) in incubation solution on logarithmic scale. Apparent chemical activities of PFOS of incubation solution were obtained from EVA measurements (i.e., $C_{EVA} \cdot F \div S_{EVA}$).**

For $a_{Soln}$ (unitless) obtained by dividing $C_{EVA}$ (mg/L) by $S_{EVA}$ (mg/L), $K_{BSA\text{-}PBS}$ (unitless) was found to decline with increasing concentration of BSA (p-value < 0.001) and vice versa with the concentration of PFOS in the incubation solution (p-value = 0.01) (Figure 10). The relationship of $K_{BSA\text{-}PBS}$ (unitless) with respect to BSA and $C_{PBS}$ was estimated on logarithmic scale with standard error as ($R^2$ = 0.66, F(2, 77) = 73.5, p-value < 0.001):

$$\log K_{BSA-PBS} = (-0.5191 \pm 0.04) \cdot \log BSA + (0.1143 \pm 0.04) \cdot \log C_{PBS} + (5.0246 \pm 0.05) \quad (33)$$

For $a_{Soln}$ (unitless) derived from $C_{EVA}$ using Equation (31) as described in Section 4.2.4., $K_{BSA-PBS}$ (unitless) was also found to decrease with increasing concentration of BSA (p-value < 0.001). However, $K_{BSA-PBS}$ (unitless) was found to decrease slightly with the concentration of PFOS in the incubation solution (p-value = 0.002) (Figure 11). The relationship of $K_{BSA-PBS}$ (unitless) with respect to BSA and $C_{PBS}$ was estimated on logarithmic scale with standard error as ($R^2$ = 0.55, F(2, 77) = 47.2, p-value < 0.001):

$$\log K_{BSA-PBS} = (-0.3808 \pm 0.05) \cdot \log BSA - (0.1762 \pm 0.05) \cdot \log C_{PBS} + (5.7016 \pm 0.06) \quad (34)$$

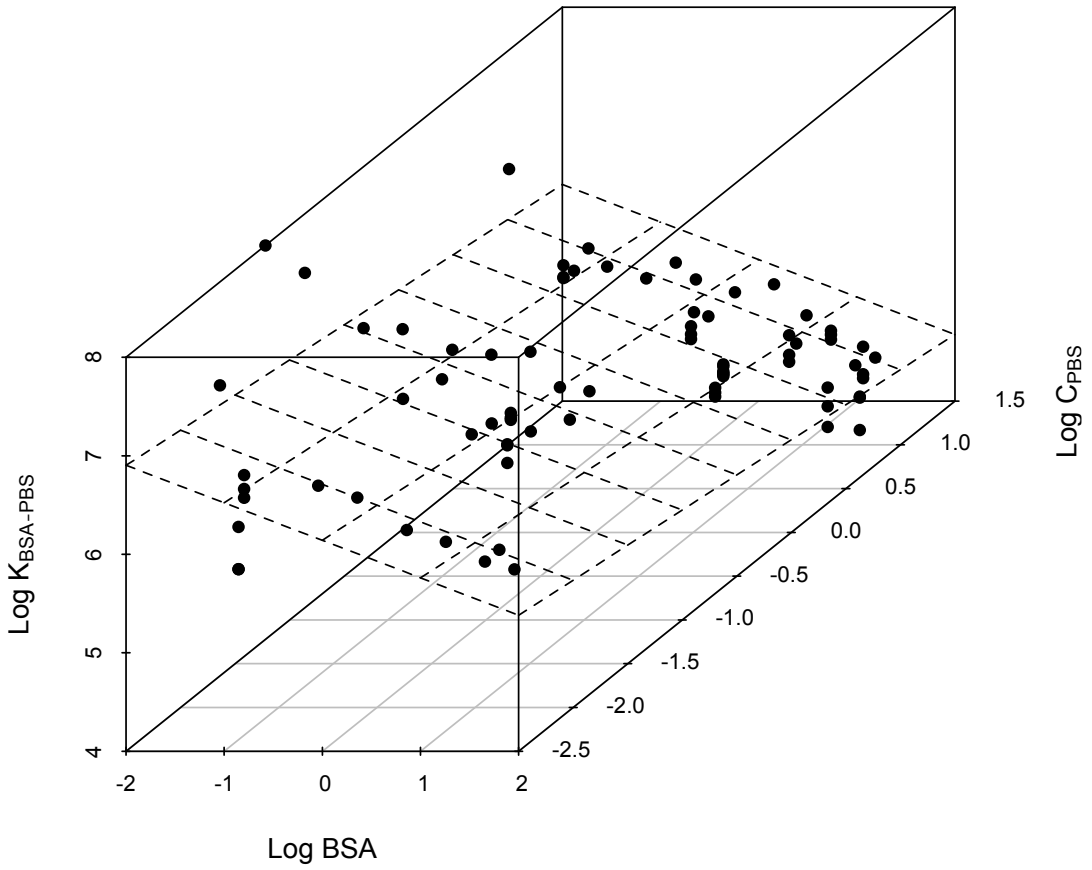


**Figure 11. $K_{BSA-PBS}$ (unitless) relative to the concentration of BSA (g/L) and concentration of PFOS (mg/L) in incubation solution on logarithmic scale. Apparent chemical activities of PFOS of incubation solution were obtained from the power regression of $a_{Soln}$ and $C_{EVA}$.**

The determination and resulting $K_{BSA-PBS}$ from EVA measurements are presented in Table F1. It is important to note that due to the non-constant behaviour of $K_{EVA-Soln}$, the determination of $K_{BSA-PBS}$ through the division of $C_{EVA}$ by $S_{EVA}$ may be underestimated,

particularly for incubation solutions with high $C_{PBS}$. Conversely, the power function from Equation (31) may offer a more practical approach as it takes into account the variability of $K_{EVA\text{-}PBS}$. Therefore, the power function using Equation (31) can provide a more reliable and accurate means to determine the partition coefficient of PFOS between BSA and solution compared to the direct division of $C_{EVA}$ by $S_{EVA}$.

In Figure 11, the regression plane illustrates the significant influence of both BSA and PFOS concentrations in the incubation solution on $K_{BSA\text{-}PBS}$. Based on the biological function of serum albumin as a transporter protein, it is possible that its conformation and binding affinity are adaptable in response to cellular conditions such as varying ligand concentrations. Consequently, the sorptive capacity of BSA for PFOS varies with both concentrations of BSA and PFOS in the incubation solution. Overall, the regression model explains up to 55% of the data variation, there may be additional factors contributing to the interaction of PFOS between BSA and the solution.

Interestingly, the molar ratio of PFOS:BSA (mol/mol) in the incubation solution appeared to not affect the partitioning of PFOS between the solution and BSA. As shown in Figure 12, $K_{BSA\text{-}PBS}$ modeled at various levels of BSA (0.01 g/L to 60 g/L) and $C_{PBS}$ (0.0008 mg/L to 45 mg/L) in the incubation solution was not found to vary among different PFOS:BSA molar ratios. Instead, the variation in $K_{BSA\text{-}PBS}$ was observed based on the levels of BSA and $C_{PBS}$ within the same molar ratio, as indicated by the colour gradient in Figure 13. This suggests that the specific molar ratio of PFOS:BSA may not be as relevant in the partitioning behaviour of PFOS, compared to their concentrations in the incubation solution.

On average, the logarithmic $K_{BSA\text{-}PBS}$ (unitless) estimated over the range of PFOS:BSA molar ratios was found to be 5.65 (SD = 0.74). However, when the PFOS:BSA molar ratio was maintained at 0.02 mol/mol, the average logarithmic $K_{BSA\text{-}PBS}$ (unitless) was 5.33 (SD = 0.52). In comparison to the logarithmic $K_{BSA\text{-}PBS}$ (unitless) values reported in the literature at 4.10 (SE = 0.10) (Bischel et al. 2011) and 4.67 (SD = 0.07) (Allendorf et al. 2019), the values obtained in this thesis were approximately 10 times larger. These differences in $K_{BSA\text{-}PBS}$ (unitless) can be explained by the differing experimental conditions, such as temperature (room temperature vs. 37 °C), equilibration techniques (EVA SPME vs. dialysis), as well as the ionic strength of the solutions. However, it is crucial to note that the values reported in the literature were

obtained under one specific condition of fixed concentrations of PFOS and BSA, whereas the values in this thesis represent an average determined from a wide range of PFOS and BSA concentration combinations. Therefore, it is challenging to directly compare the values of $K_{BSA\text{-}PBS}$, given the unique conditions under which each set of data was obtained.

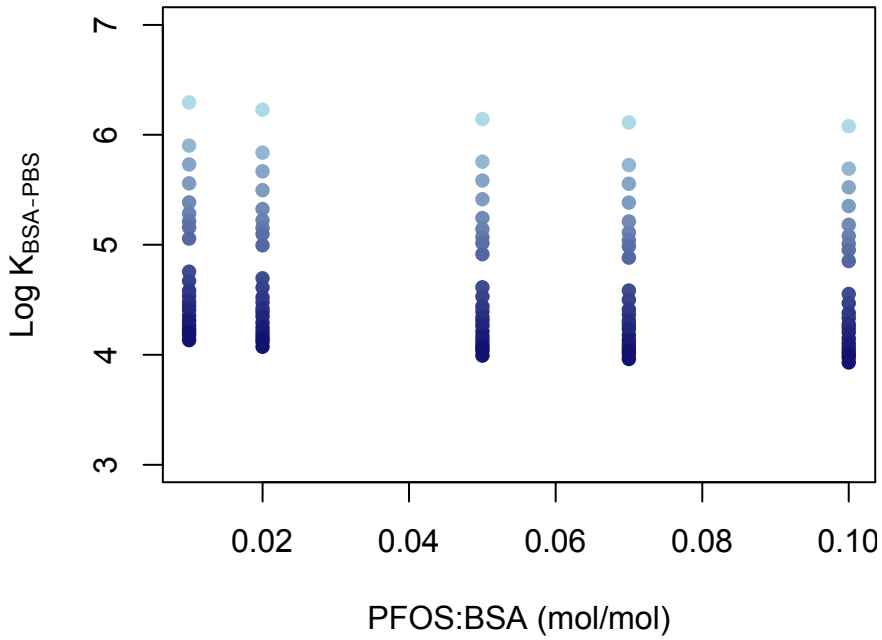


**Figure 12. Logarithmic partition coefficient of PFOS between BSA and incubation solution (Log $K_{BSA\text{-}PBS}$, unitless) relative to PFOS:BSA molar ratio (mol/mol). Colour gradient indicates increasing concentrations of BSA (0.01 g/L to 60 g/L) and PFOS (0.0008 mg/L to 45 mg/L) in the incubation solution.**

Given the intricate variables that can influence the estimation of $K_{BSA\text{-}PBS}$, using EVA SPME and the power function from Equation (31) to determine the sample's apparent chemical activity may offer a more practical approach in the environmental risk assessment of PFOS. This method facilitates the direct comparison of sample concentrations based on their apparent chemical activities. Further work is required to extend the application of the power function to lower concentration ranges of PFOS, as this will improve the model in current environmental and physiological scenarios.

### 4.3.3. Determination of the Sorptive Capacity of BSA for PFOS ($S_{BSA}$, mg/L)

The determination of the sorptive capacity of BSA for PFOS ($S_{BSA}$, mg/L) from the power function are listed in Table F1. On average, $S_{BSA}$ was $1.28 \times 10^8$ mg/L (SD = $5.18 \times 10^8$) and $1.82 \times 10^7$ mg/L (SD = $2.39 \times 10^7$ mg/L) when the PFOS:BSA molar ratio was maintained at 0.02 mol/mol.

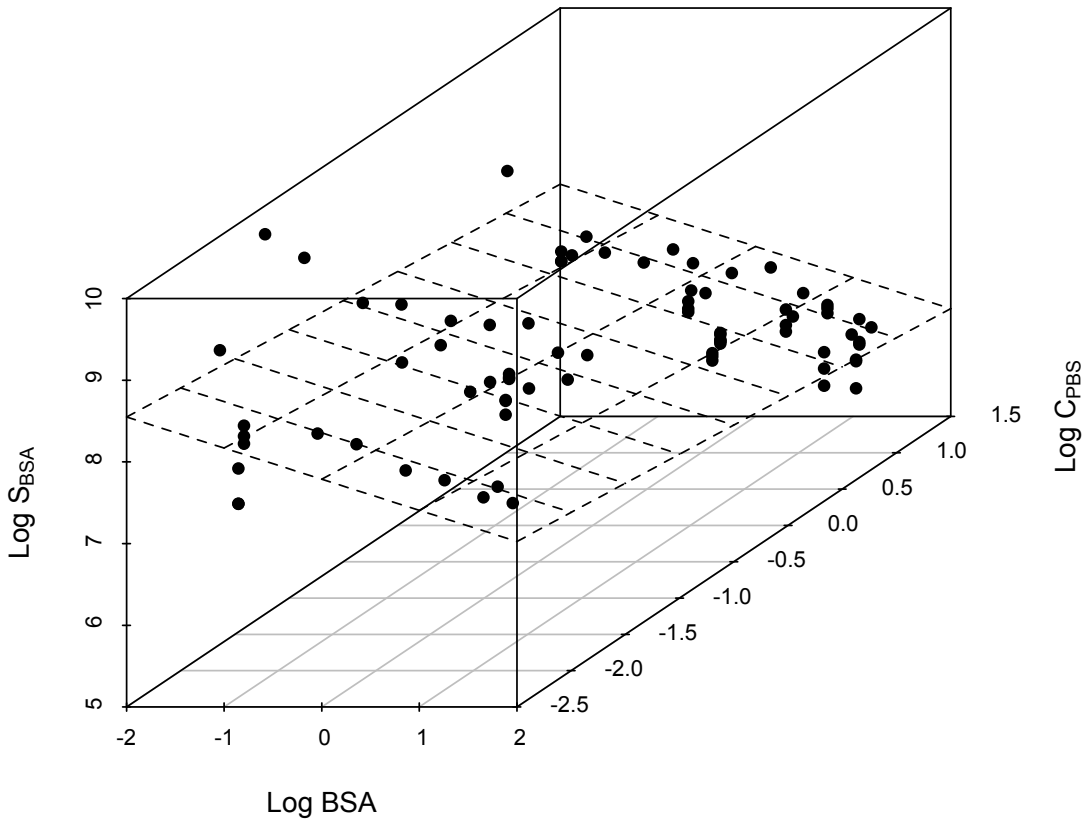


**Figure 13. The sorptive capacity of BSA for PFOS ($S_{BSA}$, mg/L) relative to the concentration of BSA (g/L) and concentration of PFOS in incubation solution on logarithmic scale. Apparent chemical activities of PFOS of incubation solution were obtained from the power regression of $a_{Soln}$ and $C_{EVA}$.**

As illustrated in Figure 13, the values of $S_{BSA}$ (mg/L) followed the same trend as Log $K_{BSA\text{-}PBS}$ (unitless) with respect to the concentration of BSA (g/L) and PFOS in the incubation solution. This is expected as $S_{BSA}$ and $K_{BSA\text{-}PBS}$ have a proportional relationship. The regression plane in Figure 13 can be described on logarithmic scale with standard error as ($R^2$ = 0.55, F(2, 77) = 47.2 , p-value <0.001):

$$\log S_{BSA} = (-0.3809 \pm 0.05) \cdot \log BSA - (0.1766 \pm 0.05) \cdot \log C_{PBS} + (7.3463 \pm 0.06) \quad (35)$$

## 4.4. Application of the Chemical Activity Approach

This section demonstrates a preliminary application of the chemical activity approach in the environmental risk assessment of PFOS. It is important to acknowledge that these apparent chemical activities may differ from absolute chemical activities. Furthermore, the results should be interpreted with caution, considering that assumptions were made to compensate for the lack of specific information on factors such as temperature, water composition, and lipid and protein contents in biological media. Additionally, the data were obtained from different studies, each with their own unique experimental or field conditions. Moreover, the apparent chemical activities of PFOS in fish were based on concentration data collected from multiple species, while those in bird were based on concentration data from a single species with only one sample. Despite these limitations, the following section demonstrate that the activity concept serves as a practical tool for evaluating environmental PFOS concentrations.

### 4.4.1. Environmental Distribution of PFOS

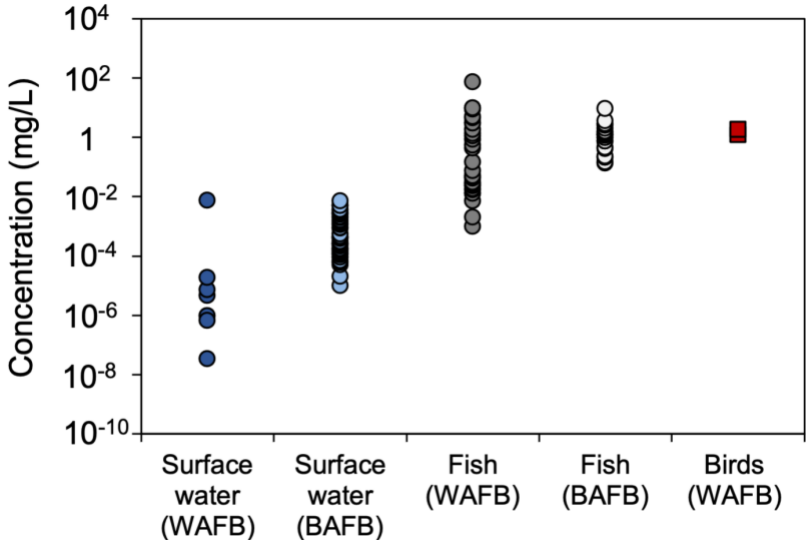


**Figure 14. Concentrations (mg/L) of PFOS in surface water, fish, and birds at the US Barksdale Air Force Base (BAFB) and Wurtsmith Air Force Base (WAFB).**

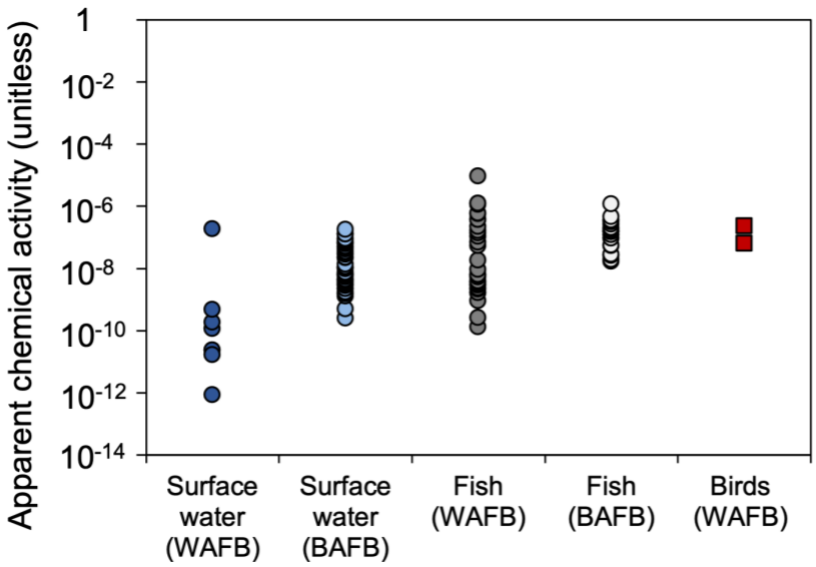


**Figure 15. Apparent chemical activities (unitless) of PFOS in surface water, fish, and birds at the US Barksdale Air Force Base (BAFB) and Wurtsmith Air Force Base (WAFB).**

As shown in Figures 14 and 15, the data of PFOS in surface water (n = 8 for WAFB and n = 50 for BAFB), fish (n = 34 for WAFB and n = 25 for BAFB), and birds (n = 2 for WAFB) at selected study sites are illustrated in concentrations (mg/L) and apparent chemical activities (unitless). A comparison of the two figures showed that the range of variation decreased by 1000-fold when the concentration data were expressed in apparent chemical activities. Specifically, PFOS concentrations ranged from $10^{-8}$ to $10^{2}$ mg/L, while apparent chemical activities ranged from $10^{-12}$ to $10^{-6}$ (unitless).

In Figure 15, non-parametric Kruskal-Wallis analysis ($\chi^2 = 40.61$, df = 4, p-value < 0.001) showed significant differences between media types expressed in apparent chemical activities. Further pairwise-comparison analysis revealed that the apparent chemical activities were higher at BAFB than WAFB in both surface water (p-value = 0.002) and fish (p-value = 0.025), indicating a heavier contamination of PFOS at BAFB than WAFB. In addition, within each site, the apparent chemical acitivities in fish were found higher than those in surface water (BAFB p-value = $5.2\times10^{-8}$, WAFB p-value = 0.017). This finding suggests a net movement of PFOS from water into fish, indicating amplification or bioconcentration of PFOS in fish at BAFB and WAFB.

### 4.4.2. Evaluation of Toxicity Risks Associated with PFOS for Biota

Toxicity references showed apparent chemical activities of PFOS ranging from $10^{-7}$ to $10^{-1}$ for fish and $10^{-6}$ to $10^{-4}$ for birds. These values are lower than the fugacity ratios calculated for biota ($10^{-0.5}$ for fish and $10^{-1.4}$ for birds), indicating that the PFOS dosages were appropriately prepared for exposure in the environmental media. If the apparent chemical activities had exceeded the fugacity ratio, it would have suggested that PFOS dosages were prepared above the sorptive capacity of the environmental media. Thus, the toxicity references used in this study can be used to evaluate the levels of PFOS contamination in fish and birds in the study sites.

Compared to the toxicity references in Figure 16, the apparent chemical activities of PFOS in fish and birds from both study sites ranged from $10^{-10}$ and $10^{-5}$. Biota data showed that approximately 10% of fish at BAFB and 30% of fish WAFB were within the range associated with NOEL. Conversely, the PFOS levels in birds at WAFB were outside the range of toxicity. These results suggest that the PFOS concentrations in fish at BAFB and WAFB were approaching levels where adverse effects could occur, whereas the concentrations in birds were not toxic. However, it is important to note that the sample size for birds at WAFB was only 2, thus more data will be necessary to confirm the toxicity risks associated with PFOS for birds.

Given that the apparent chemical activities of toxic concentrations are lower for birds than fish, as illustrated in Figure 16, it is evident that birds may be more sensitive to PFOS than fish. This comparison of toxicity concentrations among wildlife species can be useful for formulating wildlife tissue guidelines. For examples, these guidelines can be developed by applying a safety factor to the $5^{th}$ percentile of the lowest cumulative probability distribution of the apparent chemical activities for the most sensitive species. Subsequently, the guideline can be converted into a concentration-based value by multiplying it with the sorptive capacity of the specific tissue type for PFOS. For a more comprehensive evaluation of species sensitivity and formulation of wildlife tissue guidelines, a more extensive collection of monitoring data encompassing species across the food web will be needed.

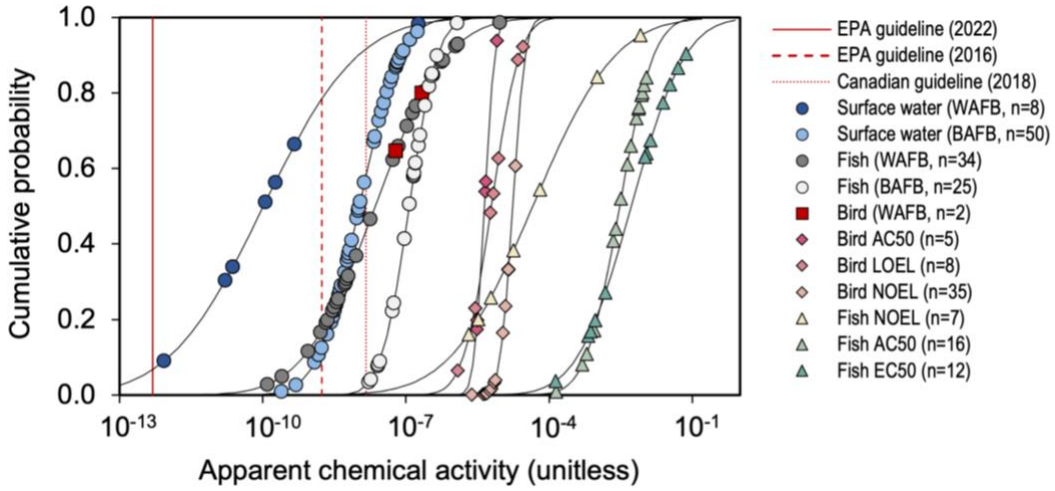


**Figure 16. Cumulative probability distributions of apparent chemical activities (unitless) of PFOS in surface water, fish, and birds from US Barksdale Air Force Base (BAFB) and Wurtsmith Air Force Base (WAFB) and chemical activities corresponded with biological effects.**

NOEL = no-observed-effect levels; LOEL = lowest-observed-effect levels; AC50 = concentrations at which 50% maximum activity was noted in high-throughput US EPA ToxCast tests; EC50 = median effect concentrations.

The evaluation of PFOS concentrations for biota and toxicity may be simplified. In particular, while the apparent chemical activities for PFOS in biota and toxicity effects in Figure 16 were calculated using the sorptive capacities summed from various biological components (Table 3), this calculation can be simplified by using only the sorptive capacity of the albumin or transporter proteins. This approach is justified by the fact that albumin accounts for at least 60 to 80 percent of the total sorptive capacity for a given tissue or biota (Table 5). Therefore, as long as this approach is consistently applied across the concentration data of biota and toxicity references, the estimation of apparent chemical activities can be simplified for the purpose of risk assessment. Table 5 provides a comparison of the sorptive capacities for different tissues and biota based on different estimations. It can be seen that despite albumin having a lower sorptive capacity compared to polar lipids, it dominates the overall sorption of PFOS due to its higher volume fraction and moderate sorptive capacity. For additional comparison, the water phase, which constitutes at least 80% of volume within a tissue or biota, is not a significant sorption phase for PFOS due to its low sorptive capacity.

Lastly, the observations drawn from the toxicity data in Figure 16 suggest a potential replacement of traditional *in vivo* studies with *in vitro* studies. As shown in the figure, the distribution of apparent chemical activities of PFOS corresponding with AC50 resemble the distribution of *in-vivo* based results. For birds, the AC50 values are approximately within the same order of magnitude as LOEL and NOEL, encompassing effects on fecundity, reproduction, feeding behaviour, and mortality. For fish, the range of AC50 coincide with EC50, encompassing effects on reproduction, development, and physiology. These overlaps of apparent chemical activities between AC50 and traditional *in vivo* toxicity tests provide support towards using AC50 data obtained from high-throughput, *in vitro* studies as alternatives to *in vivo* studies. However, it is worth noting that there remains a significant difference between NOEL and AC50 in fish, as they differ by several orders of magnitude. Hence, further research may be necessary to establish the relationship between these two toxicity measurements.

**Table 5. Comparison of different estimations for the sorptive capacity of whole fish, eggs, plasma for PFOS.**

| Estimation[a] | Unit | Whole fish | Eggs | Plasma |
|---|---|---|---|---|
| TP + PL + SP + NL + PBS | mol/m$^3$ | 175.7 | 381.4 | 168.2 |
| TP only | mol/m$^3$ | 107.0 | 321.0 | 119.9 |
| PL only | mol/m$^3$ | 60.3 | 60.3 | 48.3 |
| PBS only | mol/m$^3$ | 0.07 | 0.07 | 0.08 |

[a] Volume fractions of biological phases and their sorptive capacities for PFOS are listed in Table 3. TP = transporter protein or albumin, PL = polar lipids, SP = structural protein, NL = neutral lipids, and PBS = 30mM phosphate buffered saline at pH 7.4.

### 4.4.3. Evaluation of Water Guidelines for PFOS

Figure 16 also provides insights into the evaluation of surface waters from BAFB and WAFB with regards to recent water guidelines. As presented in the figure, the guidelines include those set by the US EPA at 70 ng/L in 2016 and 0.02 ng/L in 2022, as well as Health Canada at 600 ng/L in 2018. These represent the most stringent and the highest allowable level among current international guidelines listed in Table 1. Notably, all three guidelines fall outside the range of apparent chemical activities associated with toxic effects in birds and fish. If the most recent EPA guideline at 0.02 ng/L is applied, almost all surface water samples from BAFB (100%) and WAFB (95%) would be considered unsafe for human consumption. On the other hand, if the Canadian guideline

of 600 ng/L is used, the majority of surface water samples from WAFB (90%) and almost 60% of those from BAFB would be deemed safe for drinking. Clearly, these results highlight the significant impact of the choice of water guideline on the interpretation of current PFOS contamination levels and the subsequent actions taken. Given these results, it is crucial to continue monitoring efforts in PFOS-affected sites to improve the understanding of its environmental distribution and biological processes such as bioaccumulation, biomagnification, and biotransformation. These research will help guide the making of more realistic and context-specific environmental guidelines and subsequent management decisions for PFOS.

### 4.4.4. Discussion

In summary, the concept of chemical activity provided a comprehensive metric to integrate and compare PFOS data of various sources. The analysis successfully incorporated a total of 119 environmental, 83 toxicity, and 3 water guideline concentration data. The results showed that a fraction of fish at BAFB and WAFB contained PFOS levels associated with NOELs, indicating potential ecological risks. Based on toxicity data, birds may be more sensitive to PFOS than fish. The apparent chemical activities of surface water at both sites, external to biota, were found to be well below the ranges associated with biological effects. Additionally, birds at WAFB were not found to be within the ranges associated with toxicities. These findings emphasize the need for continued monitoring studies and data collection across abiotic and biotic media to better understand the distribution of PFOS. Through the use of the chemical activity concept, these data can contribute to improving current environmental risk assessments and guideline developments.

# Chapter 5. Conclusion

PFOS is an emerging persistent organic pollutant with unique characteristics that can be measured through EVA SPME and described in apparent chemical activities. This thesis demonstrates that the chemical activity concept can be applied for PFOS through its aqueous concentrations. The use of EVA SPME was used to measure various thermodynamic parameters for PFOS, including $S_{EVA}$, $a_{medium}$, $K_{EVA\text{-}Soln}$, $K_{BSA\text{-}Soln}$, and $S_{BSA}$, in support of a chemical activity-based evaluation of 205 PFOS concentration data of various environmental phases, metrics, and sources. The results and points for consideration outlined in this thesis are as follows:

### *The aqueous solubility of PFOS.*

While pure liquid forms of ionic PFOS are not available for the direct determination of its solubility, various aqueous solubility measurements through the salt forms provide very close estimates to the ionic form. Therefore, the application of chemical activity through aqueous concentrations is supported.

Despite uncertainties in reported aqueous solubilities in this study, their impact on the comparison of apparent chemical activities is minimal. However, it is important to distinguish between the solubility of PFOS in pure water and buffered saline, as they differ by almost 15 times. Temperature is not a significant factor when comparing apparent chemical activities between media types that are at similar temperatures, such as those between fish and their exposure water. However, when comparing subjects with temperature differences up to 5 times, such as lake water and birds, the temperature difference through the fugacity ratio can affect their comparison of apparent chemical activities.

### *EVA SPME.*

This study demonstrated that EVA can be relied as a sorbent and reference phase in SPME for the determination of various properties of PFOS, including concentration, apparent chemical activity, and partition coefficients ($K_{EVA\text{-}W}$, $K_{EVA\text{-}PBS}$, and $K_{BSA\text{-}PBS}$). Although the adsorption behaviour of EVA is not constant with respect to the concentration of PFOS in the incubation solution, a chemical activity meter can be calibrated using water. The meter can be constructed through modelling the calculated

apparent chemical activity of the water with the corresponding $C_{EVA}$. This way, the apparent chemical activity of any incubation medium can be determined through EVA SPME and applying the activity meter.

### *Chemical activity-based environmental risk assessment.*

The chemical activity approach is proven a practical metric for the environmental risk assessment of PFOS, for which traditional methods are challenged due to its unique characteristics and differences compared to neutral organic pollutants. This approach effectively integrates a variety of PFOS concentration data, providing insights onto its environmental distribution, bioaccumulation potential, and adequacy of guidelines. Moreover, the estimation of apparent chemical activity of PFOS for tissues and biota can be simplified by only considering the sorptive capacity of the albumin or transporter proteins. This simplification offers a practical approach to assess the PFOS levels in biological samples. Lastly, instead of relying on the partition coefficient of PFOS between BSA and solution, which is influenced by multiple factors, it may be more practical to directly measure the sample's apparent chemical activity and base assessments in this parameter.

The chemical activity concept is well aligned with the objectives for toxicity testing in the 21st century, which advocates for the use of high-throughput assays and large databases to make the most of available information. This thesis illustrates its application as a valuable tool in the risk assessment of PFOS. By incorporating the concept, vast amount of available data can be used to bolster current understanding of its environmental fate, thereby contributing to better-informed environmental management.

# References

3M Company. 2000. Phase-out Plan for PFOS-Based Products.

Aas, C. B., E. Fuglei, D. Herzke, N. G. Yoccoz, and H. Routti. 2014. Effect of Body Condition on Tissue Distribution of Perfluoroalkyl Substances (PFASs) in Arctic Fox (Vulpes lagopus). Environmental Science & Technology 48:11654–11661.

Allendorf, F., U. Berger, K.-U. Goss, and N. Ulrich. 2019. Partition coefficients of four perfluoroalkyl acid alternatives between bovine serum albumin (BSA) and water in comparison to ten classical perfluoroalkyl acids. Environmental Science: Processes & Impacts 21:1852–1863.

Allendorf, F., K.-U. Goss, and N. Ulrich. 2021. Estimating the Equilibrium Distribution of Perfluoroalkyl Acids and 4 of Their Alternatives in Mammals. Environmental Toxicology and Chemistry 40:910–920.

Anderson, R. H., G. C. Long, R. C. Porter, and J. K. Anderson. 2016. Occurrence of select perfluoroalkyl substances at U.S. Air Force aqueous film-forming foam release sites other than fire-training areas: Field-validation of critical fate and transport properties. Chemosphere 150:678–685.

Armitage, J. M., J. A. Arnot, F. Wania, and D. Mackay. 2013. Development and evaluation of a mechanistic bioconcentration model for ionogenic organic chemicals in fish. Environmental Toxicology and Chemistry 32:115–128.

Arp, H. P. H., C. Niederer, and K.-U. Goss. 2006. Predicting the Partitioning Behavior of Various Highly Fluorinated Compounds. Environmental Science & Technology 40:7298–7304.

ATSDR. 2021. Toxicological Profile for Perfluoroalkyls. U.S. Department of Health and Human Services.

Australian Department of Health. 2017. Health based guidance values for PFAS. For use in site investigations in Australia. Australian Government, Commonwealth of Australia. Australian Government.

Bassler, J., A. Ducatman, M. Elliott, S. Wen, B. Wahlang, J. Barnett, and M. C. Cave. 2019. Environmental perfluoroalkyl acid exposures are associated with liver disease characterized by apoptosis and altered serum adipocytokines. Environmental Pollution 247:1055–1063.

BC Ministry of Environment and Climate Change Strategy. 2020. B.C. Source Drinking Water Quality Guidelines: Guideline Summary. Water Quality Guideline Series, WQG-01.

Bhattacharya, A. A., T. Grüne, and S. Curry. 2000. Crystallographic analysis reveals common modes of binding of medium and long-chain fatty acids to human serum albumin11Edited by R. Huber. Journal of Molecular Biology 303:721–732.

Bhhatarai, B., and P. Gramatica. 2011. Prediction of Aqueous Solubility, Vapor Pressure and Critical Micelle Concentration for Aquatic Partitioning of Perfluorinated Chemicals. Environmental Science & Technology 45:8120–8128.

Bischel, H. N., L. A. MacManus-Spencer, and R. G. Luthy. 2010. Noncovalent Interactions of Long-Chain Perfluoroalkyl Acids with Serum Albumin. Environmental Science & Technology 44:5263–5269.

Bischel, H. N., L. A. MacManus-Spencer, C. Zhang, and R. G. Luthy. 2011. Strong associations of short-chain perfluoroalkyl acids with serum albumin and investigation of binding mechanisms. Environmental Toxicology and Chemistry 30:2423–2430.

Buck, R. C., J. Franklin, U. Berger, J. M. Conder, I. T. Cousins, P. de Voogt, A. A. Jensen, K. Kannan, S. A. Mabury, and S. P. van Leeuwen. 2011. Perfluoroalkyl

and polyfluoroalkyl substances in the environment: Terminology, classification, and origins. Integrated Environmental Assessment and Management 7:513–541.

Budtz-Jørgensen, E., and P. Grandjean. 2018. Application of benchmark analysis for mixed contaminant exposures: Mutual adjustment of perfluoroalkylate substances associated with immunotoxicity. PLOS ONE 13:e0205388.

Canada Gazette. 2006. Perfluorooctane Sulfonate, its Salts and its Precursors 140:2150–2153.

CEPA. 2009. Regulations Adding Perfluorooctane Sulfonate and Its Salts to the Virtual Virtual Elimination List.

CEPA. 2018a. Final guideline for Canadian drinking water quality for perfluorooctane sulfonate.

CEPA. 2018b. Final guideline for Canadian drinking water quality for perfluorooctanoic acid.

CEPA. 2018c. Federal Environmental Quality Guidelines, Perfluorooctane Sulfonate (PFOS). Environment and Climate Change Canada.

ChemSpider. 2023. Melting Temperature of PFOS acid, CSID:67068.

Chen, J., A. Adegbule, J. Huang, and M. Brooks. 2021. Surface Tension, pH, and Specific Conductance of Select PFAS and their Mixtures (Record ID 354206). American Geophysical Union Fall Meeting (US EPA), New Orleans, LA,.

Cheng, J., E. Psillakis, M. R. Hoffmann, and A. J. Colussi. 2009. Acid Dissociation versus Molecular Association of Perfluoroalkyl Oxoacids: Environmental Implications. The Journal of Physical Chemistry A 113:8152–8156.

Convertino, M., T. R. Church, G. W. Olsen, Y. Liu, E. Doyle, C. R. Elcombe, A. L. Barnett, L. M. Samuel, I. R. MacPherson, and T. R. J. Evans. 2018. Stochastic Pharmacokinetic-Pharmacodynamic Modeling for Assessing the Systemic Health Risk of Perfluorooctanoate (PFOA). Toxicological Sciences 163:293–306.

Costanza, J., L. M. Abriola, and K. D. Pennell. 2020. Aqueous Film-Forming Foams Exhibit Greater Interfacial Activity than PFOA, PFOS, or FOSA. Environmental Science & Technology 54:13590–13597.

Cousins, I., J. DeWitt, J. Glüge, G. Goldenman, D. Herzke, R. Lohmann, M. Miller, C. A. Ng, M. Scheringer, L. Vierke, and Z. Wang. 2020. Strategies for grouping per- and polyfluoroalkyl substances (PFAS) to protect human and environmental health. Environmental Science: Processes & Impacts 22:1444–1460.

Custer, C. M., T. W. Custer, P. M. Dummer, M. A. Etterson, W. E. Thogmartin, Q. Wu, K. Kannan, A. Trowbridge, and P. C. McKann. 2014. Exposure and Effects of Perfluoroalkyl Substances in Tree Swallows Nesting in Minnesota and Wisconsin, USA. Archives of Environmental Contamination and Toxicology 66:120–138.

Droge, S. T. J. 2019. Membrane–Water Partition Coefficients to Aid Risk Assessment of Perfluoroalkyl Anions and Alkyl Sulfates. Environmental Science & Technology 53:760–770.

East, A., R. H. Anderson, and C. J. Salice. 2021. Per- and Polyfluoroalkyl Substances (PFAS) in Surface Water Near US Air Force Bases: Prioritizing Individual Chemicals and Mixtures for Toxicity Testing and Risk Assessment. Environmental Toxicology and Chemistry 40:859–870.

Ebert, A., F. Allendorf, U. Berger, K.-U. Goss, and N. Ulrich. 2020. Membrane/Water Partitioning and Permeabilities of Perfluoroalkyl Acids and Four of their Alternatives and the Effects on Toxicokinetic Behavior. Environmental Science & Technology 54:5051–5061.

EFSA. 2008. Perfluorooctane sulfonate (PFOS), perfluorooctanoic acid (PFOA) and their salts. Scientific Opinion of the Panel on Contaminants in the Food chain.

Ellefson, M. 2001. Solubility of PFOS in Water, Project number E00-1716. 3M Environmental Laboratory.

Endo, S., J. Hammer, and S. Matsuzawa. 2023. Experimental Determination of Air/Water Partition Coefficients for 21 Per- and Polyfluoroalkyl Substances Reveals Variable Performance of Property Prediction Models. Environmental Science & Technology.

Environment Canada. 2006. Canadian Environmental Protection Act, 1999 (CEPA 1999): Ecological Screening Assessment Report on Perfluorooctane Sulfonate, Its Salts and Its Precursors that Contain the C8F17SO2 or C8F17SO3, or C8F17SO2N Moiety.

Fair, P. A., T. Romano, A. M. Schaefer, J. S. Reif, G. D. Bossart, M. Houde, D. Muir, J. Adams, C. Rice, T. C. Hulsey, and M. Peden-Adams. 2013. Associations between perfluoroalkyl compounds and immune and clinical chemistry parameters in highly exposed bottlenose dolphins (Tursiops truncatus). Environmental Toxicology and Chemistry 32:736–746.

Former WAFB. 2013. The United States Air Force Installation Restoration Program Record Of Decision, Sites LF-30 and LF-31, Wurtsmith AR#300140. US Department of Air Force.

Franco, A., and S. Trapp. 2010. A multimedia activity model for ionizable compounds: Validation study with 2,4-dichlorophenoxyacetic acid, aniline, and trimethoprim. Environmental Toxicology and Chemistry 29:789–799.

Freundlich, H. 1926. Colloid and Capillary Chemistry. New York, E. P. Dutton and Company.

Giesy, J. P., and K. Kannan. 2001. Global Distribution of Perfluorooctane Sulfonate in Wildlife. Environmental Science & Technology 35:1339–1342.

Gobas, F. A. P. C., P. Mayer, T. F. Parkerton, R. M. Burgess, D. van de Meent, and T. Gouin. 2018. A chemical activity approach to exposure and risk assessment of chemicals. Environmental Toxicology and Chemistry 37:1235–1251.

Gobas, F. A. P. C., S. V. Otton, L. F. Tupper-Ring, M. A. Crawford, K. E. Clark, and M. G. Ikonomou. 2017. Chemical activity–based environmental risk analysis of the plasticizer di-ethylhexyl phthalate and its main metabolite mono-ethylhexyl phthalate. Environmental Toxicology and Chemistry 36:1483–1492.

Gobas, F. A. P. C., S. Xu, G. Kozerski, D. E. Powell, K. B. Woodburn, D. Mackay, and A. Fairbrother. 2015. Fugacity and activity analysis of the bioaccumulation and environmental risks of decamethylcyclopentasiloxane (D5). Environmental Toxicology and Chemistry 34:2723–2731.

Golding, C. J., F. A. P. C. Gobas, and G. F. Birch. 2008. A fugacity approach for assessing the bioaccumulation of hydrophobic organic compounds from estuarine sediment. Environmental Toxicology and Chemistry 27:1047–1054.

Groffen, T., R. Lasters, A. Lopez-Antia, E. Prinsen, L. Bervoets, and M. Eens. 2019. Limited reproductive impairment in a passerine bird species exposed along a perfluoroalkyl acid (PFAA) pollution gradient. Science of The Total Environment 652:718–728.

Han, X., P. M. Hinderliter, T. A. Snow, and G. W. Jepson. 2004. Binding of Perfluorooctanoic Acid to Rat Liver-form and Kidney-form α2u-Globulins. Drug and Chemical Toxicology 27:341–360.

He, X. M., and D. C. Carter. 1992. Atomic structure and chemistry of human serum albumin. Nature 358:209–215.

Health Canada. 2018. Guidelines for Canadian Drinking Water Quality: Guideline Technical Document, Perfluorooctane Sulfonate (PFOS).

Hedgespeth, M. L., D. L. Taylor, S. Balint, M. Schwartz, and M. G. Cantwell. 2023. Ecological characteristics impact PFAS concentrations in a U.S. North Atlantic food web. Science of The Total Environment 880:163302.

Inoue, Y., N. Hashizume, N. Yakata, H. Murakami, Y. Suzuki, E. Kikushima, and M. Otsuka. 2012. Unique Physicochemical Properties of Perfluorinated Compounds and Their Bioconcentration in Common Carp Cyprinus carpio L. Archives of Environmental Contamination and Toxicology 62:672–680.

Jones, P. D., W. Hu, W. De Coen, J. L. Newsted, and J. P. Giesy. 2003. Binding of perfluorinated fatty acids to serum proteins. Environmental Toxicology and Chemistry 22:2639–2649.

Kelly, B. C., M. G. Ikonomou, J. D. Blair, B. Surridge, D. Hoover, R. Grace, and F. A. P. C. Gobas. 2009. Perfluoroalkyl contaminants in an Arctic marine food web: trophic magnification and wildlife exposure. Environmental Science & Technology 43:4037–4043.

KEMI. 2017. The 16 New PoPs. Stockholm: Swedish Chemicals Agency.

Kesic, R., J. E. Elliott, K. H. Elliott, S. L. Lee, and F. Maisonneuve. 2023. Perfluoroalkyl Substances in Seabird Eggs from Canada's Pacific Coast: Temporal Trends (1973–2019) and Interspecific Patterns. Environmental Science & Technology 57:10792–10803.

Key, B. D., R. D. Howell, and C. S. Criddle. 1997. Fluorinated Organics in the Biosphere. Environmental Science & Technology 31:2445–2454.

Krafft, M. P., and J. G. Riess. 2015. Selected physicochemical aspects of poly- and perfluoroalkylated substances relevant to performance, environment and sustainability—Part one. Chemosphere 129:4–19.

Lampic, A., and J. M. Parnis. 2020. Property Estimation of Per- and Polyfluoroalkyl Substances: A Comparative Assessment of Estimation Methods. Environmental Toxicology and Chemistry 39:775–786.

Larson, E. S., J. M. Conder, and J. A. Arblaster. 2018. Modeling avian exposures to perfluoroalkyl substances in aquatic habitats impacted by historical aqueous film forming foam releases. Chemosphere 201:335–341.

Lee, K., J. J. Alava, P. Cottrell, L. Cottrell, R. Grace, I. Zysk, and S. Raverty. 2023. Emerging Contaminants and New POPs (PFAS and HBCDD) in Endangered Southern Resident and Bigg's (Transient) Killer Whales (Orcinus orca): In Utero Maternal Transfer and Pollution Management Implications. Environmental Science & Technology 57:360–374.

Lewis, G. N. 1907. Outlines of a New System of Thermodynamic Chemistry. Proceedings of the American Academy of Arts and Sciences 43:259–293.

Li, H., S. Hammarstrand, B. Midberg, Y. Xu, Y. Li, D. S. Olsson, T. Fletcher, K. Jakobsson, and E. M. Andersson. 2022. Cancer incidence in a Swedish cohort with high exposure to perfluoroalkyl substances in drinking water. Environmental Research 204:112217.

Liu, Y.-L., and M. Sun. 2021. Ion exchange removal and resin regeneration to treat per- and polyfluoroalkyl ether acids and other emerging PFAS in drinking water. Water Research 207:117781.

Luebker, D. J., K. J. Hansen, N. M. Bass, J. L. Butenhoff, and A. M. Seacat. 2002. Interactions of flurochemicals with rat liver fatty acid-binding protein. Toxicology 176:175–185.

Mackay, D. 2001. Multimedia Environmental Models: The Fugacity Approach. Second edition. CRC Press.

Mackay, D., and J. A. Arnot. 2011. The Application of Fugacity and Activity to Simulating the Environmental Fate of Organic Contaminants. Journal of Chemical & Engineering Data 56:1348–1355.

Mackay, D., J. A. Arnot, E. P. Petkova, K. B. Wallace, D. J. Call, L. T. Brooke, and G. D. Veith. 2009. The physicochemical basis of QSARs for baseline toxicity. SAR and QSAR in Environmental Research 20:393–414.

Mackay, D., J. A. Arnot, F. Wania, and R. E. Bailey. 2010. Chemical activity as an integrating concept in environmental assessment and management of contaminants. Integrated Environmental Assessment and Management 7:248–255.

Mayer, P., J. Tolls, J. L. M. Hermens, and D. Mackay. 2003. Peer Reviewed: Equilibrium Sampling Devices. Environmental Science & Technology 37:184A-191A.

Meloche, L. M., A. M. H. deBruyn, S. V. Otton, M. G. Ikonomou, and F. A. P. C. Gobas. 2009. Assessing exposure of sediment biota to organic contaminants by thin-film solid phase extraction. Environmental Toxicology and Chemistry 28:247–253.

Moody, C. A., and J. A. Field. 2000. Perfluorinated Surfactants and the Environmental Implications of Their Use in Fire-Fighting Foams. Environmental Science & Technology 34:3864–3870.

Moody, C. A., G. N. Hebert, S. H. Strauss, and J. A. Field. 2003. Occurrence and persistence of perfluorooctanesulfonate and other perfluorinated surfactants in groundwater at a fire-training area at Wurtsmith Air Force Base, Michigan, USA. Journal of Environmental Monitoring 5:341–345.

OECD. 2002. Hazard Assessment of Perfluorooctane Sulfonate (PFOS) and its Salts JT00135607.

Ontario Minister of the Environment. 2021. Minister's annual report on drinking water.

Otton, S. V. 2004. Master thesis: A method to measure the sorptive capacity of sediment and plankton for selected organochlorines. Simon Fraser University.

Peters, T. Jr. 1996. All About Albumin: Biochemistry, Genetics, and Medical Applications. Academic Press.

Quist, E. M., A. J. Filgo, C. A. Cummings, G. E. Kissling, M. J. Hoenerhoff, and S. E. Fenton. 2015. Hepatic Mitochondrial Alteration in CD-1 Mice Associated with Prenatal Exposures to Low Doses of Perfluorooctanoic Acid (PFOA). Toxicologic Pathology 43:546–557.

Rewerts, J. N., E. C. Christie, A. E. Robel, T. A. Anderson, C. McCarthy, C. J. Salice, and J. A. Field. 2021. Key Considerations for Accurate Exposures in Ecotoxicological Assessments of Perfluorinated Carboxylates and Sulfonates. Environmental Toxicology and Chemistry 40:677–688.

Robuck, A. R., J. P. McCord, M. J. Strynar, M. G. Cantwell, D. N. Wiley, and R. Lohmann. 2021. Tissue-Specific Distribution of Legacy and Novel Per- and Polyfluoroalkyl Substances in Juvenile Seabirds. Environmental Science & Technology Letters 8:457–462.

Salice, C. J., T. A. Anderson, R. H. Anderson, and A. D. Olson. 2018. Ecological risk assessment of perfluooroctane sulfonate to aquatic fauna from a bayou adjacent to former fire training areas at a US Air Force installation. Environmental Toxicology and Chemistry 37:2198–2209.

Schaefer, C. E., V. Culina, D. Nguyen, and J. Field. 2019. Uptake of Poly- and Perfluoroalkyl Substances at the Air–Water Interface. Environmental Science & Technology 53:12442–12448.

Steinle-Darling, E., and M. Reinhard. 2008. Nanofiltration for Trace Organic Contaminant Removal: Structure, Solution, and Membrane Fouling Effects on the Rejection of Perfluorochemicals. Environmental Science & Technology 42:5292–5297.

Stock, N. L., V. I. Furdui, D. C. G. Muir, and S. A. Mabury. 2007. Perfluoroalkyl Contaminants in the Canadian Arctic: Evidence of Atmospheric Transport and Local Contamination. Environmental Science & Technology 41:3529–3536.

Tomy, G. T., S. A. Tittlemier, V. P. Palace, W. R. Budakowski, E. Braekevelt, L. Brinkworth, and K. Friesen. 2004. Biotransformation of N-ethyl perfluorooctanesulfonamide by rainbow trout (Onchorhynchus mykiss) liver microsomes. Environmental Science & Technology 38:758–762.

UK Health Protection Agency. 2007. Maximum acceptable concentrations of perfluorooctane sulfonate (PFOS) and perfluorooctanoic acid (PFOA) in drinking water.

US DoD. 2017. Aqueous Film Forming Foam Report to Congress No.18-C-0270.

US EPA. 2016. Fact Sheet PFOA and PFOS Drinking Water Health Advisories. EPA800-F-16-003.

US EPA. 2022a. Lifetime Drinking Water Health Advisories for Four Perfluoroalkyl Substances, 87 FR 36848.

US EPA. 2022b. ToxCast & Tox21.

US EPA. 2023a. Proposed PFAS National Primary Drinking Water Regulation.

US EPA. 2023b. CompTox Chemicals Dashboard. U.S. Environmental Protection Agency.

Vierke, L., U. Berger, and I. T. Cousins. 2013. Estimation of the Acid Dissociation Constant of Perfluoroalkyl Carboxylic Acids through an Experimental Investigation of their Water-to-Air Transport. Environmental Science & Technology 47:11032–11039.

Wang, Z., I. T. Cousins, M. Scheringer, and K. Hungerbuehler. 2015. Hazard assessment of fluorinated alternatives to long-chain perfluoroalkyl acids (PFAAs)

and their precursors: Status quo, ongoing challenges and possible solutions. Environment International 75:172–179.

Wang, Z., J. C. DeWitt, C. P. Higgins, and I. T. Cousins. 2017. A Never-Ending Story of Per- and Polyfluoroalkyl Substances (PFASs)? Environmental Science & Technology 51:2508–2518.

Wang, Z., M. MacLeod, I. T. Cousins, M. Scheringer, K. Hungerbühler, Z. Wang, M. MacLeod, I. T. Cousins, M. Scheringer, and K. Hungerbühler. 2011. Using COSMOtherm to predict physicochemical properties of poly- and perfluorinated alkyl substances (PFASs). Environmental Chemistry 8:389–398.

Wilcockson, J. B., and F. A. P. C. Gobas. 2001. Thin-Film Solid-Phase Extraction To Measure Fugacities of Organic Chemicals with Low Volatility in Biological Samples | Environmental Science & Technology 35:1425–1431.

Witt, G., G. A. Liehr, D. Borck, and P. Mayer. 2009. Matrix solid-phase microextraction for measuring freely dissolved concentrations and chemical activities of PAHs in sediment cores from the western Baltic Sea. Chemosphere 74:522–529.

World Health Organization. 2022. PFOS and PFOS in Drinking-water, Background document for development of WHO guidelines for Drinking-water Quality.

Worley, R. R., S. M. Moore, B. C. Tierney, X. Ye, A. M. Calafat, S. Campbell, M. B. Woudneh, and J. Fisher. 2017. Per- and polyfluoroalkyl substances in human serum and urine samples from a residentially exposed community. Environment International 106:135–143.

# Appendix A.

## Physical and Chemical Properties of PFOS

**Table A1. Solubilities (mg/L) of PFOS in pure water**

| Form | Value (mg/L) | Temperature | Type | Source |
|---|---|---|---|---|
| acid | $3.10 \times 10^{-3}$ | NR | P-EPIsuite | 1 |
| | 2.36 | NR | P-TEST | 1 |
| | 60 | NR | P-COSMOtherm | 2 |
| | 409 | 25 | P-OPERA | 1 |
| | 2701 | NR | P-ACD Lab | 1 |
| ion | 406 | 25 | P-OPERA | 1 |
| | 2695 | NR | P-ACD Lab | 1 |
| DEA salt | 2.86 | NR | P-TEST | 1 |
| | 494 | 25 | P-OPERA | 1 |
| | 3268 | NR | P-ACD Lab | 1 |
| K salt | 0.12 | NR | P-EPIsuite | 1 |
| | 2.54 | 25 | P-TEST | 1 |
| | 440 | 25 | P-OPERA | 1 |
| | 498 | NR | E | 1 |
| | 519 | 25 | E | 3 |
| | 570 | 20 | E | 4 |
| | 680 | 25 | E | 5 |
| | 910 | 25 | E | 6 |
| | 2906 | NR | P-ACD Lab | 1 |
| Li salt | 0.20 | NR | P-EPIsuite | 1 |
| | 2.39 | NR | P-TEST | 1 |
| | 413 | 25 | P-OPERA | 1 |
| | 557 | NR | E | 1 |
| | 2733 | NR | P-ACD Lab | 1 |
| Na salt | 2.46 | NR | P-TEST | 1 |
| | 427 | 25 | P-OPERA | 1 |
| | 2819 | NR | P-ACD Lab | 1 |
| $NH_4$ salt | 2.44 | NR | P-TEST | 1 |
| | 423 | 25 | P-OPERA | 1 |
| | 2793 | NR | P-ACD Lab | 1 |

**Table A2. Melting temperatures (°C) of PFOS**

| Form | Value (°C) | Temperature | Type | Source |
|---|---|---|---|---|
| acid | 15.2 | | P-TEST | 1 |
| | 51.9 | | P-EPIsuite | 1 |
| | 90 | | P | 7 |
| | 185 | | P-OPERA | 1 |
| ion | 185 | | P-OPERA | 1 |
| DEA salt | 15.2 | | P-TEST | 1 |
| | 182 | | P-OPERA | 1 |
| K salt | 15.2 | | P-TEST | 1 |
| | 192 | | P-EPIsuite | 1 |
| | 285 | | E | 1 |
| | 285 | | E | 4 |
| | 285 | | P | 7 |
| | 400 | | P-OPERA | 1 |
| Li salt | 15.20 | | P-TEST | 1 |
| | 192 | | P-EPIsuite | 1 |
| | 193 | | P-OPERA | 1 |
| Na salt | 15.20 | | P-TEST | 1 |
| | 242 | | P-OPERA | 1 |
| $NH_4$ salt | 15.20 | | P-TEST | 1 |
| | 209 | | P-OPERA | 1 |

**Table A3. Vapour pressures (Pa) of PFOS**

| Form | Value (Pa) | Temperature | Type | Source |
|---|---|---|---|---|
| acid | $3.31 \times 10^{-4}$ | 25 | P-OPERA | 1 |
| | 1.60 | 25 | P-COSMOtherm | 8 |
| | 3.50 | 25 | P-SPARC | 8 |
| | 6.80 | NR | P-COSMOtherm | 2 |
| | 17 | 25 | P | 9 |
| | 34 | 25 | P-EPIsuite | 8 |
| ion | $3.31 \times 10^{-4}$ | 25 | P-OPERA | 1 |
| K salt | $3.31 \times 10^{-4}$ | 25 | P-OPERA | 1 |
| | $3.31 \times 10^{-4}$ | 20 | E | 4 |
| Li salt | $3.31 \times 10^{-4}$ | 25 | P-OPERA | 1 |
| Na salt | $3.31 \times 10^{-4}$ | 25 | P-OPERA | 1 |

| | | | | |
|---|---|---|---|---|
| $NH_4$ salt | $3.31 \times 10^{-4}$ | 25 | P-OPERA | 1 |

**Table A4. Henry's constants (Pa-m$^3$/mol) of PFOS**

| Form | Value (Pa-m$^3$/mol) | Temperature | Type | Source |
|---|---|---|---|---|
| ion | $1.82 \times 10^{-6}$ | 25 | P-OPERA | 1 |
| acid | $1.82 \times 10^{-6}$ | 25 | P-OPERA | 1 |
| | 6.30 | 25 | P-COSMOtherm | 10 |
| | 9.90 | 25 | P-COSMOtherm | 8 |
| | 100 | 25 | P-ABSOLV | 10 |
| | 120 | 25 | P-SPARC | 10 |
| | 220 | 25 | P-SPARC | 8 |
| | 1100 | 25 | P-EPIsuite | 10 |
| | $4.80 \times 10^{6}$ | 25 | P | 9 |
| DEA salt | $1.82 \times 10^{-6}$ | 25 | P-OPERA | 1 |
| K salt | $1.82 \times 10^{-6}$ | 25 | P-OPERA | 1 |
| Li salt | $1.82 \times 10^{-6}$ | 25 | P-OPERA | 1 |
| Na salt | $1.82 \times 10^{-6}$ | 25 | P-OPERA | 1 |
| $NH_4$ salt | $1.82 \times 10^{-6}$ | 25 | P-OPERA | 1 |

**Table A5. Critical micelle concentrations (mg/L) of PFOS**

| Form | Value (mg/L) | Temperature | Type | Source |
|---|---|---|---|---|
| acid | 536 | 25 | E | 11 |
| | 1200 | 25 | P | 11 |
| K salt | 4537 | NR | P | 12 |

**Table A6. p$K_a$ of PFOS**

| Form | Value | Temperature | Type | Source |
|---|---|---|---|---|
| acid | -1.64 | 25 | P-OPERA | 1 |
| | 0.14 | NR | P-SPARC | 14 |
| ion | -1.64 | 25 | P-OPERA | 1 |
| | 0.14 | NR | P-SPARC | 15 |
| K salt | -1.64 | 25 | P-OPERA | 1 |

| | | | | |
|---|---|---|---|---|
| | <0.3 | NR | E | 13 |
| | <1 | NR | E | 16 |
| Li salt | -1.64 | 25 | P-OPERA | 1 |
| Na salt | -1.64 | 25 | P-OPERA | 1 |
| $NH_4$ salt | -1.64 | 25 | P-OPERA | 1 |

1-(US EPA 2023b)
2-(Wang et al. 2011)
3-(OECD 2002)
4-(3M Company 2000)
5-(Ellefson 2001)
6-(Inoue et al. 2012)
7-(ChemSpider 2023)
8-(Arp et al. 2006)
9-(Kim et al. 2015)
10-(Zhang et al. 2010)
11-(Bhhatarai and Gramatica 2011)
12-(Yu et al. 2008)
13-(Vierke et al. 2013)
14-(ATSDR 2021)
15-(Steinle-Darling and Reinhard 2008)
16-(Cheng et al. 2009)
NR: Not reported; E: Experimental; P: Predicted (models indicated when available); DEA: Diethanolamine.

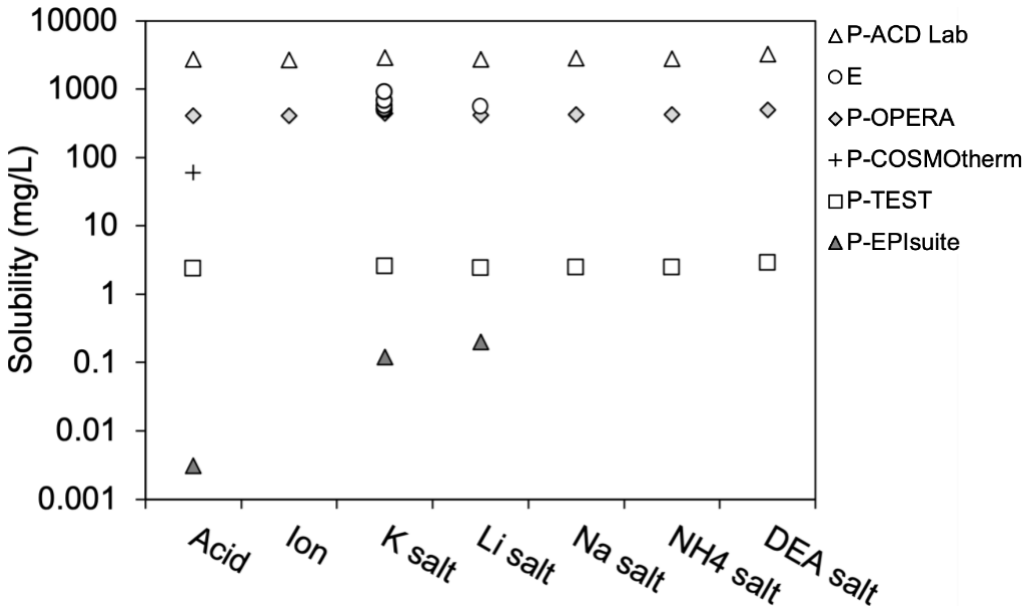


**Figure A1. Predicted (P) and experimentally measured (E) solubilities (mg/L) of PFOS in pure water.**

DEA: Diethanolamine

# Preparation of Potassium Phosphate Buffered Saline

**Table A7. Formulation of 30mM potassium phosphate buffered saline at pH 7.4**

| | Conjugate base | Conjugate acid |
|---|---|---|
| **Name** | Potassium phosphate dibasic | Potassium dihydrogen phosphate |
| **Molecular formula** | $K_2HPO_4$ | $KH_2PO_4$ |
| **Molecular weight (g/mol)** | 174.18 | 136.09 |
| **CAS #** | 7758-11-4 | 7778-77-0 |
| **Concentration (M)** | 0.0209 | 0.0091 |

**Table A8. Calculation of ionic strength of 30 mM potassium phosphate buffered saline at pH 7.4**

| | Ions | $c_i$ (M) | $z^2$ | $(c_i \cdot z^2)$ |
|---|---|---|---|---|
| **Conjugate base** | $K^+$ | 0.0418 | 1 | $0.0418 \cdot 1^2$ |
| | $HPO_4^{2-}$ | 0.0209 | 2- | $0.0209 \cdot (-2)^2$ |
| **Conjugate acid** | $K^+$ | 0.0091 | 1 | $0.0091 \cdot 1^2$ |
| | $H_2PO_4^-$ | 0.0091 | 1- | $0.0091 \cdot (-1)^2$ |
| **Ionic strength (M)** | | | | 0.0717 |

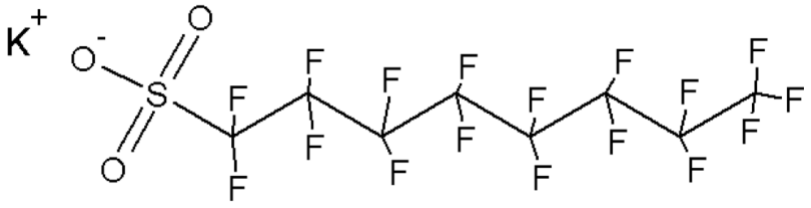


**Figure A2. Structural formula of PFOS as its potassium salt.**

## pH of PFOS-K in Water and PBS at pH 7.4

As illustrated in Figures A3 and A4, the pH of PFOS-K in water decreased from 5.898 to 5.030 as its concentration increased. In contrast, the pH of PFOS in PBS remained stable at an average of 7.421, irrespective of changes in concentration (data not shown in figures). The pH of deionized water was measured at 6.499. Overall, these pH measurements at different concentrations of PFOS-K in water are consistent with the findings by Chen and Colleagues (2021), as shown in Figure A3.

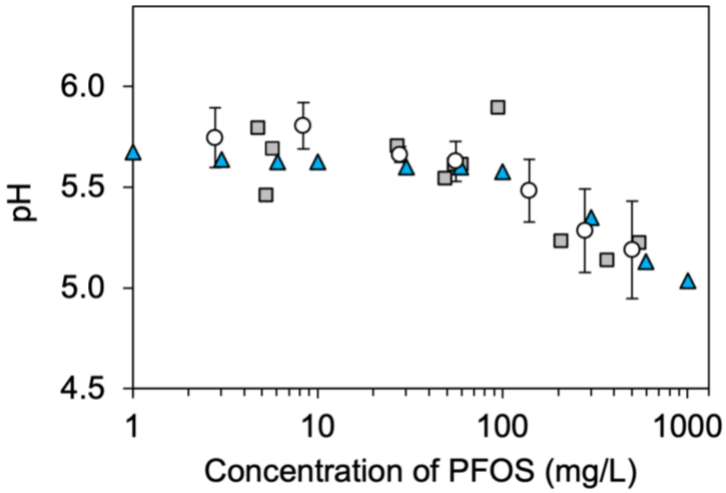


**Figure A3.** **pH of PFOS-K in deionized water. Circles (n=3) and squares (n=1) are measurements from this study, while triangles are measurements from Chen et al. 2021. PFOS concentrations shown in circles are nominal, while those in squares are quantified by the LC MS/MS.**

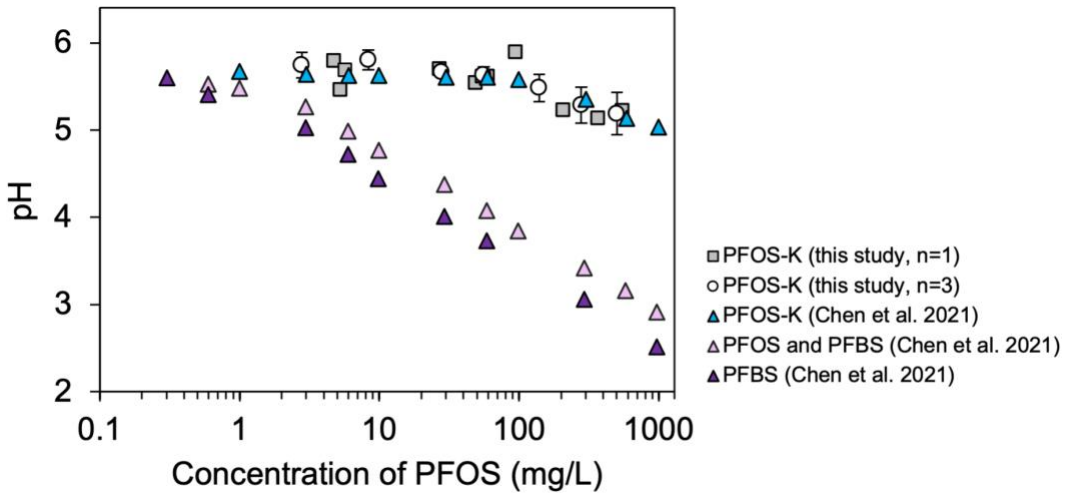


**Figure A4. pH of PFOS-K, PFBS, and mixture of PFOS ad PFBS in deionized water. Data in triangles are obtained from Chen et al. 2021.**

Additionally, the authors also observed a decrease in pH for the mixture of the acid form of PFOS and perfluorobutane sulfonate (PFBS) at increasing concentrations. Figure A4 shows that both the mixture of PFOS and PBBS and PFBS alone exhibit similar downward slopes in pH, both of which are steeper than those observed for PFOS-K in water. These findings may suggest that the potassium counter ion of PFOS-K limits the overall variation in pH, and that the acid PFOS on its own would otherwise show a steep decline in pH as its concentration increases in water.

The recorded pH values in this study were also used to calculate the dissociation status of PFOS acid using the modeled p$K_a$ of 0.3. Figure A4 shows that the anionic form overwhelmingly dominates the solution for the tested concentrations ranging from 5 mg/L to 550 mg/L. Even when the lowest modeled p$K_a$ at -5.45 was applied, the predominant form was still anionic.

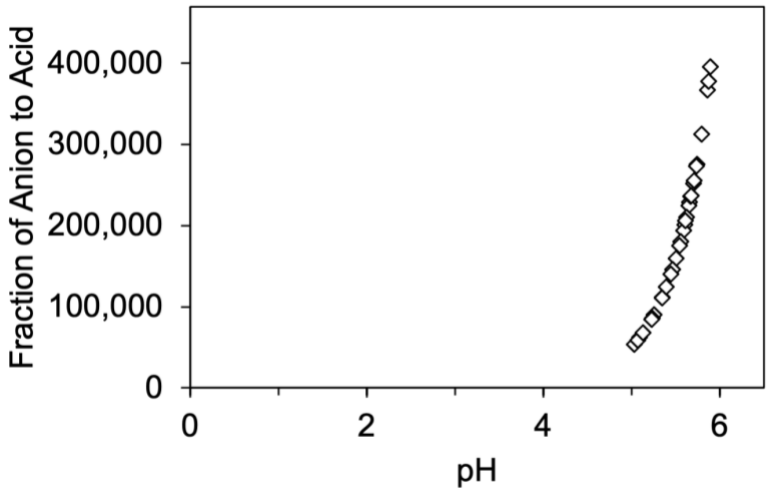


**Figure A3. Relationship between pH of PFOS-K in deionized water and dissociation status. The fractiion of anion to acid was derived with the highest modeled p$K_a$ of 0.3.**

The observed pH variability in this study can be explained by uncertainties related to measurements taken under high-concentration and high-ionic strength solutions. Generally, highly concentrated samples can impede the mobility of hydrogen ions, making it difficult for electrodes to accurately detect them for pH analysis. Additionally, high-ionic strength samples can cause a charge imbalance with the electrode filling solution, resulting in fluctuations in the liquid junction potential. The use of the potassium-PFOS salt may also influence the overall pH due to the presence of potassium counter ions. These factors could have each contributed to the noise observed in the pH data. Future studies on other forms of PFOS, such as salts of ammonium, diethanolamine, and lithium, may help to clarify the effects of PFOS concentration and counter ions on pH.

# Appendix B.

## Solid Phase Microextraction via PDMS

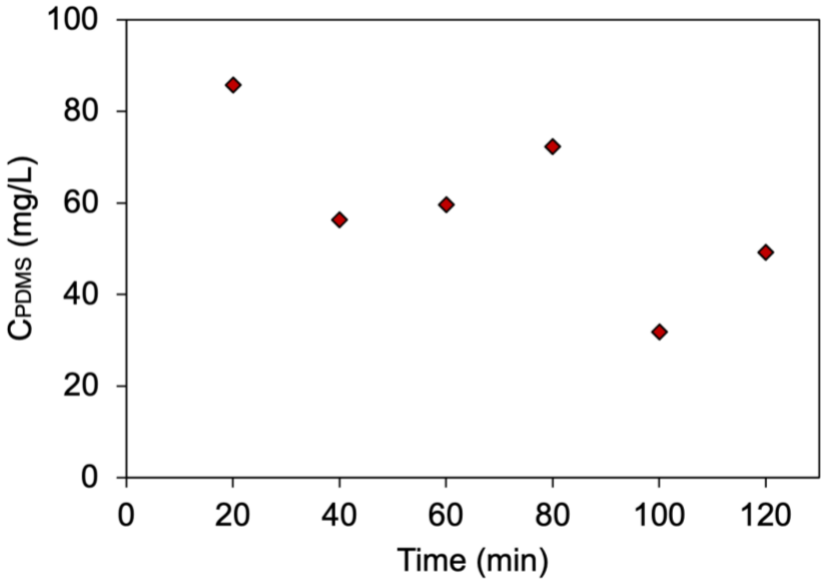


**Figure B1. PDMS sorption of PFOS ($C_{PDMS}$, mg/L) over duration of 2 hours.**
Partitioning was conducted at room temperature between PDMS (Supelco, No. 57308) and solution of PFOS in water at 55 mg/L. Extracted concentrations in methanol were near the detection limits by the LC MS/MS. Overall extraction efficiency of PFOS via methanol was 76.1%. Polyacrylate (Supelco, No. 57304) sorption of PFOS is not shown as its sorption was 10 times lower than that of PDMS.

## Omittance of the Air Phase

The air phase was omitted in the EVA system as the head space was negligible compared to the water phase. PFOS also has very low volatility with a Henry's Law constant at $3.45 \times 10^{-4}$ Pa m$^3$/mol (EFSA 2008), therefore it can be assumed that PFOS does not readily partition into the head space. The following equations further demonstrate the insignificance of the air phase at equilibrium between the water and air.

$$a_w = a_{air}$$

$$\frac{C_w}{S_w} = \frac{C_{air}}{S_{air}}$$

At equilibrium, the activities of PFOS (a, unitless) across different compartments become the identical. The solubility of PFOS in air ($S_{air}$, ng/mL) can be substituted with

$\frac{H \cdot S_w}{R \cdot T}$, the product of Henry's Law constant (H, Pa $m^3$/mol) and the solubility in water ($S_w$, ng/mL) divided by the product of the universal gas constant (R, 8.314 Pa $m^3$/mol K) and the system temperature (T, Kelvin). Both concentrations in the numerator can be replaced with mass (M, ng) over volume (V, mL).

$$\frac{M_w}{S_w \cdot V_w} = \frac{M_{air} \cdot R \cdot T}{V_{air} \cdot H \cdot S_w}$$

$$M_{air} = \frac{M_w \cdot V_{air} \cdot H}{V_w \cdot R \cdot T}$$

After the mass of PFOS in the air phase ($M_{air}$, ng) is isolated, it becomes clear that $M_{air}$ is negligible when the low Henry's constant for PFOS is substituted in.

## EVA Extraction Efficiency via Methanol

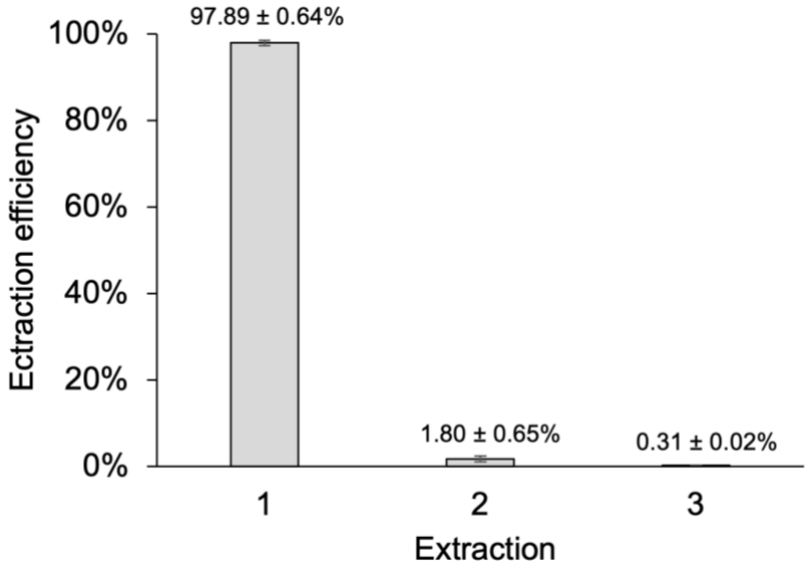


**Figure B2. EVA extraction efficiency of PFOS via methanol (n=3, errors indicated in standard deviations).**

# Appendix C.

## LC MS/MS Methodology and Calibration Curve

**Table C1. LC MS/MS method conditions for PFOS, including A) MS parameters, B) target compounds, C) source and gas parameters, D) LC method conditions, E) optimized MS parameters.**

**A) MS Parameters**

| Field | Value |
|---|---|
| Scan type | Q1 MA (Q1) |
| Start (Da) | 450 |
| Stop (Da) | 550 |
| Duration (min) | 3 |
| Time (sec) | 1 |
| Polarity | Negative |

**B) Target compounds**

| Compound | Q1 Mass (Da) | Q3 Mass (Da) |
|---|---|---|
| $^{13}C_8$ PFOS 1 | 507 | 80 |
| $^{13}C_8$ PFOS 2 | 507 | 99 |
| TPFOS 1 | 499 | 80 |
| TPFOS 2 | 499 | 99 |

**C) Source and gas parameters**

| Field | Value |
|---|---|
| Curtain gas | 40 |
| IonSpray Voltage | -4500 |
| Temperature | 350 |
| Ion Source Gas 1 | 50 |
| Ion Source Gas 2 | 50 |
| CAD | Medium |
| Column | Gemini Phenomenex |

**D) LC method conditions**

| Time (min) | Flow (µL/min) | % 20 mM ammonium acetate | % Methanol |
|---|---|---|---|
| 0.01 | 400 | 40 | 60 |
| 2.50 | 400 | 5 | 95 |
| 2.51 | 400 | 40 | 60 |
| 4.50 | 400 | 40 | 60 |

Injection volume was at 5 µL, and the column temperature at 40 °C.
Mobile phase A: 20 mM Ammonium acetate; Mobile phase B: Methanol

**E) Optimized MS parameters**

| ID | Q1 (Da) | Q3 (Da) | Dwell time (msec) | DP (volts) | CE (volts) | CXP (volts) |
|---|---|---|---|---|---|---|
| $^{13}C_8$ PFOS 1 | 507 | 80* | 150 | -115 | -94 | -1 |
| $^{13}C_8$ PFOS 2 | 507 | 99 | 150 | -95 | -72 | -7 |
| TPFOS 1 | 499 | 80* | 150 | -90 | -94 | -3 |
| TPFOS 2 | 499 | 99 | 150 | -90 | -72 | -5 |

*Used for quantitation

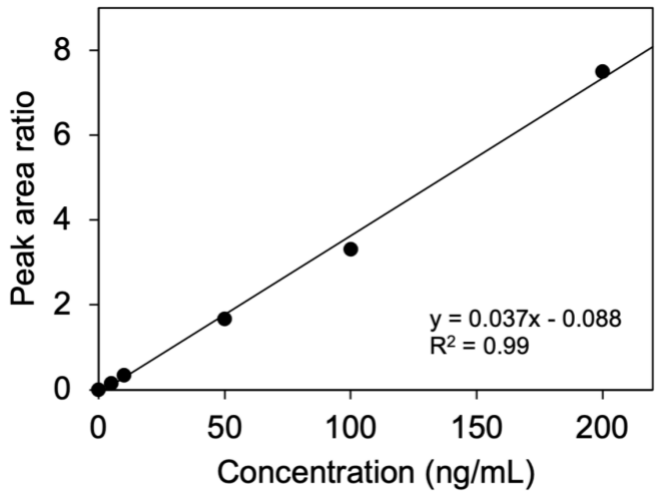


**Figure C3. Calibration curve for PFOS-K based on the peak area of the native PFOS (technical grade) relative to the internal standard ($^{13}C_8$ PFOS) as a function of concentrations of PFOS (ng/mL).**

**Table C2. Limits of detection (LOD) for PFOS in average and standard deviation (SD) by each study**

| Study | LOD ± SD (ng/mL) | Sample size |
|---|---|---|

| | | |
|---|---|---|
| Aqueous solubility | 0.96 ± 0.75 | n = 10 |
| Partitioning of EVA-water | 0.40 ± 0.24 | n = 4 |
| Partitioning of EVA-PBS | 0.96 ± 0.65 | n = 7 |
| Partitioning of EVA-BSA | 1.25 ± 0.62 | n = 10 |

# Appendix D.

## Data on the Solubility of PFOS in Water and PBS at pH 7.4

**Table D1. Solubility (mg/L) of PFOS in water measured at different temperatures (°C).**

| Temperature (°C) | Sample | Time (day) | Solubility (mg/L) | Average solubility (mg/L) | SD (mg/L) |
|---|---|---|---|---|---|
| 2 | 1 | 2 | 445.7 | 400.3 | 49.7 |
| | | 4 | 342.1 | | |
| | | 7 | 375.9 | | |
| | | 10 | 437.3 | | |
| | 2 | 2 | 464.6 | 422.1 | 56.7 |
| | | 4 | 340.8 | | |
| | | 7 | 426.2 | | |
| | | 10 | 456.8 | | |
| | 3 | 2 | 419.2 | 417.3 | 22.3 |
| | | 4 | 386.2 | | |
| | | 7 | 425.2 | | |
| | | 10 | 438.5 | | |
| 12 | 1 | 3 | 495.1 | 527.9 | |
| | | 7 | 560.7 | | |
| | 2 | 3 | 539.6 | | |
| | | 7 | 954.9[a] | | |
| | 3 | 3 | 519.0 | 557.1 | |
| | | 7 | 595.3 | | |
| 21 | 1 | 3 | 506.3 | 502.9 | |
| | | 7 | 499.5 | | |
| | 2 | 3 | 391.6 | 461.8 | |
| | | 7 | 532.0 | | |
| | 3 | 3 | 302.5 | 394.8 | |
| | | 7 | 487.2 | | |
| 22.5[b] | 1 | 2 | 702.9 | 729.0 | 22.4 |
| | | 4 | 720.1 | | |
| | | 7 | 754.8 | | |
| | | 10 | 738.1 | | |
| | 2 | 2 | 549.6 | 584.7 | 23.4 |
| | | 4 | 597.9 | | |

| | | | | | |
|---|---|---|---|---|---|
| | | 7 | 596.1 | | |
| | | 10 | 595.2 | | |
| | 3 | 2 | 593.4 | 618.2 | 57.0 |
| | | 4 | 576.8 | | |
| | | 7 | 702.3 | | |
| | | 10 | 600.1 | | |
| 37 | 1 | 3 | 479.0 | 498.3 | |
| | | 7 | 517.6 | | |
| | 2 | 3 | 406.3 | 418.2 | |
| | | 7 | 430.0 | | |
| | 3 | 3 | 466.2 | 495.4 | |
| | | 7 | 524.6 | | |
| 37 | 1 | 2 | 588.5 | 581.7 | 54.3 |
| | | 3 | 566.3 | | |
| | | 4 | 605.3 | | |
| | | 7 | 500.7 | | |
| | | 10 | 647.8 | | |
| | 2 | 2 | 510.4 | 511.1 | 9.9 |
| | | 3 | 497.3 | | |
| | | 4 | 524.7 | | |
| | | 7 | 513.9 | | |
| | | 10 | 509.4 | | |
| | 3 | 2 | 582.0 | 606.1 | 27.7 |
| | | 3 | 572.8 | | |
| | | 4 | 612.1 | | |
| | | 7 | 628.7 | | |
| | | 10 | 635.1 | | |

[a] excluded as outlier, [b] PFOS was dissolved in MS-grade water.

**Table D2. Solubility (mg/L) of PFOS in 30mM phosphate buffered saline at pH 7.4 measured at different temperatures (°C).**

| Temperature (°C) | Sample | Time (day) | Solubility (mg/L) | Average solubility (mg/L) | SD (mg/L) |
|---|---|---|---|---|---|
| 12 | 1 | 5 | 16.4 | 15.2 | |
| | | 7 | 14.1 | | |
| | 2 | 5 | 18.5 | 18.4 | |
| | | 7 | 18.2 | | |
| | 3 | 5 | 21.5 | 22.1 | |
| | | 7 | 22.7 | | |
| 21 | 1 | 3 | 37.9 | 38.3 | |
| | | 7 | 38.6 | | |
| | 2 | 3 | 29.2 | 30.1 | |
| | | 7 | 31.1 | | |
| | 3 | 3 | 30.6 | 29.7 | |
| | | 7 | 28.7 | | |
| 22 | 1 | 2 | 61.1 | 52.5 | 11.8 |
| | | 7 | 51.2 | | |
| | | 8 | 50.2 | | |
| | | 13 | 30.6 | | |
| | | 15 | 62.0 | | |
| | | 19 | 47.1 | | |
| | | 21 | 65.2 | | |
| | 2 | 2 | 43.5 | 42.6 | 7.9 |
| | | 4 | 37.4 | | |
| | | 8 | 37.1 | | |
| | | 10 | 39.4 | | |
| | | 15 | 45.7 | | |
| | | 18 | 36.6 | | |
| | | 30 | 58.6 | | |
| | 3 | 1 | 49.3 | 49.4 | 6.8 |
| | | 2 | 56.6 | | |
| | | 13 | 40.4 | | |
| | | 21 | 51.3 | | |
| 37 | 1 | 3 | 33.5 | 34.6 | |
| | | 7 | 35.6 | | |
| | 2 | 3 | 35.0 | 34.6 | |
| | | 7 | 34.2 | | |

| | | | | | |
|---|---|---|---|---|---|
| | 3 | 3 | 33.6 | 36.4 | |
| | | 7 | 39.2 | | |
| | 1 | 2 | 15.9 | 17.8 | 3.6 |
| | | 3 | 14.2 | | |
| | | 4 | 16.3 | | |
| | | 7 | 19.4 | | |
| | | 10 | 23.3 | | |
| 37 | 2 | 2 | 23.3 | 25.18 | 3.6 |
| | | 3 | 23.2 | | |
| | | 4 | 23.6 | | |
| | | 7 | 24.2 | | |
| | | 10 | 31.6 | | |
| | 3 | 2 | 24.3 | 31.04 | 8.0 |
| | | 3 | 25.2 | | |
| | | 4 | 42.0 | | |
| | | 7 | 26.7 | | |
| | | 10 | 37.0 | | |

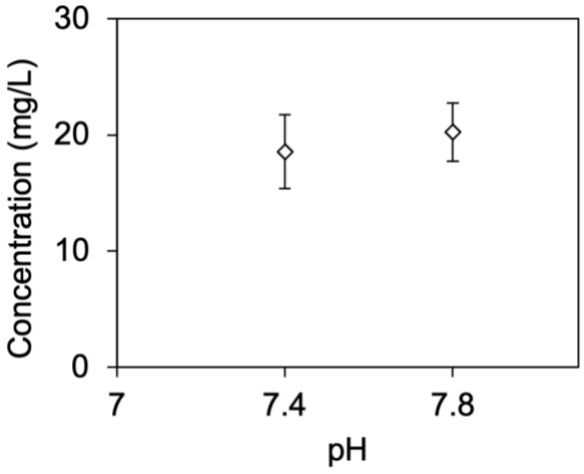


**Figure D4. Solubility (mg/L) of PFOS in 30mM phosphate buffered saline at pH 7.4 (n=3) and pH 7.8 (n=3) at 12 °C. Error bars indicated in standard deviation.**

The student t-test concluded no significant difference between the solubilities of PFOS in PBS at pH 7.4 and pH 7.8 (p-value = 0.2383).

# Appendix E.

## Data on the Partitioning of EVA-Water and EVA-PBS

**Table E1. Details on the partitioning of PFOS from water to EVA, including the concentration of PFOS in water ($C_W$, mg/L), concentration of PFOS in EVA ($C_{EVA}$, mg/L), partition coefficient of PFOS between EVA-water ($K_{EVA-W}$, unitless), calculated apparent chemical activity of PFOS in water ($a_W$, unitless), and EVA-measured apparent chemical activity of PFOS in EVA ($a_{EVA}$, unitless).**

| $C_W$ | $C_{EVA}$ | $K_{EVA-W}$[a] | $a_W$[b] | $a_{EVA}$[c] |
|---|---|---|---|---|
| mg/L | mg/L | unitless | unitless | unitless |
| 0.014 | 7.9 | 578 | 4.75E-07 | 1.83E-05 |
| 0.028 | 4.8 | 174 | 9.57E-07 | 1.12E-05 |
| 0.032 | 10.4 | 332 | 1.08E-06 | 2.40E-05 |
| 0.064 | 10.3 | 163 | 2.18E-06 | 2.39E-05 |
| 0.070 | 24.0 | 346 | 2.39E-06 | 5.56E-05 |
| 0.074 | 12.1 | 164 | 2.53E-06 | 2.79E-05 |
| 0.106 | 15.4 | 145 | 3.62E-06 | 3.55E-05 |
| 0.177 | 20.5 | 116 | 6.05E-06 | 4.75E-05 |
| 0.199 | 25.5 | 128 | 6.81E-06 | 5.91E-05 |
| 0.202 | 31.5 | 156 | 6.89E-06 | 7.29E-05 |
| 0.322 | 23.5 | 73.1 | 1.10E-05 | 5.43E-05 |
| 1.88 | 81.6 | 43.4 | 6.43E-05 | 1.89E-04 |
| 1.89 | 87.6 | 46.4 | 6.45E-05 | 2.03E-04 |
| 1.91 | 53.1 | 27.8 | 6.53E-05 | 1.23E-04 |
| 3.54 | 202.0 | 57.1 | 1.21E-04 | 4.68E-04 |
| 3.68 | 96.0 | 26.1 | 1.26E-04 | 2.22E-04 |
| 4.05 | 207.5 | 51.3 | 1.38E-04 | 4.81E-04 |
| 4.06 | 214.0 | 52.6 | 1.39E-04 | 4.95E-04 |
| 4.99 | 293.6 | 59.0 | 1.70E-04 | 6.80E-04 |
| 4.99 | 321.4 | 64.6 | 1.70E-04 | 7.44E-04 |
| 4.99 | 247.0 | 49.6 | 1.70E-04 | 5.72E-04 |
| 5.98 | 343.7 | 57.6 | 2.04E-04 | 7.96E-04 |
| 10.0 | 516.0 | 51.6 | 3.42E-04 | 1.19E-03 |
| 31.2 | 1038.3 | 33.3 | 1.07E-03 | 2.40E-03 |
| 60.2 | 1586.3 | 26.4 | 2.06E-03 | 3.67E-03 |
| 143.7 | 3137.9 | 21.9 | 4.91E-03 | 7.27E-03 |

| | | | | |
|---|---|---|---|---|
| 278.3 | 5305.0 | 19.1 | 9.51E-03 | 1.23E-02 |
| 278.3 | 5433.4 | 19.5 | 9.51E-03 | 1.26E-02 |
| 278.3 | 4545.5 | 16.3 | 9.51E-03 | 1.05E-02 |
| 343.2 | 4242.7 | 12.4 | 1.17E-02 | 9.82E-03 |
| 463.8 | 8861.6 | 19.1 | 1.58E-02 | 2.05E-02 |
| 463.8 | 7676.0 | 16.6 | 1.58E-02 | 1.78E-02 |
| 463.8 | 7944.4 | 17.1 | 1.58E-02 | 1.84E-02 |
| 525.6 | 6550.9 | 12.5 | 1.80E-02 | 1.52E-02 |
| 525.6 | 8712.0 | 16.6 | 1.80E-02 | 2.02E-02 |
| 525.6 | 9133.9 | 17.4 | 1.80E-02 | 2.11E-02 |
| 618.3 | 10526.2 | 17.0 | 2.11E-02 | 2.44E-02 |
| 618.3 | 11142.2 | 18.0 | 2.11E-02 | 2.58E-02 |
| 618.3 | 10308.1 | 16.7 | 2.11E-02 | 2.39E-02 |
| 684.9 | 9928.4 | 14.5 | 2.34E-02 | 2.30E-02 |

[a] Calculated by $C_{EVA}$ (mg/L) ÷ $C_W$ (mg/L), where $C_W$ was mass-adjusted for PFOS loss to EVA.
[b] Calculated using $S_W$ (mg/L) = 664.3, F = 0.023.
[c] Calculated using $S_{EVA}$ (mg/L) = 9933.99, F = 0.023.

**Table E2. Details on the partitioning of PFOS from 30mM phosphate buffered saline (pH 7.4) to EVA, including the concentration of PFOS in PBS ($C_{PBS}$, mg/L), concentration of PFOS in EVA ($C_{EVA}$, mg/L), partition coefficient of PFOS between EVA-PBS ($K_{EVA-PBS}$, unitless), calculated apparent chemical activity of PFOS in PBS ($a_{PBS}$, unitless), and EVA-measured apparent chemical activity of PFOS in EVA ($a_{EVA}$, unitless).**

| $C_{PBS}$ | $C_{EVA}$ | $K_{EVA-PBS}$[a] | $a_{PBS}$[b] | $a_{EVA}$[c] |
|---|---|---|---|---|
| mg/L | mg/L | unitless | unitless | unitless |
| 0.010 | 10.47 | 1083 | 5.14E-06 | 2.43E-05 |
| 0.012 | 25.52 | 2312 | 6.07E-06 | 5.91E-05 |
| 0.012 | 25.24 | 2285 | 6.07E-06 | 5.84E-05 |
| 0.012 | 18.86 | 1678 | 6.07E-06 | 4.37E-05 |
| 0.026 | 52.70 | 2135 | 1.35E-05 | 1.22E-04 |
| 0.026 | 35.08 | 1392 | 1.35E-05 | 8.12E-05 |
| 0.026 | 30.24 | 1193 | 1.35E-05 | 7.00E-05 |
| 0.028 | 24.99 | 901 | 1.47E-05 | 5.79E-05 |
| 0.047 | 34.99 | 767 | 2.40E-05 | 8.10E-05 |
| 0.11 | 67.24 | 623 | 5.66E-05 | 1.56E-04 |
| 0.25 | 111.7 | 457 | 1.27E-04 | 2.59E-04 |
| 0.27 | 264.3 | 1003 | 1.40E-04 | 6.12E-04 |
| 0.47 | 270.2 | 581 | 2.44E-04 | 6.26E-04 |

| | | | | |
|---|---|---|---|---|
| 0.96 | 375.8 | 397 | 4.93E-04 | 8.70E-04 |
| 2.02 | 1039.3 | 527 | 1.04E-03 | 2.41E-03 |
| 2.62 | 1211.7 | 471 | 1.35E-03 | 2.81E-03 |
| 3.92 | 1425.8 | 369 | 2.02E-03 | 3.30E-03 |
| 7.05 | 2733.6 | 394 | 3.63E-03 | 6.33E-03 |
| 8.06 | 2222.4 | 279 | 4.15E-03 | 5.15E-03 |
| 8.08 | 1755.7 | 219 | 4.16E-03 | 4.06E-03 |
| 11.0 | 1917.4 | 176 | 5.64E-03 | 4.44E-03 |
| 11.2 | 5933.4 | 543 | 5.75E-03 | 1.37E-02 |
| 18.6 | 5104.7 | 278 | 9.56E-03 | 1.18E-02 |
| 21.7 | 3389.3 | 157 | 1.12E-02 | 7.85E-03 |
| 32.5 | 5044.2 | 156 | 1.67E-02 | 1.17E-02 |
| 32.5 | 10899.7 | 340 | 1.67E-02 | 2.52E-02 |
| 32.5 | 5148.6 | 160 | 1.67E-02 | 1.19E-02 |
| 36.8 | 8915.8 | 245 | 1.89E-02 | 2.06E-02 |
| 36.8 | 14065.7 | 388 | 1.89E-02 | 3.26E-02 |
| 36.8 | 15826.1 | 438 | 1.89E-02 | 3.66E-02 |
| 39.0 | 12284.1 | 319 | 2.00E-02 | 2.84E-02 |
| 39.0 | 13442.3 | 350 | 2.00E-02 | 3.11E-02 |
| 39.0 | 11135.3 | 289 | 2.00E-02 | 2.58E-02 |
| 43.3 | 14409.1 | 338 | 2.23E-02 | 3.34E-02 |
| 43.3 | 11056.9 | 258 | 2.23E-02 | 2.56E-02 |
| 43.3 | 14013.8 | 328 | 2.23E-02 | 3.24E-02 |

[a] Calculated by $C_{EVA}$ (mg/L) ÷ $C_{PBS}$ (mg/L), where $C_{PBS}$ was mass-adjusted for PFOS loss to EVA.
[b] Calculated using $S_{PBS}$ (mg/L) = 44.1, F = 0.023.
[c] Calculated using $S_{EVA}$ (mg/L) = 9933.99, F = 0.023.

# Appendix F.

## Data on the Partitioning of PFOS between BSA solution and EVA

**Table F1.** **Details on the partitioning of PFOS between BSA solution and EVA at various PFOS:BSA molar ratios, including concentration of PFOS ($C_{Soln}$, mg/L) and BSA (BSA, g/L) in incubation solution, equilibrated EVA concentration ($C_{EVA}$, mg/L), apparent chemical activity of incubation solution ($a_{Soln}$, unitless) calculated through $C_{EVA} \times F \div S_{EVA}$ and Equation (31), sorptive capacity of BSA for PFOS ($S_{BSA}$, mg/L), and Log partition coefficient of PFOS between BSA and solution (Log $K_{BSA-PBS}$, unitless).**

| PFOS:BSA | $C_{Soln}$[a] | BSA[b] | $C_{EVA}$ | $a_{Soln}$[c] | $S_{BSA}$[d] | Log $K_{BSA-PBS}$ | $a_{Soln}$[e] | $S_{BSA}$[d] | Log $K_{BSA-PBS}$ |
|---|---|---|---|---|---|---|---|---|---|
| mol/mol | mg/L | g/L | mg/L | unitless | mg/L | unitless | unitless | mg/L | unitless |
| 2.80E-04 | 0.023 | 10 | 2.59 | 6.00E-06 | 3.79E+05 | 3.93 | 4.33E-07 | 5.31E+06 | 5.08 |
| 3.70E-04 | 0.060 | 20 | 0.25 | 5.83E-07 | 5.15E+06 | 5.07 | 2.04E-08 | 1.47E+08 | 6.52 |
| 4.00E-04 | 0.023 | 7 | 2.38 | 5.50E-06 | 5.88E+05 | 4.12 | 3.86E-07 | 8.46E+06 | 5.28 |
| 5.70E-04 | 0.023 | 5 | 3.84 | 8.88E-06 | 5.08E+05 | 4.06 | 7.23E-07 | 6.34E+06 | 5.16 |
| 7.40E-04 | 0.060 | 10 | 0.40 | 9.35E-07 | 6.41E+06 | 5.16 | 3.79E-08 | 1.58E+08 | 6.56 |
| 1.43E-03 | 0.023 | 2 | 5.36 | 1.24E-05 | 9.03E+05 | 4.31 | 1.12E-06 | 1.02E+07 | 5.36 |
| 1.48E-03 | 0.060 | 5 | 0.36 | 8.35E-07 | 1.44E+07 | 5.51 | 3.27E-08 | 3.67E+08 | 6.92 |
| 3.40E-03 | 0.138 | 5 | 4.06 | 9.40E-06 | 2.93E+06 | 4.82 | 7.79E-07 | 3.55E+07 | 5.91 |
| 3.56E-03 | 0.023 | 0.80 | 8.73 | 2.02E-05 | 1.35E+06 | 4.49 | 2.12E-06 | 1.34E+07 | 5.48 |
| 3.71E-03 | 0.060 | 2 | 0.76 | 1.77E-06 | 1.69E+07 | 5.58 | 8.72E-08 | 3.43E+08 | 6.89 |
| 8.50E-03 | 0.138 | 2 | 9.95 | 2.30E-05 | 2.97E+06 | 4.83 | 2.52E-06 | 2.73E+07 | 5.79 |
| 9.27E-03 | 0.060 | 0.80 | 1.40 | 3.25E-06 | 2.29E+07 | 5.72 | 1.93E-07 | 3.86E+08 | 6.94 |
| 1.14E-02 | 0.023 | 0.25 | 11.88 | 2.75E-05 | 3.12E+06 | 4.85 | 3.18E-06 | 2.84E+07 | 5.81 |
| 0.02 | 0.0078 | 0.05 | 13.67 | 3.16E-05 | 3.67E+06 | 4.92 | 3.82E-06 | 3.66E+07 | 5.92 |
| 0.02 | 0.0078 | 0.05 | 27.12 | 6.28E-05 | 1.31E+06 | 4.47 | 9.39E-06 | 1.36E+07 | 5.49 |
| 0.02 | 0.0078 | 0.05 | 27.24 | 6.31E-05 | 1.30E+06 | 4.47 | 9.44E-06 | 1.35E+07 | 5.49 |

| | | | | | | | | | |
|---|---|---|---|---|---|---|---|---|---|
| 0.02 | 0.0088 | 0.05 | 9.91 | 2.30E-05 | 6.39E+06 | 5.16 | 2.51E-06 | 6.56E+07 | 6.17 |
| 0.02 | 0.0088 | 0.05 | 8.50 | 1.97E-05 | 7.66E+06 | 5.24 | 2.05E-06 | 8.10E+07 | 6.26 |
| 0.02 | 0.0088 | 0.05 | 6.75 | 1.56E-05 | 9.96E+06 | 5.35 | 1.52E-06 | 1.11E+08 | 6.40 |
| 0.02 | 0.157 | 1 | 26.11 | 6.04E-05 | 2.54E+06 | 4.76 | 8.93E-06 | 1.74E+07 | 5.60 |
| 0.02 | 0.157 | 1 | 25.59 | 5.93E-05 | 2.59E+06 | 4.77 | 8.70E-06 | 1.79E+07 | 5.61 |
| 0.02 | 0.157 | 1 | 35.31 | 8.17E-05 | 1.86E+06 | 4.63 | 1.33E-05 | 1.17E+07 | 5.42 |
| 0.02 | 0.169 | 1 | 16.27 | 3.77E-05 | 4.43E+06 | 5.00 | 4.81E-06 | 3.51E+07 | 5.90 |
| 0.02 | 0.169 | 1 | 18.31 | 4.24E-05 | 3.93E+06 | 4.95 | 5.61E-06 | 3.00E+07 | 5.83 |
| 0.02 | 0.169 | 1 | 17.69 | 4.10E-05 | 4.07E+06 | 4.97 | 5.36E-06 | 3.14E+07 | 5.85 |
| 0.02 | 1.59 | 10 | 45.29 | 1.05E-04 | 1.51E+06 | 4.53 | 1.84E-05 | 8.61E+06 | 5.29 |
| 0.02 | 1.59 | 10 | 49.27 | 1.14E-04 | 1.38E+06 | 4.50 | 2.05E-05 | 7.71E+06 | 5.24 |
| 0.02 | 1.59 | 10 | 53.20 | 1.23E-04 | 1.28E+06 | 4.46 | 2.27E-05 | 6.97E+06 | 5.20 |
| 0.02 | 1.89 | 10 | 47.70 | 1.10E-04 | 1.70E+06 | 4.59 | 1.97E-05 | 9.57E+06 | 5.34 |
| 0.02 | 1.89 | 10 | 39.58 | 9.16E-05 | 2.05E+06 | 4.67 | 1.54E-05 | 1.22E+07 | 5.44 |
| 0.02 | 1.89 | 10 | 45.41 | 1.05E-04 | 1.79E+06 | 4.61 | 1.84E-05 | 1.02E+07 | 5.36 |
| 0.02 | 1.89 | 10 | 45.33 | 1.05E-04 | 1.79E+06 | 4.61 | 1.84E-05 | 1.02E+07 | 5.37 |
| 0.02 | 1.89 | 10 | 43.52 | 1.01E-04 | 1.86E+06 | 4.63 | 1.74E-05 | 1.08E+07 | 5.39 |
| 0.02 | 1.89 | 10 | 38.08 | 8.82E-05 | 2.13E+06 | 4.68 | 1.46E-05 | 1.29E+07 | 5.46 |
| 0.02 | 5.54 | 35 | 104.9 | 2.43E-04 | 6.49E+05 | 4.17 | 5.53E-05 | 2.86E+06 | 4.81 |
| 0.02 | 5.54 | 35 | 213.2 | 4.94E-04 | 3.19E+05 | 3.86 | 1.40E-04 | 1.13E+06 | 4.41 |
| 0.02 | 5.54 | 35 | 147.5 | 3.42E-04 | 4.61E+05 | 4.02 | 8.64E-05 | 1.83E+06 | 4.62 |
| 0.02 | 5.94 | 35 | 42.16 | 9.76E-05 | 1.74E+06 | 4.60 | 1.67E-05 | 1.01E+07 | 5.36 |
| 0.02 | 5.94 | 35 | 49.45 | 1.14E-04 | 1.48E+06 | 4.53 | 2.06E-05 | 8.22E+06 | 5.27 |
| 0.02 | 5.94 | 35 | 45.13 | 1.04E-04 | 1.62E+06 | 4.57 | 1.83E-05 | 9.27E+06 | 5.32 |
| 0.02 | 7.92 | 50 | 157.1 | 3.64E-04 | 4.33E+05 | 3.99 | 9.38E-05 | 1.68E+06 | 4.58 |
| 0.02 | 7.92 | 50 | 160.3 | 3.71E-04 | 4.24E+05 | 3.98 | 9.63E-05 | 1.64E+06 | 4.57 |
| 0.02 | 7.92 | 50 | 285.8 | 6.62E-04 | 2.37E+05 | 3.73 | 2.05E-04 | 7.66E+05 | 4.24 |
| 0.02 | 8.48 | 50 | 72.17 | 1.67E-04 | 1.01E+06 | 4.36 | 3.38E-05 | 5.01E+06 | 5.06 |

| | | | | | | | | | |
|---|---|---|---|---|---|---|---|---|---|
| 0.02 | 8.48 | 50 | 124.6 | 2.88E-04 | 5.87E+05 | 4.12 | 6.92E-05 | 2.45E+06 | 4.74 |
| 0.02 | 8.48 | 50 | 117.7 | 2.72E-04 | 6.21E+05 | 4.15 | 6.42E-05 | 2.64E+06 | 4.78 |
| 0.02 | 0.138 | 0.80 | 17.35 | 4.02E-05 | 4.23E+06 | 4.98 | 5.23E-06 | 3.28E+07 | 5.87 |
| 0.02 | 8.08 | 44 | 103.3 | 2.39E-04 | 7.66E+05 | 4.24 | 5.42E-05 | 3.39E+06 | 4.89 |
| 0.03 | 10.95 | 50 | 125.4 | 2.90E-04 | 7.53E+05 | 4.23 | 6.98E-05 | 3.14E+06 | 4.85 |
| 0.03 | 0.023 | 0.10 | 18.97 | 4.39E-05 | 4.68E+06 | 5.03 | 5.88E-06 | 3.78E+07 | 5.93 |
| 0.03 | 0.060 | 0.25 | 2.36 | 5.46E-06 | 4.34E+07 | 5.99 | 3.82E-07 | 6.22E+08 | 7.15 |
| 0.03 | 0.138 | 0.50 | 30.26 | 7.01E-05 | 3.82E+06 | 4.94 | 1.08E-05 | 2.52E+07 | 5.76 |
| 0.06 | 10.26 | 2.00 | 412.5 | 9.55E-04 | 5.34E+06 | 5.08 | 3.32E-04 | 1.54E+07 | 5.54 |
| 0.07 | 0.138 | 0.25 | 19.14 | 4.43E-05 | 1.22E+07 | 5.44 | 5.95E-06 | 9.23E+07 | 6.32 |
| 0.07 | 0.060 | 0.10 | 4.58 | 1.06E-05 | 5.49E+07 | 6.10 | 9.13E-07 | 6.43E+08 | 7.16 |
| 0.09 | 8.08 | 11 | 202.1 | 4.68E-04 | 1.56E+06 | 4.55 | 1.30E-04 | 5.62E+06 | 5.11 |
| 0.09 | 7.59 | 10 | 272.1 | 6.30E-04 | 1.20E+06 | 4.43 | 1.93E-04 | 3.93E+06 | 4.95 |
| 0.09 | 7.59 | 10 | 170.1 | 3.94E-04 | 1.92E+06 | 4.64 | 1.04E-04 | 7.28E+06 | 5.22 |
| 0.09 | 7.59 | 10 | 239.0 | 5.53E-04 | 1.37E+06 | 4.49 | 1.63E-04 | 4.66E+06 | 5.02 |
| 0.14 | 10.95 | 10 | 202.4 | 4.69E-04 | 2.33E+06 | 4.72 | 1.31E-04 | 8.36E+06 | 5.28 |
| 0.17 | 0.138 | 0.10 | 54.44 | 1.26E-04 | 1.03E+07 | 5.37 | 2.34E-05 | 5.77E+07 | 6.12 |
| 0.25 | 10.26 | 5 | 180.3 | 4.17E-04 | 4.90E+06 | 5.05 | 1.12E-04 | 1.82E+07 | 5.62 |
| 0.28 | 0.023 | 0.01 | 18.29 | 4.24E-05 | 4.87E+07 | 6.04 | 5.60E-06 | 3.97E+08 | 6.95 |
| 0.74 | 0.060 | 0.01 | 6.03 | 1.40E-05 | 4.13E+08 | 6.97 | 1.31E-06 | 4.45E+09 | 8.00 |
| 0.94 | 7.59 | 1 | 831.7 | 1.93E-03 | 3.88E+06 | 4.94 | 8.33E-04 | 9.03E+06 | 5.31 |
| 0.94 | 7.59 | 1 | 958.1 | 2.22E-03 | 3.36E+06 | 4.88 | 1.00E-03 | 7.49E+06 | 5.23 |
| 0.94 | 7.59 | 1 | 1038.4 | 2.40E-03 | 3.10E+06 | 4.85 | 1.11E-03 | 6.73E+06 | 5.18 |
| 0.95 | 8.08 | 1 | 683.8 | 1.58E-03 | 4.79E+06 | 5.04 | 6.45E-04 | 1.18E+07 | 5.43 |
| 1.35 | 10.95 | 1 | 1173.6 | 2.72E-03 | 3.97E+06 | 4.95 | 1.31E-03 | 8.29E+06 | 5.27 |
| 1.58 | 10.26 | 0.80 | 665.1 | 1.54E-03 | 8.25E+06 | 5.27 | 6.22E-04 | 2.05E+07 | 5.67 |
| 1.70 | 0.138 | 0.01 | 33.4 | 7.73E-05 | 1.73E+08 | 6.59 | 1.23E-05 | 1.11E+09 | 7.40 |
| 2.53 | 10.26 | 0.50 | 707.8 | 1.64E-03 | 1.24E+07 | 5.45 | 6.74E-04 | 3.03E+07 | 5.84 |

| | | | | | | | | | |
|---|---|---|---|---|---|---|---|---|---|
| 5.07 | 10.26 | 0.25 | 1575.6 | 3.65E-03 | 1.10E+07 | 5.40 | 1.92E-03 | 2.10E+07 | 5.68 |
| 12.67 | 10.26 | 0.10 | 2558.4 | 5.92E-03 | 1.67E+07 | 5.58 | 3.63E-03 | 2.75E+07 | 5.80 |
| 16.67 | 8.08 | 0.06 | 2827.0 | 6.55E-03 | 1.96E+07 | 5.65 | 4.14E-03 | 3.14E+07 | 5.85 |
| 18.74 | 7.59 | 0.05 | 2710.0 | 6.27E-03 | 2.30E+07 | 5.72 | 3.92E-03 | 3.73E+07 | 5.93 |
| 18.74 | 7.59 | 0.05 | 3325.0 | 7.70E-03 | 1.85E+07 | 5.62 | 5.12E-03 | 2.82E+07 | 5.81 |
| 18.74 | 7.59 | 0.05 | 3345.8 | 7.75E-03 | 1.84E+07 | 5.62 | 5.16E-03 | 2.80E+07 | 5.80 |
| 24.58 | 10.95 | 0.06 | 3157.2 | 7.31E-03 | 2.61E+07 | 5.77 | 4.79E-03 | 4.03E+07 | 5.96 |
| 126.67 | 10.26 | 0.01 | 2573.1 | 5.96E-03 | 1.66E+08 | 6.58 | 3.66E-03 | 2.73E+08 | 6.79 |

[a] Measured concentration by LC MS/MS.

[b] Nominal concentration.

[c] Calculated using $C_{EVA}$ (mg/L) × F ÷ $S_{EVA}$ (mg/L), where $S_{EVA}$ (mg/L) = 9933.99 and F = 0.023 at 21°C.

[d] Calculated using $S_{PBS}$ (mg/L) = 44.1.

[e] Calculated using Equation (31), as described in Section 4.2.4.

# Appendix G.

# Supplementary Information

**Description:**

The accompanying Excel spreadsheet shows PFOS concentration data collected from US DoD sites (Former Wurtsmith Air Force Base and Barksdale Air Force Base) and toxicity studies. The sheet “Field data” consists of PFOS concentration data of surface water, fishes, and birds; column headings include details on site, medium, units, PFOS concentration (minimum and maximum), author, study, source, and year. The sheet “Toxicity data” consists of PFOS concentrations measured at AC50, EC50, LOEL, and NOEL in fishes and birds; column headings include details on animal, species, exposure duration, exposure, exposure type, exposure temperature, exposure media, metric, effect, response site, concentration, units, author, study, source, and year.

**Filename:**

S.HSU-Supplementary Info-MRM thesis_Chemical activity assessment of PFOS.xlsx